Utilization of Geogenic Contaminated Soil in Embankments with Water Interception Approaches

2020

FEYZULLAH GULSEN

ABSTRACT

The utilization of recycled and reusable materials in the construction industry has become an alternative way to substitute natural materials. However, national regulations might discourage to use them in construction works. With accepting this struggle, two alternative methods for the utilization of geogenic contaminated soils in embankments, which is a reusable material from the construction industry, are proposed and experimentally investigated. At the first one, the contaminated soil is considered to be placed as a core material in the embankment with a simple earthen cover, which is obtained from available in-situ soil. In the second one, the contaminated soil is also suggested to place as a core material in the embankment; however, instead of a cover layer, a drainage layer system is recommended as a countermeasure for preventing water contact to the contaminated soil. The cover layer system is proposed for the coarse-grained contaminated soil (coarser than the available in-situ soil), while the drainage layer system is for the fine-grained contaminated soils (finer-than the available in-situ soil). The efficiency of both methods is tested with a two-dimensional infiltration box test.

A cover may be used to reduce water infiltration inside the core of embankment, which geogenic contaminated soil is considered to locate. A capillary barrier (CB) cover system is a type of cover layer which uses the hydraulic properties difference between fine and coarse-grained layers under unsaturated conditions to create water interception. In the first proposed method, a capillary barrier system was designed by utilizing the coarse contaminated soil in the core of embankment under the in-situ available clean fine soil. The capillary barrier models were verified for the utilization of geogenic contaminated soil in the embankment. A series of laboratory experiments were conducted on the capillary barrier model with a different combination of medium sand over gravel or silica sand. In summary, it concluded that the medium sand with gravel capillary barrier models are effective for the water interception approach. However, a material combination with medium sand over silica sand did not create any capillary barrier effect, although both layers were prepared initially at fully dry conditions.

A drainage layer system is concerned with minimizing the amount of water that might contact with geogenic contaminated soil inside the embankment using a gravity flow phenomenon. This layer might prevent the existence of a potential leachate generation. The efficiency of the proposed drainage layer system is also confirmed with a laboratory infiltration box test. Three different drainage layer models were investigated using two different materials. During the experiments, all three models are tested with two different initial preparation conditions: optimum moisture content preparation case and drawdown case (free drainage after the saturation). According to experimental results, it is found that a drainage layer system with

coarse-grained material at the embankment shoulder and fine-grained material (contaminated soil) in the embankment core is an alternative way for the utilization of geogenic contaminated soil in the embankment. If the contaminated soil which is placed only under the impermeable pavement layer, more than 90% of drained water flows out from the drainage layer.

Numerical studies are also included to understand the in-situ performance of the proposed methods. The analysis was solved in two stages. At first, a water balance analysis was conducted using conventional equations for the cover layer. Kyoto city, Japan, is selected as the investigation site, and its average monthly precipitation and mean temperature over the past thirty years (1985-2015) used as the primary input data. Results show that approximately 28% of precipitation percolated to the surface cover layer annually. Even if the occurrence of the maximum precipitation in summer, oppositely the maximum percolation, takes place in March. This is due to high temperatures in summer. The evapotranspiration increases in this season. Due to the high demand for water, the summer percolation becomes less according to spring. In the second stage, a 1D contaminant transport model was used. Both seepage flow and advection/dispersion properties were considered in the model. Based on the proposed solution, the influences of time and depth from the source were investigated. The result shows that the contamination level 1.5 m from the source reaches the same input contamination level after 2190 days, although unit constant concentration and infiltration are applied during analysis.

From the overall results presented in this study, it can be inferred that both capillary barrier system and drainage layer system methods show encouraging experimental results. If a suitable soil combination is selected, both suggested systems might be a promising output for the utilization of naturally contaminated soil in the embankments with an appropriate design concept.

ACKNOWLEDGEMENTS

I owe the deepest gratitude to my family for their supports, unending encouragement, and guidance throughout all my life.

I would like to express my sincere appreciation to my supervisor, Dr. Takeshi Katsumi, Professor of Graduate School of Global Environmental Studies, Kyoto University, for his tremendous expertise, knowledge, valuable suggestions and guidance, throughout this research.

I also would like to thank Dr. Atsushi Takai, Associate Professor of Graduate School of Global Environmental Studies, Kyoto University, for his endless patience and comments during the research. Special thanks to Professors Toru Inui from Osaka University and Giancarlo Flores from Universidad de Ingeniería & Tecnología (UTEC) for their extremely valuable helps, advises, and supports as well as their continuous encouragement.

I also would like to express gratitude to Professor Mamoru Mimura and Dr. Yousuke Higo from the Graduate School of Engineering, Kyoto University, for letting me use their laboratory, freely. Moreover, I would like to express my sincere thanks to Dr. Mai Sawada, and Dr.Takao Yano for all their affords during the experimental works and brainstorming that saved my research.

It is also a pleasure to be a member of The Katsumi Sensei research group. I would like to thank all the members, including Lincoln, Purba, Mikata, Shimuzu, Akama, Arakama, Mikata, and others, for their tremendous companions. Thank you to all students and friends who provided a nice break before return to study. I also would like to express my appreciation to Yasumoto-san, Laboratory Assistant, Environmental Infrastructure Engineering Laboratory at Kyoto University for her continuous cooperation.

I would also like to thank Mr. Mitsugu Yoshimura from Soil and Rock Engineering Co., Ltd. for the preparation of experimental system.

Finally, financial support from the Ministry of Education, Culture, Sports, Science and Technology (MEXT) is also gratefully acknowledged.

TABLE OF CONTENTS

LIST OF FIGURES

LIST OF TABLES

CHAPTER 1: INTRODUCTION

1.1 General Remarks

The amount of waste and contaminated soil is increasing all over the world. The sources of these waste materials can be different, for example, municipal waste incineration plants, residue from waste recycling or industrial processing residue, etc. Likewise, the contaminated soils might be generated from the construction works such as excavation, earthworks, and rehabilitation of contaminated sites, etc. In addition, there are areas where hazardous heavy metals and metalloids are concentrated in soil due to its geological nature. Due to the excavations or other construction works in such areas, leaching of these elements may be triggered by contact to water and air. As a result, the geogenic (naturally) contaminated soils occur. Some of them may be utilized in construction works in terms of favorable mechanical properties. However, their potential contaminated nature has a question mark.

In-situ and ex-situ remediation techniques have been developed to clean the heavy metal-contaminated sites. These techniques include surface capping, encapsulation, landfilling, soil flushing, soil washing, electrokinetic extraction, stabilization, solidification, vitrification, phytoremediation, and bioremediation. They have specific advantages, disadvantages, and applicability. Most of the techniques are in-situ applicable, while landfilling and soil washing are ex-situ based, which are more expensive than the others due to their transportation fee. The cost and duration of soil remediation are technique-dependent and site-specific (Liu et al. 2018). Therefore, in this dissertation, it is proposed the utilization of these soils containing naturally derived metals and metalloids at a low concentration level as embankment cores with suitable design aspects for being an alternative way to substitute natural resources. Reusing of them would reduce the use of natural resources as a construction material. This aim will prevent the deposition of slightly contaminated soils in disposal areas and save space in the landfills. In conclusion, that effort would be particularly beneficial in countries with limited space such as Japan; also, it will be helpful for non-using of natural construction materials for highway embankments.

In 2002, Soil Contamination Countermeasures Act was established in Japan. It prescribes the state of soil contamination and shows countermeasures for health hazards associated with soil contamination (Ministry of the Environment 2019). However, this act initially did not comprise the naturally contaminated soil. In 2010, the scope of it was extended, and the naturally contaminated soil was also included. It is suggested to apply countermeasure when the geogenic contaminated soil is wanted to use in construction works (Inazumi et al. 2018).

The naturally contaminated soil may have arisen from arsenic, lead, fluorine, etc. The regulatory limit for arsenic and lead is 0.01 mg/L, and one for fluorine is 0.8 mg/L. This study focuses on soils which are slightly above the regulatory limits. For example, arsenic or lead-contaminated soils do not exceed 0.05 mg/L. The utilization of these materials without any protection involves some environmental risks such as spreading around the construction area, contact with the living creatures and contamination of the natural water resources, etc. (Von Maubeuge et al. 2015). An application of a cover layer or a drainage layer might be one of the solutions for these environmental risks.

In Japan, the concept of underground space utilization was introduced as early as the 1980s (Hanamura 1990). Due to that large-scale construction projects such as envisioning the use of underground space for transportation (e.g., roads, railways, and pedestrian tunnels), utilities and telecommunications (e.g., water, sewage, gas, and electric lines), public use (e.g., shopping centers, hospitals, and civil defense structures), and private/personal use (e.g., car garages), excavated soils and rocks with geogenic contamination were generated (Tabelin et al. 2018). A summary of notable tunneling projects which have contaminated soil or rocks around Japan is listed in Table 1-1. One of the primary contaminants is arsenic from these projects. In Japan, arsenic (As) and lead (Pb) exist at a higher concentration compared to the global average. The location of Japan is the main reason for the occurrence of these elements. It is located in the area where the Eurasian and Pacific Plates connect, and geological activities, including volcanic action, have been active. In these environments, some trace elements such as As and Pb may be accumulated (Katsumi 2015). Leaching behavior of these excavated soils and rocks were studied by several researchers (Igarashi et al. 2008; Tabelin et al. 2014; Li et al. 2016; Tabelin et al. 2018). It was pointed out that the leaching concentrations were slightly higher than the regulatory limits. Moreover, these results are relatively low compared to those of anthropogenic contaminated soils and rocks.

Table 1.1 Some of the projects in Japan that generated geogenic contaminated soil

Project	Geogenic heavy metal	Reference
Seikan Undersea Tunnel	Cu, Zn, Pb, Mo	(Mizukami et al. 1995)
Hakkouda Tunnel	As, Pb, Cd, Se	(Hattori et al. 2003)
Hokkaido Shinkansen Tunnel	As, Cd, Cu, Zn	(Yokobori et al. 2015)
Nakakoshi	As	(Tabelin et al. 2018)
Otoineppu bypass	As, B, Se	(Tabelin et al. 2018)

Cover layers have been used traditionally as a safeguard for any waste deposition facilities. The conventional cover design was designed for placing over landfills. They are mostly employed with low-permeable materials such as compacted clay layers, geomembrane, geosynthetic clay liners, or composite liners to minimize rainfall infiltration (Koerner and Daniel 1997). The use of earthen materials is a common alternative way for an engineered cover system (Benson et al. 2001). Although applying geosynthetic in the cover is convenient for safer design, according to economic concern, that is an expensive trial.

The use of geosynthetics and earthen natural material as cover in landfills were investigated widely in previous works (Koerner and Daniel 1997; Merrill et al. 2002; Heerten and Koerner 2008; Zornberg et al. 2003). However, their usage as an embankment cover for contaminated soil utilization was focused by only a few researchers (Von Maubeuge et al. 2015; Birle et al. 2010). Birle et al. (2010) compared various construction methods with slightly contaminated soils in the embankments. The researchers stated that a safeguard is usually necessary as a sealing system. Conversely, if the contaminated soil has low permeability using a geomembrane or additional clay liners as sealing is not required. With this viewpoint, this research focuses on the utilization of naturally contaminated soil in embankments without any artificial materials shown in Figure 1.1.

Figure 1.1 Utilization of geogenic contaminated using a capillary barrier system

In this research, two utilization methods were proposed. At the first approach, a utilization way is suggested when the geogenic contaminated soil is coarser than available in-situ soil. In this case, the contaminated soil is deposited and appropriately compacted under a cover inside the highway embankment. The cover is considered to construct with available in-situ soil (Figure 1 - 1). The performance of the earthen covers depends on soil type and compaction status. Besides, the structure and hydraulic properties of the covers can be affected by desiccation cracks, frost, or roots in the long-term perspective. A thicker cover layer might be a solution to these problems (Koerner and Daniel 1997). Moreover, Birle et al. (2010) mentioned that, if the use of contaminated soils is limited underneath the impermeable pavement, an artificial sealing material will not be necessary. Therefore, in the research, a

simple thick earthen cover without any additional sealing materials is proposed, as shown in Figure 1 - 1.

In this approach, the proposed system will work as a capillary barrier. The capillary barrier is a tilted soil layer system that is composed of a fine-grained soil underlain by a coarse-grained, as shown in Figure 1 - 2. Water is held in the fine layer until horizontal drainage, evapotranspiration, or percolation removes it. Differences in pore size distribution between the coarse and fine soils cause infiltrated water to be retained in the upper fine soil layer under unsaturated flow conditions. As long as the contrast in unsaturated hydraulic conductivities of the fine and coarse soils (k_{fine} and k_{coarse}) is sufficiently large, the capillary barrier system continues to work (Ross 1990). At the low suction range (wet region), the hydraulic conductivity of coarse soil is higher than the fine one ($k_{coarse} > k_{fine}$). On the other hand, at the high suction range (dry region), the hydraulic conductivity of fine soil is higher than the coarse one ($k_{fine} > k_{coarse}$). Due to this hydraulic conductivity difference, the water is directed horizontally inside the fine layer until breakthrough hydraulic conductivity is reached (when the hydraulic conductivity of coarse soil becomes higher than fine one).

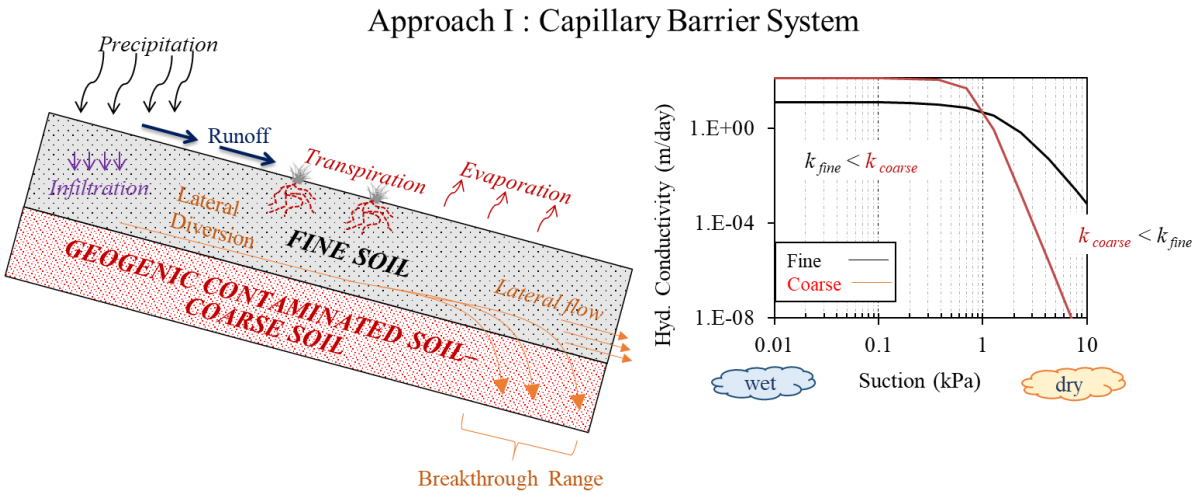

Figure 1 - 2 Schematic of the capillary barrier system

In the second approach, it is studied that the contaminated soil is finer than the available in-situ soil. In this case, the in-situ available coarse-grained soil is considered to use as a drainage layer for the utilization of contaminated soil. The contaminated soil is placed under the pavement layer. Additional sealing layers are not necessary if slightly contaminated soils are placed only within the core of the embankment, underneath the impermeable pavement shown in Figure. 1 – 3 (Birle et al., 2010).

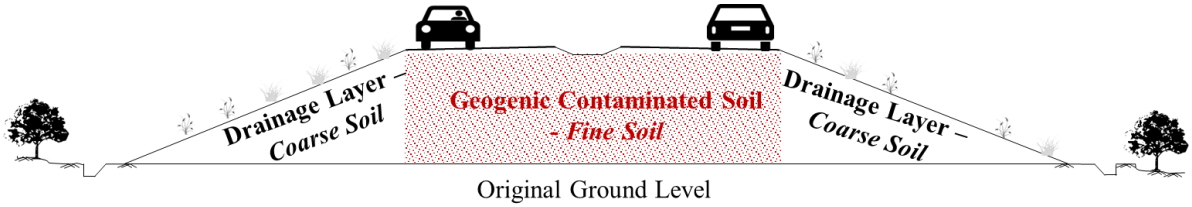

Figure 1 - 3 Utilization of geogenic contaminated using a drainage layer system

In the second approach, the design consideration is different from the capillary barrier system, since the different soil configuration inside the embankment. In this case, two different materials are selected for the core and the side sections of the embankment, separately. This approach is suggested when the contaminated soil has lower hydraulic conductivity than available in-situ soil. In other words, the design is proposed for a coarse in-situ available clean soil and fine contaminated soil. The coarse soil is suggested to use as a drainage layer at the shoulder; however, the fine contaminated soil is at the core of the embankment. Due to the higher hydraulic conductivity of the shoulder region (coarse layer), the water will tend not to enter the contaminated area. It is desired that the water will drain inside the drainage layer, and it will not contact the contaminated region (Figure. 1 - 4). Also, the pavement layer is almost impervious (Azizian et al. 2003). The water may not drain under the impermeable pavement layer. Therefore, it is suggested to place the contaminated soil under the impervious pavement layer. Also, other replacement geometries for the drainage layer system are discussed in Chapter 5.

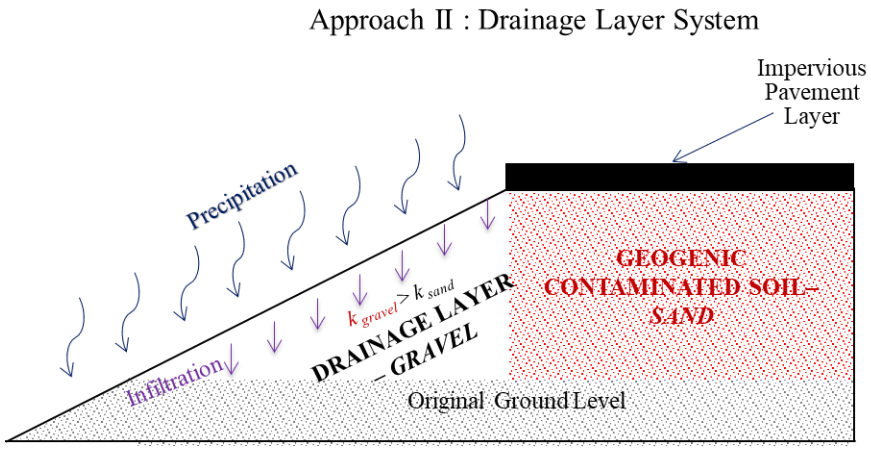

Figure 1 - 4 Schematic of the drainage layer system

This research is investigated to the possibility of the utilization of geogenic contaminated soil in the embankments. For that purpose, two different approaches are suggested. The performance of proposed utilization systems is assessed by using the experimental works.

1.2 Objectives and Scope

The overall objective of this research is to find out alternative ways when utilizing geogenic contaminated soils in the highway embankments. For that reason, two different approaches were proposed—capillary barrier system and drainage layer system. The specific objectives of this dissertation are:

(1) Evaluating the effectiveness of the capillary barrier system when the geogenic-contaminated coarse-grained soil is overlain by in-situ available fine-grained soil.

(2) Assessing the efficiency of the drainage layer system when the geogenic-contaminated fine-grained soil in the core of embankment and in-situ available coarse-grained soil in the shoulder of the embankment.

(3) Clarify the effects of preparation water content on both the performance of the capillary barrier system and the drainage layer system.

(4) Checking the repeatability and the recoverability of both suggested systems.

(5) Evaluating the effect of drainage layer geometry for the utilization of geogenic contaminated soils in the embankment.

To achieve these objectives, at the beginning of the research, the basic geotechnical experiments, including hydraulic conductivity, grain-size distribution, standard Proctor, and relativity density, were conducted to evaluate the geotechnical properties soils which were used in the research. Also, the unsaturated hydraulic conductivity characteristics of the soils estimated using experimental results and literature available equation. Moreover, the effectiveness of the suggested systems was experimentally checked using a two-dimensional laboratory infiltration box test. For understanding the field performance, a water balance analysis is analytically predicted with consideration of the metrological conditions in Kyoto, Japan. Besides, a one- dimensional contaminant transport analysis is solved using water balance analysis results.

1.3 Outline of the Dissertation

This dissertation has been divided into six chapters. The flowchart of the thesis is shown in Figure 1 – 5.

The first chapter (Chapter 1) aims to clarify the objectives and to outline the contents of this research. General information about the proposed systems is presented.

Chapter 2 reviews the sources and origins of heavy metals, as well as their treatment methods, focused on the cover soils and capillary barrier system. Also, it includes literature reviews about drainage layer saturated and unsaturated water flow and contaminated transport in the soil media.

Chapter 3 discusses the basic geotechnical experiments and unsaturated soil mechanics experiment and their results. Also, this chapter gives information about the experimental setup for the infiltration box testes, which are used for the capillary barrier system. It provides results and discussion for the capillary barrier system experimental works.

Chapter 4 describes the experimental system for the drainage layer system. It also shows the experimental results and discussions about the drainage layer system for the utilization of the geogenic contaminated soil in the embankment.

Chapter 5 provides a water balance analysis and a one-dimensional numerical simulation. A water balance analysis is conducted for the Kyoto city, and a one-dimensional contaminant transport analysis is performed using the water balance analysis results.

Chapter 6 presents the conclusion of the result, and it gives suggestions about future research direction.

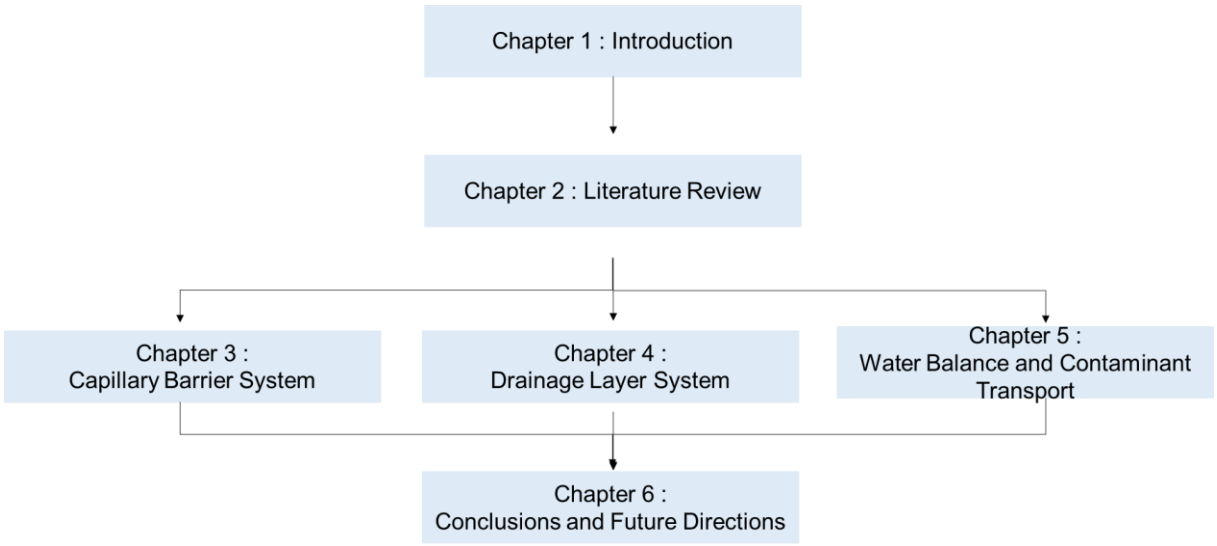

Figure 1 - 5 Outline of the Dissertation

CHAPTER 2: LITERATURE REVIEW

2.1 General Remarks

Metals and/or metalloids contaminated soils are global environmental problems. Heavy metals and/or metalloids present in soils include arsenic (As), cadmium (Cd), copper (Cu), lead (Pb), mercury (Hg), nickel (Ni), chromium (Cr), nickel (Ni), zinc (Zn), manganese (Mn), molybdenum (Mo), selenium (Se), boron (B), and thallium (Tl) all of which represent risks to human health and the environment, especially when they are not degradable by natural processes. There are some methods to control them for not getting in contact with living organisms. This chapter gives a general introduction about heavy metal contamination sources, the basic information about remediation techniques with emphasizing cover soil. It is also summarized literature about the capillary barrier and drainage layer system. Besides, fundamental knowledge about saturated and unsaturated water flow and contaminant transport is presented.

2.2 Sources and Origins of Heavy Metals in Soils and Rocks

Soils may be contaminated by heavy metals or/and metalloids. The term heavy metal represents to any metallic chemical element that has a relatively high density greater than $4\,g\ cm^{-3}$ (Edelstein and Ben-Hur 2018). They are mostly toxic or poisonous at low concentrations and may be found at the contaminated sites. The most common heavy metals found in the soil contamination sites are As, Pb, Cr, Zn, Cd, Cu, Hg, and Ni, etc.

The heavy metals may arise from two different ways in the soil: geogenic(naturally) or anthropogenic. As a geogenic way, the pedogenesis processes of parent materials weathering at levels that are regarded as trace (< 1000 mg/kg) and rarely toxic (Zhao and Kaluarachchi 2002; Pierzynski et al. 2005). Due to the disturbance and acceleration of nature's slowly occurring geochemical cycle of metals by man, most soils of rural and urban environments may accumulate one or more of the heavy metals above-defined background values high enough to cause risks to human health, plants, animals, ecosystems, or other media (D'Amore et al. 2005). A simple mass balance of the heavy metals in the soil can be expressed as follows (Wuana and Okieimen 2011).

$$M_{total} = \left(M_p + M_a + M_f + M_{ag} + M_{ow} + M_{ip}\right) - \left(M_{cr} + M_l\right) \qquad (2.1)$$

where M is the mass of heavy metal, p is the parent material, a is the atmospheric deposition, f is the fertilizer sources, *ag* is agrochemical sources, *ow* is the organic waste sources, *ip* is the other inorganic pollutants, *cr* is crop removal, and l is the losses by leaching, volatilization, and so forth.

2.2.1 Geogenic (Natural) Sources

The heavy metals naturally occur in the environment from rocks and soils. The origin and generation processes of these geological materials affect contaminant nature. Geogenic contaminated rocks or soils that pose risks of releasing hazardous and toxic elements into the environment fall into three different categories according to their origin (Bradl 2005): (1) Igneous (Magmatic) Rocks, (2) Sedimentary Rocks, and (3) Metamorphic Rocks.

2.2.1.1 Igneous (Magmatic) Rocks

The primary rocks are called igneous or magmatic and have a wide range of mineral and chemical composition. They formed through the cooling and solidification of magma. The magma can be derived from partial melts of existing rocks in either an earth`s mantle or crust. It contains more than 3000 minerals known is unique in its chemical composition and its orderly internal crystalline structure. Naturally, the melting of magma is caused by one or more of three processes: an increase in temperature, a decrease in pressure, or a change in composition. If the solidification into rock occurs below the surface, it is named as an intrusive rock, or if the solidification occurs on the surface, it is called extrusive rocks. Intrusive rocks cool within the earth slowly and comprise of minerals that solidify into large crystals. On the other hand, extrusive rocks that rapidly cool when magma is extruded onto the earth's surface by volcanic activity have fine crystals.

During the mineral crystallization of magma, a process called chemical differentiation occurs. Different minerals precipitate according to their stability fields at limited ranges of temperature, pressure, and chemical composition conditions (Siegel 2002). The chemical composition of the magma is subjected to changes during the cooling. Most heavy metals concentrate mostly inside the residual magma. Only a few heavy metals form their mineral or component of a principal mineral. One example is Cr, which crystallizes as the mineral chromite ($FeCr_2O_4$), or Ni, which occurs in the mineral forsterite ($Mg_2[Ni]SiO_4$) as a substitute for Mg during the early stages of differentiation. In the later stages of differentiation, metal concentrations increase, which may lead to precipitation as their mineral such as uraninite (U), beryl (Be) or be hosted in late stage-forming accessory minerals such as zircon, which contains such elements as U and rare earths (Bradl 2005).

Most heavy metals concentrations in the hot residual hydrothermal fluids during the final stages of magma differentiation. When these fluids infiltrate into the enclosing rock, chemical reactions occur between the enclosing rock and the hydrothermal fluid, and minerals precipitate as ores. Examples are Hg as cinnabar (HgS), As arsenopyrite (FeAsS), Pb as galena (PbS), Zn as sphalerite (ZnS), Cu as chalcopyrite ($CuFeS_2$), Mo in molybdenite (MoS_2), Fe as pyrite (FeS_2), and U as uraninite (UO_2). Cd can substitute in part for Zn in sphalerite (Zn [Cd]S), and As can accompany Fe in pyrite (Fe[As]S_2). Ore most often occurs as a group of several minerals, so that smelting and processing of one metal often result in the release of other metals in the environment (Bradl 2005).

2.2.1.2 Sedimentary Rocks

Sedimentary rocks are one of the three main rock groups. They are formed in four main ways: by the deposition of the weathered other rocks, by the accumulation of sediments, by the deposition of the results of biogenic activity, and by precipitation from solution. Disintegrated particles of them are named as sediments (Wilkinson et al. 2009).

The most chemical and biogenic sediments comprise of the mineral calcite, which can be precipitated either by living organisms such as corals or precipitates directly if the chemical conditions for precipitation are given. If evaporation exceeds water inflow into ocean basins, chemical sediments precipitate directly. Among these precipitations, products are the minerals halite (NaCl), gypsum ($CaSC{\cdot}2H_2O$), anhydrite ($CaSO_4$), calcite ($CaCO_3$), phosphorite ($Ca_3(PO_4)_2$), and goethite (FeOOH) (Siegel 2002). The sedimentary rocks have a porous structure than the other rocks types. This structure enables the storage of fluids and helps to create a hydraulic flow (permeability). Because of that, the sedimentary rocks are used for water and energy supply. They contain oil, natural gas, and coal-bearing strata, which provides about 80% of global energy needs. On the other hand, this structure may confine ore deposits from hydrothermal fluids, which have many potentially toxic metals (e. g., Pb, Zn, and U) (Warren 2010).

2.2.1.3 Metamorphic Rocks

Metamorphic rocks derive from some other type of rock; however, they have been substantially altered from their original igneous, sedimentary, or earlier metamorphic form. Metamorphic rocks form when rocks are subjected to high heat, high pressure, hot mineral-rich fluids or, some combination of these factors. These conditions may be found within the deep earth or where tectonic plates meet. Under high temperature/pressure conditions, chemically active fluids may be generated. The chemistry of metamorphic rocks may show the chemistry of the

parent rocks which they derive. Metal-bearing ore deposits originate during metamorphism (Floyd and Winchester 1978).

2.2.1.4 Soil

Another source of the toxic elements and heavy metals for the environment is the soil. Soil is a mixture of mineral matter produced by the weathering of bedrock or other parent material. These materials are modified by continued weathering, downward leaching with infiltrating rainwater. Weathering is a key source of the soil-forming process (Naidu et al. 1998). The process of soil formation generally involves the downward movement of water, fine soil particles, dissolved ions, and a common result of that is the development of chemically and texturally different layers known as soil horizons. When a soil develops from rock, soil profiles developed, as illustrated in Figure 2 - 1, are (DiVenere 2019):

O — 100% organic matters (leaf litter, grasses, etc.)

A — the layer of partially decayed organic matter mixed with mineral material

B — organic poor, enriched in fine materials and soluble ions the layer of accumulation of clay, (Fe) oxyhydroxides, and other elements from the overlying soil

C — physically and chemically weathered parent material the C horizon grades down into unaltered parent material

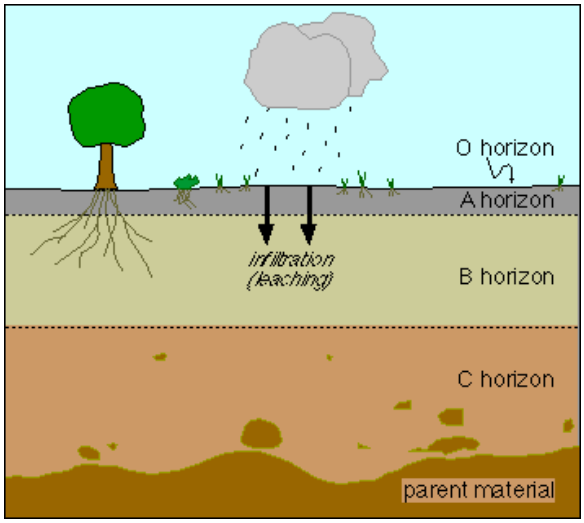

Figure 2 - 1 Soil horizons (DiVenere 2019)

According to the type of parent rock, climate, time, and soil organisms, soil composition may change. Its chemical composition primarily depends on the parent rock. Typical concentrations of a range of heavy metal(loid)s found in the upper earth's crust, and the most common types of igneous and sedimentary rocks are shown in Table 2 – 1 (Alloway 2013).

Table 2 - 1 Geological sources of heavy metals and metalloids (mg/kg) (Alloway 2013)

Element	Upper Crust	Granite, Granodiorite	Gabbro, Basalt	Ultramafic rock	Sandstone	Shales	Black/Oil Shales	Limestone	Coal
Ag	0.07	0.04	0.10	0.06	0.25	0.07	1.90	0.12	–
As	2.00	3.00	0.70	0.70	0.50	13.00	<500.00	1.50	10.00
Ba	668.00	600.00	330.00	5.00	300.00	550.00	67.00	90.00	250.00
Cd	0.10	0.10	0.20	0.05	<0.04	0.25	<240.00	0.10	1.00
Co	12.00	4.00	45.00	110.00	0.30	20.00	67.00	0.10	10.00
Cr	35.00	10.00	250.00	2300.00	35.00	100.00	<700.00	5.00	20.00
Cu	14.00	12.00	90.00	40.00	2.00	45.00	<300.00	6.00	20.00
Mn	527.00	400.00	1500.00	1200.00	100.00	850.00	–	15.00	40.00
Mo	1.40	1.50	1.20	0.30	0.30	2.00	<570.00	0.30	3.00
Ni	19.00	5.00	130.00	2000.00	2.00	70.00	<300.00	5.00	20.00
Pb	17.00	20.00	4.00	0.05	10.00	22.00	<100.00	5.00	20.00
Sb	0.30	0.30	0.20	0.10	0.05	1.00	<10.00	0.15	2.00
Sn	2.50	3.60	0.90	0.30	0.60	5.00	<10.00	0.30	8.00
U	2.50	4.00	0.50	0.02	1.30	3.20	<1.25	1.00	2.00
V	53.00	70.00	260.00	80.00	20.00	130.00	<2.42	15.00	40.00
Zn	52.00	50.00	100.00	60.00	20.00	100.00	<2.31	40.00	50.00

2.2.2 Anthropogenic Sources

Potentially toxic metals can be released into the environment by human activities that are named as anthropogenic sources of contamination. Some example of anthropogenic processes caused to the soil contaminations is the emissions from the industrial areas, mine tailings, disposal of metal wastes, leaded gasoline and paints, application of fertilizers, animal manures, sewage sludge, pesticides, land application of treated wastewater (TWW), coal combustion residues, spillage of petrochemicals, and atmospheric deposition, etc...(Khan et al. 2008; Zhang et al. 2010; Edelstein and Ben-Hur 2018).

2.3 Heavy Metal Treatment Methods

Contamination of soils with heavy metals is a global problem for human health and the environment. Globally more than 5 million sites are covering 20 million ha of land in which the soils are contaminated by different heavy metal(loid)s. The heavy metals in contaminated soil damage the natural ecosystem and eventually damage human health (Wuana and Okieimen 2011; Jaishankar et al. 2014; Liu et al. 2018).

Over the years, various in-situ and ex-situ remediation techniques have been developed to contain, clean up, or restore heavy metal-contaminated soils, such as surface capping, soil flushing, electrokinetic extraction, solidification, vitrification, and phytoremediation (Figure 2 - 2). These techniques can be classified into five categories: physical, chemical, electrical, thermal, and biological remediation or three divisions: containment-based (e.g., capping/encapsulation), transformation-based (e.g., stabilization/immobilization), and transport-based (e.g., extraction/removal) methods. Generally, these soil remediation methods have different working mechanisms and suggested for a specific application with their advantages and limitations. There is some literature for the soil heavy metal remediation technologies (Khan et al. 2004; Bradl 2005; Wuana and Okieimen 2011; Liu et al. 2018). However, in this thesis, it is aimed to use one of the primary remediation techniques for heavy metal contaminated soils. It is the covering.

Surface covering is to simply cover the contaminant with a layer of water interception design to form a stable, protection surface for contaminated materials. The covering technique is not truly a soil remediation method, because no efforts are made to remove the heavy metal contaminants or at least reduce their reactivity. However, the method enables to eliminate the risk of contact to the contaminated soil with living creatures and//or environment. Also, it serves as an impermeable barrier to surface water infiltration, preventing soil contaminants' leaching from surfacing water and groundwater (Liu et al. 2018).

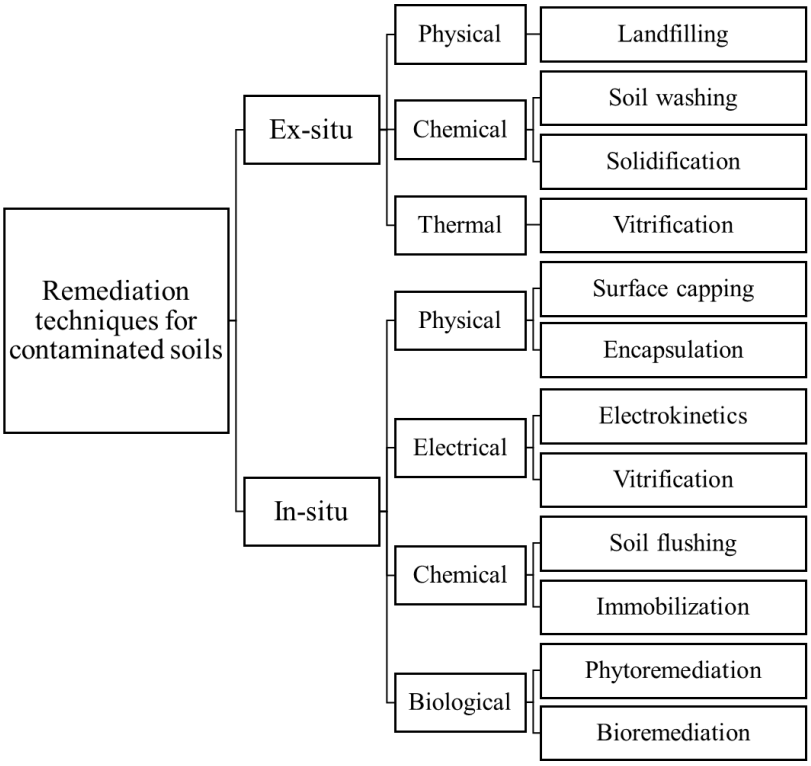

Figure 2 - 2 Common remediation techniques for heavy metal-contaminated soils (Liu et al. 2018)

2.4 Cover Technologies

Cover systems for waste containment and remediation sites may consist of multiple layers of different types of soils and/or geosynthetics, each with one or more specific functions. A final cover system should semi-permanently prevent the infiltration of rainwater into the underlying contaminated layer. The primary purposes of final landfill cover systems are: (1) to minimize the infiltration of rain and melted snow into the contaminated layer after the construction has been completed, (2) to limit the uncontrolled release of gases, (3) to suppress the proliferation of vectors, (4) to limit the potential for fire, (5) to provide a suitable surface for vegetation at the site, and (6) to serve as the central element in the reclamation at the site (Koerner and Daniel 1997).

To attain these goals, landfill final cover systems must be able to: (1) withstand climatic extremes (e.g., hot/cold, wet/dry, and freeze/thaw), (2) resist water and erosion, (3) maintain stability against slumping, cracking, slope failure, and downward slippage or creep, (4) resist differential settlement caused by the compression of waste and foundation soil, (5) resist deformation caused by earthquakes, and (6) resist disruptions caused by plants, burrowing animals, worms, and insects (Koerner and Daniel 1997; Kamon et al. 2002). It is essential that considerations should exist, which corresponds to attaining those mentioned above.

In this research, a cover (sometimes called caps), which is different from traditional landfill cover, is the focus of an embankment. It is planning to place under the highway pavement layer. The proposed cover remains in place as an essential part of the utilization of geogenic contaminated soil in the embankment.

The cover system is based on one or more of three different principles for preventing or minimizing water percolation into waste. It can be work as a hydraulic barrier, capillary barriers, or evapotranspirative barrier. The hydraulic barrier type of cover system uses a low permeability to block the downward migration of water into the waste. Hydraulic barrier materials most commonly include compacted clay layers (CCLs), geosynthetic clay liners (GCLs), geomembranes, and combinations of these materials (Bonaparte and Yanful 2001).

The capillary barrier consists of a fine-grained soil overlying of coarse-grained soil. At a low degree of soil saturation, i.e., at high matric suction in the hydraulic conductivity of the coarse-grained soil is much less than that of the fine-grained soil. This is the reverse of the condition that occurs when the coarse-grained soil is at a high degree of soil saturation. Capillary barriers either: (1) store water by increased moisture content in the fine-grained soil for subsequent evapotranspiration, or (2) divert infiltrating water via unsaturated lateral flow in the fine-grained soil (above the soil interface). Sometimes a drainage layer is installed between the coarse and fine layers to accelerate lateral flow. At a high degree of soil saturation in the coarse-grained soil, the capillary effect breaks down, and percolation through the system can occur.

Evapotranspirative cover system has also been developed primarily for use at arid and semi-arid sites. They consist of a thick layer of relatively fine-grained soil capable of supporting vegetation. Evapotranspirative covers use two characteristics of fine-grained soils: (a) significant soil water storage capacity, and (b) low hydraulic conductivity. Low hydraulic conductivity limits the progression of the soil wetting front during seasonal wet periods. High water storage capacity allows storage of moisture, which infiltrates until it can later be removed by evapotranspiration. An evapotranspirative barrier must be sufficiently thick that changes in moisture content.

One of the essential issues is the total bottom percolation amount for the covers. The evapotranspirative covers are generally used at semi-arid and arid sites, however, they also used for places in humid climates, but to a lesser extent than for sites in drier climates and generally only when a relatively high level of drainage (percolation through the barrier) is acceptable, e.g., 50 mm/yr drainage in a humid climate (Benson et al. 2001). To minimize the percolation, an evapotranspirative cover should generally be sufficiently thick such that the soil water content does not change near the base of the cover. The minimum required barrier thickness is

a function of the frequency and intensity of precipitation, the magnitude of potential evapotranspiration when most precipitation occurs, the unsaturated hydraulic properties of the soil, the type of vegetative cover, and other factors. The barrier should be thick enough to store excess precipitation during times of vegetation dormancy and/or low evaporation rates (Zornberg et al. 2003).

If the cover system is designed as evapotranspirative, it must be served as a rooting. Instead of being compacted in thin 0.15-m thick lifts to achieve a relatively high bulk density (dry unit weight), e.g., 95% of the standard Proctor maximum dry density, and low saturated hydraulic conductivity, evapotranspirative barriers are often placed in thicker lifts with less compaction effort, e.g., 80 to 90% of the standard Proctor maximum dry density. Soil compaction reduces the volume and continuity of the larger soil pores, which are more conductive to the water and air needed for root growth (Gross 2005).

2.5 Capillary Barrier System

The capillary barrier consists of a fine-grained soil overlying of coarse-grained soil. It uses a slope and a textural difference between an overlying finer soil layer, and an underlying coarser soil layer. Engineered capillary barriers have been interested in their potential to limit the interaction between waste disposal facilities and the surface water. In arid and semiarid climates, engineered capillary barriers have adequately been considered to store, release, and funnel water away from sensitive underground structures (Ross 1990; J. C. Stormont 1996; Morris and Stormont 1997).

On the other hand, the capillary barriers are also used in humid climates as oxygen barriers to limit the production of acid mine drainage (Choo and Yanful 2000). Moreover, the engineered capillary barriers are also suggested as a potential application as a slope stabilization method against rainfall-induced landslides (Tami et al. 2004; Rahardjo et al. 2012). Another application of the capillary barrier system is suggested as a preservation method for tumulus (Sawada et al. 2017). From these studies, it is apparent that an engineered capillary barrier system may be applied as a cover layer for safe utilization of geogenic contaminated soils in the highway embankments as adopting a fundamental approach based on saturated–unsaturated flow theory.

A capillary barrier is a cover system that takes advantage of a capillary phenomenon. Ross (1990) defined a capillary barrier as an arrangement of unsaturated fine-grained soil overlaying unsaturated coarse-grained soil along with a sloping contact, which can lead to the diversion of infiltrating water away from the coarser material. A similar description is presented by Stormont (1996); he also expressed that a capillary barrier is effective if the combined effect

of evaporation, transpiration, and lateral divergence exceeds infiltration from precipitation, thereby retaining a sufficiently negative pressure potential, so that breakthrough into the coarse layer does not occur. Parent and Cabral 2006 developed a design method to optimize the thickness of capillary barrier layers based on minimum water infiltration. Nyhan (2005)reported that an increase in the slope of the landfill decreases percolation into the waste.

Warren et al. (1996) and Albright et al. (2004) made field measurements on the landfills who have constructed with capillary barrier cover systems. It has shown that deep percolation is less than 5% of annual rainfall. However, most of the instrumented capillary barriers were constructed in regions with arid or semi-arid climates where the annual precipitation is generally less than 1000 mm.

The capillary barrier effect primarily depends on the contrast in hydraulic conductivity between the fine and coarse soil interface layer. Figure 2 – 3 presents the changing of hydraulic conductivity during the wetting process in two soils. At the beginning of wetting, the coarse soil has smaller hydraulic conductivity than the fine one. If the wetting process continues, the water content of the fine-grain layer will increase, and suction will be reduced. As a result, the *k* of the fine layer will be increased progressively. However, the water will not infiltrate from fine to coarse layer due to the relatively smaller hydraulic conductivity of the coarse layer. Therefore, water will be diverted along with the fine-coarse interface when it's sloped. Water can only infiltrate to the coarse layer when the suction at the interface decreases to the water-entry value of the coarse layer. If the suction value at the interface reaches a value lower than the water-entry value, water will rapidly move into the coarse layer because the high k-value coarse layer, and the barrier effect is diminished.

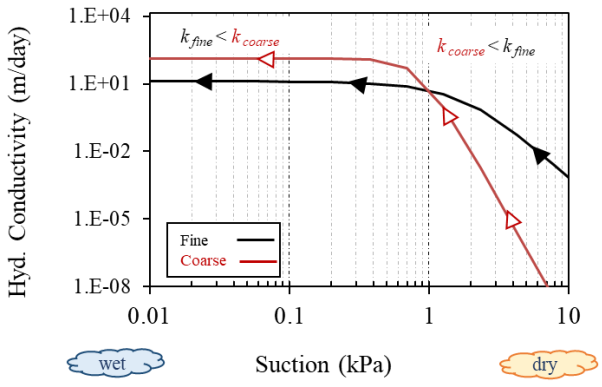

Figure 2 - 3 Typical hydraulic conductivity relationship capillary barrier effect

2.5.1 Water Storage of a Capillary Barrier

Stormont and Morris (1998) suggested a method to calculate the amount of water storage in a capillary barrier. Researchers stated that the maximum water content a soil can hold before it

drains downward is approximated as its field capacity (FC), which is the water content after free or gravity drainage. Field capacity is often arbitrarily stated as the water content at about 3,500 mm of the suction head (Stormont and Morris 1998). Below field capacity, the hydraulic conductivity is often assumed to be so low that gravity drainage becomes negligible, and the soil moisture is held in place by suction. By assuming a constant field capacity, the water storage capacity for a simple soil cover can be described by:

$$\mathrm{SC} = \int_0^z \theta_w \, dz = FC \, z \tag{2.2}$$

where *SC* is the storage capacity of a cover layer, θ is the volumetric water content, and *z* is the layer thickness. On the other hand, not all stored water can be removed by plants. Vegetation can reduce the soil moisture content to the permanent wilting point (PWP), which is typically defined as the water content at 150,000 mm of the suction head. Evaporation from the soil surface can reduce the soil moisture below the wilting point. However, evaporation is usually described as a surface process. Therefore, the net storage capacity (NSC), also called the available water capacity, of a soil layer can be approximated by (Stormont and Morris 1998):

$$NSC = (FC - PWP) z \tag{2.3}$$

To calculate the storage capacity of the capillary barrier layer, suction profile inside the fine-grained layer at breakthrough needs to be estimated. The suction profile may be computed using the Kisch method (1959) or the linear method. Stormont and Morris (1998) suggested that breakthrough occurs when the water-entry value of the coarse layer has been reached. Based on this fact, the water-entry value of the coarse layer can be selected as the boundary in the pore-water pressure profile of the fine-grained layer of the capillary barrier. The effectiveness of the capillary barrier also depends on the infiltration rate (flux) of water into the soil (Ross 1990; Stormont and Morris 1998). For a constant slow infiltration rate, it is assumed that the suction profile in the fine-grained layer behaves as a unit slope profile (dh/dz = 1). A unit slope suction profile represents that the increase in suction is equal to the increase in elevation. For a relatively fast infiltration rate, phenomena will be different from the slow one. In particular, the unit slope will not be approached in the overlying soil if the constant infiltration flux is higher than a critical flux (q_c), which is given by:

$$q_c = k (b + h_w) \tag{2.4}$$

where q_c is the infiltration rate, k is the hydraulic conductivity, b is the total height of the fine soil above the interface, and h_w is the water-entry head of the coarse-grained layer. After the height of b is reached, the suction profile inside the fine layer becomes constant up to the surface of the capillary barrier. It is represented in Figure 2 - 4.

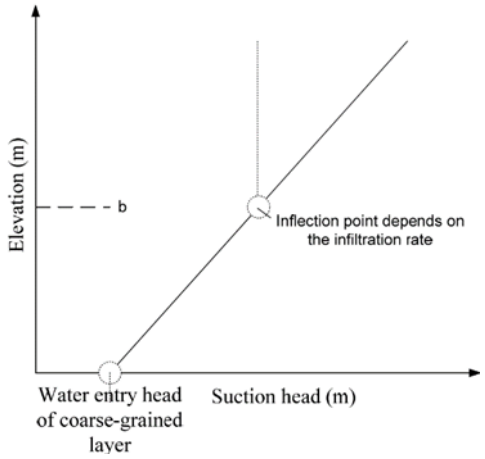

Figure 2 - 4 Pore-water pressure profile of a capillary barrier at breakthrough (Harnas 2015)

The estimated pore-water pressure profile at breakthrough is used for obtaining the volumetric water content profile inside the capillary barrier. For a slow infiltration rate, the total storage capacity can be calculated by:

$$SC = \int_0^z \theta_w \, (z + h_w) \; d_z \tag{2.5}$$

2.5.2 Lateral Diversion of a Capillary Barrier

Mechanism of lateral diversion of water in the capillary barrier system has been discussed (Ross 1990; Stormont and Morris 1998; Abdolahzadeh et al. 2011). The pioneer equation for the calculation of lateral diversion was developed by Ross (1990). He used some assumptions for obtaining the equation. These are: steady-state infiltration, a semi-infinitely thick layer, and a quasi-linear approximation for the relationship between the relative permeability and pressure head. He defined the diversion capacity as the maximum water volume, which can be diverted per unit area of the fine-grained layer above the interface before entering the coarse-grained layer. Also, the diversion length is the distance in the down-dip direction from the crest of the capillary barrier to the point where the rate of water percolation into the coarse layer. Figure 2 – 5 shows the diversion length and diversion capacity.

The total horizontal directed flow in the fine layer Q_{max} is equal to the total flux of water until a breakthrough occurs. It can be calculated by Ross (1990):

$$Q_{max} = k_s \tan\theta \int k_r \, d\psi = \tan\theta \int k_w \, d\psi \tag{2.6}$$

where Q_{max} is the maximum total horizontal flux at breakthrough, k_s is the saturated hydraulic conductivity, θ is the angle of the fine-coarse interface with respect to the horizontal, k_r is the wetting face relative hydraulic conductivity, k_w is the unsaturated hydraulic conductivity, and ψ is the matric suction. The relative permeability function used by Ross. It is a quasi-linear function.

The boundary conditions are the matric suction values at the surface and interface (bottom of the fine layer). A steady-state one-dimensional vertical flow was assumed. At the surface, the relative permeability is simply the infiltration rate and divided by the saturated permeability of the fine layer. The matric suction was considered as equal at the interface layer between the fine and coarse layers. With these integration limits, Ross's closed-form solution:

$$Q_{max} = k_s \frac{\tan\theta}{\alpha} \left[\left(\frac{q}{k_s^*} \right)^{\frac{\alpha}{\alpha^*}} - \frac{q}{k_s} \right] \tag{2.7}$$

where the unstarred and starred values are the fine and coarse layer parameters, respectively.

For a constant infiltration, the diversion length, L, is the total water volume diverted by the capillary barrier divided by the infiltration rate:

$$L = k_s \frac{\tan\theta}{q\,\alpha} \left[\left(\frac{q}{k_s^*} \right)^{\frac{\alpha}{\alpha^*}} - \frac{q}{k_s} \right] \tag{2.8}$$

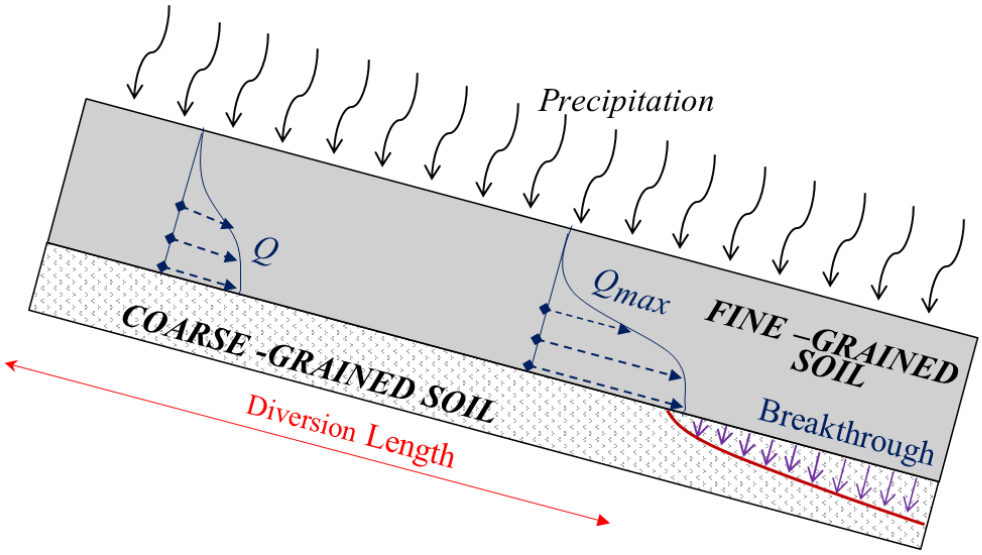

Figure 2 - 5 Illustration of diversion length and diversion capacity of a capillary barrier

2.6 Drainage Layer System

A drainage layer is generally used in embankments to control the infiltration of undesired water towards the collector systems. Modern concerns for subsurface drainage within a road or embankment began with Pierre Marie Jerome Tresaguet (1716–1796), who developed a pavement structure in which sloping interfaces. Tresaguet's system used an aggregate surface layer designed as an impervious mat to shed surface water. From the early twentieth century, rapid developments in construction materials and technologies resulted in the use of different techniques and different materials as highway drainage systems. However, using a high permeable material in the base layer as a drainage system becomes the main design criterion (Lebeau and Konrad 2009).

Especially in humid, rainy, or frost areas, the selection of appropriate embankment materials plays a key for the durability of the roads. The selection of proper drainage materials for embankment provides additional protection against heavy rain, frost action, which causes maintenance of stresses that are transmitted to the subgrade layer. In pavement engineering, there has been extensive research about highway drainage systems, which is related to the structural safety of the highway (Lebeau and Konrad 2009; Koohmishi 2019). However, alternative usage of the contaminated soil in the embankment has not been focused on detailed not only pavement engineers but also geoenvironmental engineers, too.

In Europe, Germany is the one pioneer country for reuse or recycling of materials to preserve natural resources by introducing the German Closed Substance Cycle Waste Management Act. The German Association for Research on Road Construction and Traffic Affairs (FGSV) developed various construction methods for the use of such materials. A technical safeguard or a technically safe installation is usually considered as the application of a sealing system. If the contaminated soils or recycled materials are of low permeability, the use of additional clay liners or geomembranes for sealing purposes is not necessary. However, the requirements set on the hydraulic properties of the contaminated soils and recycled materials must be defined (Birle et al. 2010; Von Maubeuge et al. 2015)

Birle et al. (2010) have shown the construction methods with slightly contaminated soils or recycled materials using the recommended by the German Association for Research on Road Construction and Traffic Affairs. The researchers stated that, if the contaminated soils or recycled materials are deposited underneath the impermeable pavement, an additional sealing material will not be necessary, too. They have suggested a method for the utilization of slightly contaminated soils in the embankment, which is shown in Figure 2 - 6. They recommend using

a shoulder material which has 50 times higher hydraulic conductivity than the contaminated soils or recycled materials.

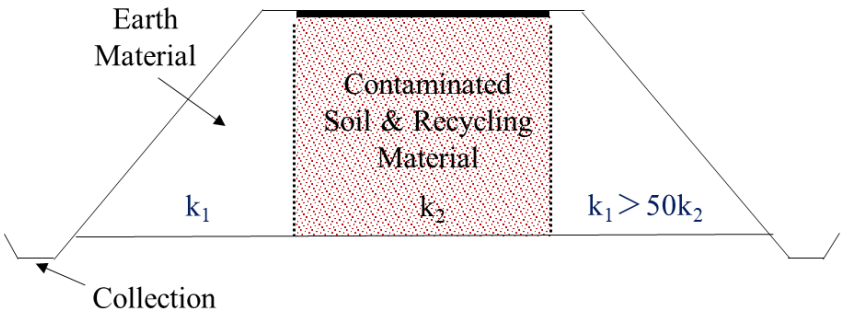

Figure 2 - 6 Embankment with a core of contaminated soils or recycled materials (Birle et al. 2010)

2.7 Water Flow in Soil Media

Water flow in soil media is divided into two main parts: saturated and unsaturated (or vadose) flow. These two parts are generally separated by the groundwater table (GWT). If the soil is located under the GWT, it is named as saturated soil, and if the soil is located above the GWT, it is called unsaturated soil. In the unsaturated case, the amount of water and air significantly influences the behavior of soils (Fredlund et al. 2012). The amount of water, air, and solid in soils is calculated using the volume – mass relationships (soil phase diagram) illustrated in Figure 2 - 7. The amount of water in the soil media is generally expressed in two ways. The gravimetric water content w is the mass of water M_w divided by the mass of solids M_s. As an alternative representation is the volumetric moisture content θ, which is defined as the volume of water in the voids V_w divided by the total volume of the soil V_T.

The volume of the void inside soil media is represented by porosity and void ratio. The porosity n, is calculated by the ratio of the volume of voids V_v divided to the total volume of the soil V_T. The voids ratio e, is an alternative representation of the volumetric variables and is the ratio of the volume of the voids V_v to the volume of the solids V_s. The degree of saturation S_r is calculated by the volume of water to the instantaneous volume of voids. These volumetric quantities are linked through mass quantities in the soil phase diagram by the dry density of the soil ρ_d, the density of water ρ_w, and the specific gravity of solids G_s. The dry density ρ_d, is the ratio of the mass of the solid particles M_s to the total volume V_T. The bulk density ρ_{bulk} is the ratio of the total mass M_T to the total volume V_T where the total mass and the total volume are the sums of the masses and volumes of the phases, respectively, as illustrated in Figure 2 -7. The relative density G_s, is the density of the soil particles ρ_s, divided by the density of water ρ_w.

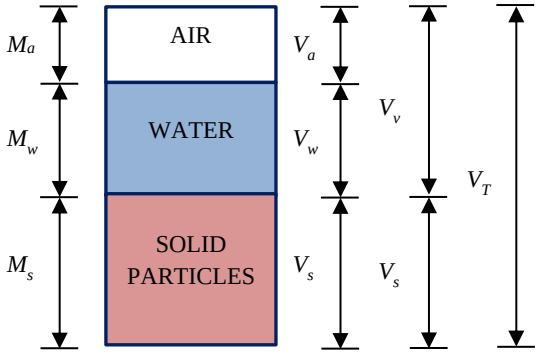

$$\rho_{bulk}=\frac{M_T}{V_T} \qquad w(\%)=\frac{M_w}{M_s}\times 100 \qquad n=\frac{V_v}{V_T}$$

$$\theta=\frac{V_w}{V_T}=n\times S_r \qquad e=\frac{V_w}{V_T}=\frac{n}{1-n} \qquad S_r=\frac{V_w}{V_v}$$

$$S_r\times e=w\times G_s \qquad G_s=\frac{\rho_s}{\rho_w}$$

$$\rho_d=\frac{M_s}{V_T}=\frac{\rho_s}{1+e}=\frac{\rho_{bulk}}{1+w}$$

Figure 2 - 7 Volume – mass relationships (soil phase diagram)

The flowing of water from one place to another place requires energy. Whether the flow is in a pipe, channels, or soil, and energy difference is the main concern. The energy level in the water system is defined in the height of water or head (h). It has three components, gravitational (elevation), pressure, and velocity, as shown in equation (2.9). The elevation (gravitational) head z, represents the potential energy. The pressure head ($u / \rho_w g$) denoted the energy stored as the pressure in the water, and the velocity head ($v^2 / 2g$) represents the kinetic energy. The velocity head in the soil is negligible because of the slow velocity of water flows through soils.

$$h = z + \frac{u}{\rho_w g} + \frac{v^2}{2g} = z + \frac{u}{\rho_w g} \tag{2.9}$$

The hydraulic gradient i, is another definition of water flow in soil. The hydraulic gradient is the ratio of the loss of total head (Δh) between two investigated points over the actual traveled distance (L) between these two points.

$$i = \frac{\Delta h}{L} \tag{2.10}$$

Many researchers have investigated the water flow through a soil media; therefore, the basis of the flow of water in a saturated soil was founded by Henry Darcy (1856) (Fredlund et al. 2012). He found that there is a linear relationship between the water velocity (v) and the hydraulic gradient (i), and the slope of that relationship is named as the hydraulic conductivity (k). Darcy's law for one-dimensional flow is:

$$Q = -Aki = -Av \tag{2.11}$$

where Q is the discharge rate in the flow direction. The minus sign is shown the decreases in the head through the flow direction. Darcy velocity or Darcy flux (q) is another term for water flow. It shows the discharge rate per unit area (A):

$$q = \frac{-kAi}{A} = -k\frac{\Delta h}{L} \tag{2.12}$$

In the soil media, the actual cross-sectional area is less than the total area (A), which is used for Darcy's law. Thus, the actual average velocity (seepage) of the water (v) is higher than the Darcy velocity. The net cross-sectional area for the water flow is equal to the porosity (n) times the total cross-sectional area (A). Therefore, the actual velocity of the water is:

$$v = \frac{q}{n} \tag{2.13}$$

A water flow problem always includes the continuity equation, which expresses the principle of mass conservation. In a control volume, the mass of groundwater, M, changes when groundwater enters or leaves at a specific time, t (Delleur 1999). The conservation of mass bases on that the net result of inflow minus outflow is balanced by the change in storage versus time.

$$Mass\ flux\ inflow - Mass\ flux\ outflow = \frac{\partial M}{\partial t}\ (mass\ change\ by\ t) \tag{2.14}$$

To make a derivation of water flow in the unsaturated zone, let's think of a soil element with one-dimensional water flow, shown in Figure 2 - 8. The element has infinitesimal dx, dy, and dz dimensions and fixed in space. To make the derivation of the flow one-dimensional flow equations, it is considered that the flow is only in the x-direction: $v_y = v_z = 0$. Using mass balance and Darcy's law, one-dimensional flow equation can be calculated using the equation below:

$$\frac{\partial}{\partial x}\left(k_x \frac{\partial h}{\partial x}\right) = S_s \frac{\partial h}{\partial t} \tag{2.15}$$

where S_s is the specific storage of the soil element. With the same consideration, if the previous calculation is converted as three-dimensional flow, there would be additional velocity terms in the y and z directions. At that case, the general equation is:

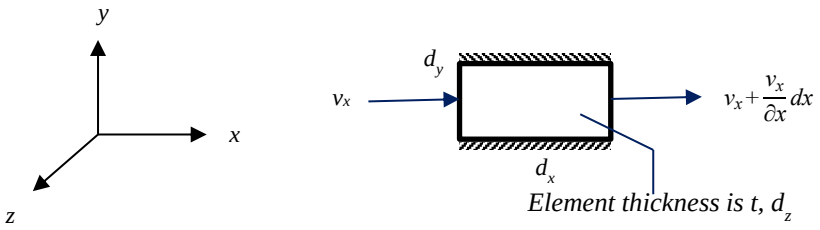

Figure 2 - 8 One-dimensional water flow through an unsaturated soil element

$$\frac{\partial}{\partial x}\left(k_x\frac{\partial h}{\partial x}\right)+\frac{\partial}{\partial y}\left(k_y\frac{\partial h}{\partial y}\right)+\frac{\partial}{\partial z}\left(k_z\frac{\partial h}{\partial z}\right)=S_s\frac{\partial h}{\partial t} \tag{2.16}$$

Equation (2.16) is the general equation for the three-dimensional flow. The real soil media is heterogeneous and anisotropic, due to that at real flow hydraulic conductivities which belong to x, y, and z directions are different for each direction ($k_x \neq k_y \neq k_z$). According to the general flow equation, the general flow equation may be separated as steady-state water flow and transient or unsteady-state flow. In the steady-state case, the changing of the head during to investigated time is zero ($\partial h/\partial h = 0$). But in some problems such as precipitation of water, water flow under a dam (Billstein et al. 1999), it is necessary to take into consideration changes in heads (or water storage). A transient flow gives a chance to solve complex water flow problems by considering time-dependent solutions. At the transient flow, the general flow equation is solve considering ($\partial h/\partial h \neq 0$).

The general forms of the flow equations can be simplified by making some assumptions. If the hydraulic conductivities are assumed to be homogenous and equal to each other's ($k_x = k_y = k_z = k$), a new format for the equation is obtained, like below:

$$k\frac{\partial^2 h}{\partial x^2}+k\frac{\partial^2 h}{\partial y^2}+k\frac{\partial^2 h}{\partial z^2}=S_s\frac{\partial h}{\partial t} \tag{2.17}$$

$$\frac{\partial^2 h}{\partial x^2}+\frac{\partial^2 h}{\partial y^2}+\frac{\partial^2 h}{\partial z^2}=\frac{S_s}{k}\frac{\partial h}{\partial t} \tag{2.18}$$

The above three-dimensional equations may be reduced to two or one dimensions by simply eliminate flows in y and/or z terms. For example, plain or axis-symmetric problem solutions equation (2.18) can be reduced to solve a two-dimensional flow problem in the horizontal plane. The depth can be assumed as unit width or equal to the x-direction terms. Therefore, these kinds of problems can be solved only at x-y or z-y planes. For the one-dimensional problems, only one direction is considered for the solution, such as x direction, y direction, or z-direction. The two-dimensional flow problem in the x, y for the homogenous and isotropic soil media can be written by below:

$$\frac{\partial}{\partial x}\left(k\frac{\partial h}{\partial x}\right)+\frac{\partial}{\partial y}\left(k\frac{\partial h}{\partial y}\right) = S_s\frac{\partial h}{\partial t} \tag{2.19}$$

For two-dimensional flow, if there is a leakage or inflow N at the boundary conditions of the investigated problem, the equation (2.18) becomes like below:

$$\frac{\partial}{\partial x}\left(k_x\frac{\partial h}{\partial x}\right)+\frac{\partial}{\partial y}\left(k_y\frac{\partial h}{\partial y}\right)+N = S_s\frac{\partial h}{\partial t} \tag{2.20}$$

For the flow in a homogeneous and isotropic media, the above equation becomes:

$$\frac{\partial}{\partial x}\left(k\frac{\partial h}{\partial x}\right)+\frac{\partial}{\partial y}\left(k\frac{\partial h}{\partial y}\right)+N = S_s\frac{\partial h}{\partial t} \tag{2.21}$$

This equation states that the difference between the flow (flux) entering and leaving an elemental volume at a point in time is equal to the change in the storage of the soil systems. More fundamentally, it states that the sum of the rates of change of flows in the x- and y-directions plus the externally applied flux is equal to the rate of change of the water amount with respect to time.

2.8 Unsaturated Soil Properties

Unlike saturated soils, which are two-phase soil systems, unsaturated soils have multiphase systems composed of three phases consisting of solid (soil particles), liquid (water), and gas (air). The air-water interface, which is commonly referred to as the contractile skin, has been postulated as the additional fourth phase of unsaturated soil (Fredlund et al. 2012). The soil above the groundwater table is named as an unsaturated soil. The total energy of water in the soil governs the interaction between water and soil particles. The energy was developed by the difference in pressure. The pressure in a soil considered to be positive when soils are saturated below a water table, whereas the pressure in the soil considered to be negative above the water table. This negative pressure is commonly known as suction.

In the early 1900s, the concept of soil suction was developed in soil physics (Edlefsen and Anderson 1943). Soil suction is quantified in terms of relative humidity and commonly referred to as total suction. Total suction consists of two components: osmotic suction and matric suction. Matric suction is associated with the capillary phenomenon arising from the surface tension of water, while osmotic suction is related to the presence of dissolved salts in a soil (Fredlund et al. 2012). In the field, the change in osmotic suction is relatively less significant as compared with the change in matric suction (Krahn and Fredlund 1972). Besides, most engineering problems in unsaturated soil are solved only using the matric suction

component. The relationship between total suction and its components can be expressed as follows:

$$\Psi = (u_a - u_w) + \Psi_{\Pi} \tag{2.22}$$

where Ψ is the total suction (L), ($u_a - u_w$) is the matric suction (L), u_a is the pore-air pressure (L), u_w is the pore-water pressure (L), Ψ_{Π} = osmotic suction.

Aitchison (1965) defined matric suction as "the equivalent suction derived from the measurement of the partial pressure of the water vapor in equilibrium with the soil water, relative to the partial pressure of the water vapor in equilibrium with a solution identical in composition with the soil water." Alternatively, matric suction can be thought of as the difference between the pore-air pressure (u_a) and the pore-water pressure (u_w) that act across the contractile skin (Aitchison 1965; Fredlund et al. 2012). The pores in the soil are like a bundle of capillary tubes of different sizes. The capillary effects cause the water to rise above the water table just like in a capillary tube; the smaller the radius of the tube generated, the higher the water rises above the water table.

The soil-water characteristic curve (SWCC) is a graphical representation of the relationship between the amount of water in soil (i.e., the degree of saturation (S), volumetric water content (θ_w) or gravimetric water content (w) and the soil suction. SWCC contains the fundamental information required for describing the mechanical behavior of unsaturated soil, such as the hydraulic conductivity function of unsaturated soils. Fredlund et al. (2012) showed that the estimation procedures for obtaining unsaturated soil properties are inexact but are generally satisfactory for analyzing unsaturated soil mechanics problems. As a result, the hydraulic conductivity is commonly estimated from SWCC instead of being measured directly because the direct measurement is time-consuming and costly.

The typical shape of SWCC is a sigmoidal curve where the water content of the soil decreases when the matric suction increases following the drying curve, and water content increase when matric suction decreases. A typical SWCC for a drying soil for the entire range of suction (i.e., from saturated to dry condition) of 0 to 1,000,000 kPa is shown in Figure 2 - 9. The curve can be divided into three zones, namely (i) the boundary effect zone, also known as the capillary zone, (ii) the transition zone is also known as desaturation zone, and (iii) the residual zone.

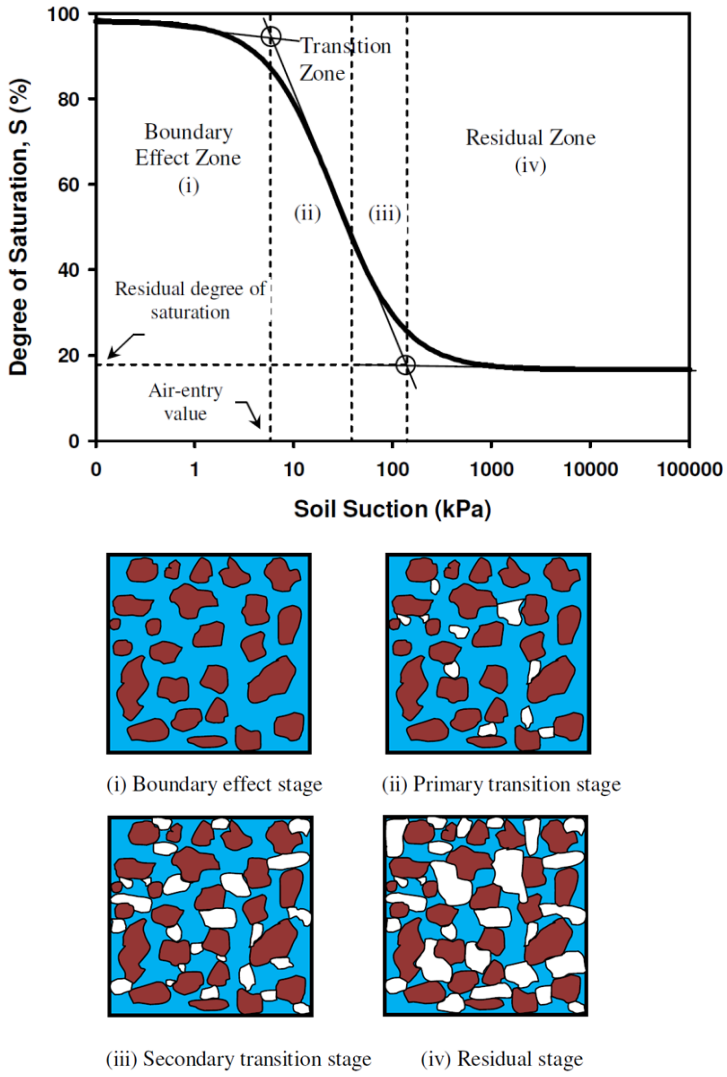

Figure 2 - 9 Typical SWCC and physical representation of air-water-solid interaction (Fredlund et al. 2012)

In the boundary effect zone, the water phase is continuous within the soil pores, although desaturation exerts tension on the water while soil suction is increasing. As the suction keeps increasing, at a specific suction value, air replaces water from the largest pore in the soil matrix. This particular suction value is known as the air-entry value or bubbling pressure of the soil, ψ_a.

Any increase in suction contributes to a significant decrease in water content or degree of saturation beyond the air- entry value (i.e., starting point of the primary transition zone). As desaturation continues in the transition zone (i.e., from primary to secondary transition zone), the area of water in contact with the soil particles decreases, and the continuous water paths are blocked with air (Figure 2 - 9). Finally, in the residual zone, water content, w, degree of saturation, S, or volumetric water content, θ decreases are small despite significant increases in suction values. The amount of water retained within the pore space in this residual state is referred to as the residual water content (w_r), residual volumetric water content (θ_r), or the

residual degree of saturation (S_r). The slope of the SWCC indicates how much water retained in the soil for a given pressure change. The slope can be very mild or very steep, depending on the pore-size distribution of the soil (Fredlund and Xing 1994).

2.9 Contaminant Transport in Soil

There are three fundamental mechanisms for contaminant transport in the: advection, diffusion, and dispersion. In this thesis, it is considered the solutes transport dissolved in water, and only a single-phase flow case. The contaminant transport equation derives by considering the mass flux q in a porous material, as illustrated in Figure 2 - 10, the absolute net mass flux across the element is = $(\partial q/\partial x)\, dx$ (GEO-SLOPE International Ltd. 2008).

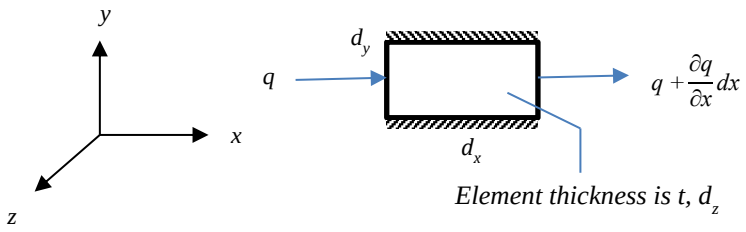

Figure 2 - 10 Mass balance in porous one-dimensional element

The first step in the development of differential equations for the transport of solutes in porous media is to consider the flux of solute into and out of a fixed elemental volume as the seen figure above. Conservation of mass can be written for the fixed elemental volume in Figure 2 - 10 (Freeze and Cherry 1979).

$$\begin{bmatrix} Net\ change\ of \\ mass\ of\ solute \\ within\ the\ element \end{bmatrix} = \begin{bmatrix} Flux\ of \\ solute\ out \\ of\ the\ element \end{bmatrix} - \begin{bmatrix} Flux\ of \\ solute\ into \\ the\ element \end{bmatrix} \pm \begin{bmatrix} Loss\ or\ gain \\ of\ solute\ mass \\ due\ to\ reaction \end{bmatrix} \quad (2.23)$$

The processes that control the flux into and out of the elemental volume are advection, diffusion, and dispersion. Loss or gain of solute mass in the elemental volume can occur as a result of chemical or biochemical reactions or radioactive decay (Freeze and Cherry 1979). A mass concentration, C is the mass of solute dissolved in a unit volume of solution, which is shown in equation (2.24). The SI unit for concentration quantity is kilograms per cubic meter (kg/m^3), or grams per liter (g/L) is commonly used.

$$C = \frac{M}{V_W} \quad (2.24)$$

where C is mass concentration, M mass of dissolved solute, V_w volume of water. The above equation can also be written as:

$$M = C \times V_W \tag{2.25}$$

The volume of water per unit volume of the element is the volumetric water content, θ as mentioned in section 2.7. The mass, M per total unit volume then is:

$$M = C \times \theta \tag{2.26}$$

2.9.1 Contaminant Transport by Advection

Advection is defined as the process by which pollutants are transported along with the flowing fluid. The mass flux of dissolved contaminants that are being transported depends on its concentration in fluid and on the quantity of water velocity. Due to advection, non-reactive solutes are carried at an average rate equal to the seepage velocity of the fluid. For saturated flow, the seepage and Darcy velocity can be associated with the concentration C; and the advective mass flux is calculated by:

$$J_{advection} = \frac{M}{At} = \frac{M}{V}\,\frac{x}{t} = C\,v = n\,v_s\,C \tag{2.27}$$

where $J_{advection}$, is the advective mass flow, A is the total cross-sectional area perpendicular to the flow, t is the increment of time, and x is the distance traveled by the contaminant during t time, n is the porosity of soil and v_s is the seepage velocity of the fluid. By considering Figure 2 -10, the governing differential equation is:

$$\frac{\partial C}{\partial t} = - \; v_s \frac{\partial C}{\partial x} \tag{2.28}$$

2.9.2 Contaminant Transport by Diffusion

Transportation by advection is associated with the water movement; however, diffusion is based on the change in concentration due to a chemical gradient. A solute in water will move from an area of higher concentration toward an area where it is less concentrated. Because of that, the diffusion will occur as long as a concentration gradient exists, even if the fluid is not moving. It can be expressed as Fick's first law; in one dimension, Fick's first law is:

$$J_{diffusion} = - \; n \, D^* \frac{\partial C}{\partial x} \tag{2.29}$$

where $J_{diffusion}$ is the diffusive mass flux, and D^* is the effective diffusion coefficient. Equation (2.29) represents the one-dimensional form of Fick's first law describing diffusion in aqueous (i.e., no porous material). For diffusion in a saturated porous material, a modified form of Fick's first law is used (Daniel 1993). The values of D^* do not change significantly, and they vary 1 x 10^{-9} to 2 x 10^{-9} m/s (Sharma and Reddy 2004). The D* also related to the tortuosity factor (τ) and self-diffusion coefficients (D_0) of the chemicals as below:

$$D^* = \tau \, D_0 \tag{2.30}$$

The tortuosity factor accounts for the increased distance of transport and the more tortuous pathways experienced by solutes diffusing through porous media. Tortuosity is expressed as

$$\tau = \left(\frac{L}{L_e} \right)^2 \tag{2.31}$$

where L is the straight-line distance between two points defining the flow path, and L_e is the actual, effective distance of transport between the same two points (Freeze and Cherry 1979; Daniel and Shackelford 1988; Daniel 1993). τ is a dimensionless tortuosity factor, approximately ranging from 0.3 to ~0.7 for most soils (Van Genuchten, and Wierenga 1986). By using Fick's first law and continuity equation, the rate at which contaminants can diffuse in the soil can be given by equation (2.32), and this equation is known as Fick's second law.

$$\frac{\partial C}{\partial t} = D^* \frac{\partial^2 C}{\partial x^2} \tag{2.32}$$

2.9.3 Contaminant Transport by Dispersion

The dispersion mechanism is associated with fluid movement in the porous medium. Fluid particles that are at one time close together tend to move spread. The spreading nature of pollutants is attributed to variations in seepage velocity. Mechanical dispersion is the transport of a solute resulting from minor differences in groundwater velocity as it flows through heterogeneous porous media (Duriez 2005). When solutes in fluid come across with clean water that does not contain a solute, mixing occurs along the flow path, resulting in a dilution of the solute at the advancing edge of the flow. The mixing occurs along the direction of the flow path

is called longitudinal dispersion. However, the contaminant will spread in directions normal to the flow path, and it is named as transverse dispersion, which is the mixing in directions normal to the flow path. Assuming that mechanical dispersion follows Fick's law for diffusion and that the amount of both longitudinal dispersion, $D_{L,}$ and transverse dispersion, D_T are a function of the average linear velocity. The longitudinal dispersion and transverse dispersion are defined by:

$$D_L = \alpha_L \, v_s \tag{2.33}$$

$$D_T = \alpha_T \, v_s \tag{2.34}$$

where D_L is the longitudinal mechanical dispersion [$L^2.T^{-1}$], D_T is the transverse mechanical dispersion [$L^2.T^{-1}$], α_L is the longitudinal dispersivity [L], α_T is the transverse dispersivity [L], v_s is the average seepage velocity in the principal direction of flow [$L.T^{-1}$]. Generally, a combination of diffusion and mechanical dispersion is used in the equations and it is named as hydrodynamic dispersion coefficient are defined as follows:

$$D_L^* = \alpha_L \, v_s + D^* \tag{2.35}$$

$$D_T^* = \alpha_T \, v_s + D^* \tag{2.36}$$

where D_L^* is the longitudinal hydrodynamic dispersion coefficient [$L^2.T^{-1}$], D_T^* is the transverse hydrodynamic dispersion coefficient [$L^2.T^{-1}$]. Macroscopically, the dispersion process is similar to the diffusion process; however, unlike diffusion, it occurs only during water movement. Field and laboratory experiments have shown that the one-dimensional dispersive transport can be described by an equation similar to diffusion as follows:

$$J_{dispersion} = - \, n \, D_L \, \frac{\partial C}{\partial x} \tag{2.37}$$

2.9.4 Chemical Reaction Processes

Advection, diffusion and dispersion simply relocate the mass of dissolved contaminants within the soil media. Neither of these processes considers changing the amount of contaminant in by chemical and biological processes in the soil media. By these processes, the contaminant may alter by transforming the solute to another form, moving the solute from the liquid

(groundwater) to solid phase (aquifer material) or degrading (Duriez 2005). Chemical and biological reaction processes include many different types; however, during the numerical analysis of this study, decay or other processes do not be considered.

One of the main chemical processes is the sorption and desorption. The sorption may occur when the contaminant becomes attached to the surface of the soil particles. Desorption is the process by which the contaminant gets detached from the surface of the particle (Bedient et al. 1999). An empirical equation of sorption is related to the mass of contaminant sorbed per unit dry mass of soil S (e.g., mg/kg or ppm) to the concentration of contaminant in solution at equilibrium C (e.g., mg/L). Sorption is affecting the real velocity of the contaminants since the solutes will move more slowly. A retardation coefficient R_d (larger than 1) then links the seepage velocity v_s, to the actual contaminant velocity. If the R_d is 1, the actual contaminant velocity is equal to the seepage velocity.

Biodegradation is another process that may be occurred when a contaminant is completely converted to mineralized end products (i.e.CO_2, H_2O, and salts) through metabolism by living organisms. It may be aerobic or anaerobic. The aerobic biodegradation takes place in the presence of oxygen, which acts as an electron acceptor from the substance; on the other hand, the anaerobic biodegradation takes place in the absence of oxygen. Some microorganisms naturally occurring in soil have the remarkable ability to degrade and transform many compounds, including hydrocarbons, polychlorinated biphenyls, polyaromatic hydrocarbons, pharmaceutical substances, radionuclides, and metals. However, for degradation to take place, the microorganism must be matched to the contaminant to be degraded (Bedient et al. 1999).

2.9.5 Transport Equation

The equation governing transport is obtained from the derivation of the advection, diffusion, and dispersion equation. This derivation is based on the law of conservation of mass of contaminants (Figure 2 -10). In this derivation, the calculation is solved for homogeneous, isotropic, and Darcy's law applies. The governing differential equation is presented only in terms of one-dimensional transport. The total mass of contaminant per unit volume of soil C_T is:

$$C_T = \rho_d C_s + \theta_w C_w + \theta_g C_g \tag{2.38}$$

where ρ_d is the dry density of the soil [$M.T^{-3}$], C_s is the concentration of contaminant in the solid phase, θ_w is the volumetric water content (volume of water over the volume of soil), C_w is the concentration of contaminant in the liquid phase [$M.T^{-3}$], θ_g is the volumetric gas content

(volume of air over volume of soil), and *Cg* is the concentration of contaminant in the gas phase [M.T^{-3}]. At saturated flow, θ_g is zero, θ_w is equal to the porosity *n*, and equation (2.38) becomes:

$$C_T = \rho_d C_s + n\, C_w \tag{2.39}$$

The contaminant mass flux due to advection, diffusion, and dispersion can be calculated combining the equation (2.26), (2.27) and (2.37):

$$\begin{aligned} J_{Total} &= J_{advection} + J_{diffusion} + J_{dispersion} \\ &= n\, v_s\, C_w - n\, D^* \frac{\partial C_w}{\partial x} - n\, D_L \frac{\partial C_w}{\partial x} \end{aligned} \tag{2.40}$$

By considering the conservation of mass, the change in concentration of mass of contaminant with time has to be equal to the slope of the curve describing the flux vs. distance along the flow path:

$$\begin{aligned} \frac{\partial C_T}{dt} &= -\frac{\partial F_T}{dx} \\ \frac{\partial(\rho_d C_s)}{\partial t} + \frac{\partial (n\, C_w)}{\partial t} &= -\frac{\partial}{\partial x}\left(n\, v_s\, C_w - \left(n\, D^* + n\, \alpha_L\, v_s\right) \frac{\partial C_w}{\partial x} \right) \pm S \end{aligned} \tag{2.41}$$

S is also included in the equation for any sources or sinks of contaminants, due to chemical reactions. The partition coefficient K_d is defined as:

$$K_d = -\frac{C_s}{C_w} \tag{2.42}$$

If the sources and sinks are ignored, the below equation is obtained:

$$\frac{\partial C_w}{\partial t} = -\frac{v_s}{\left(\frac{\rho_d K_d + n}{n}\right)} \frac{\partial C_w}{\partial x} + \frac{\left(D^* + \alpha_L\, v_s\right)}{\left(\frac{\rho_d K_d + n}{n}\right)} \frac{\partial^2 C_w}{\partial x^2} \tag{2.43}$$

After setting the retardation factor, R_d, and D_L^*:

$$R_d = \left(\frac{\rho_d K_d + n}{n}\right) = \frac{\rho_d K_d}{n} + 1 \tag{2.44}$$

The general differential equation for the contaminant transport can be obtained (Freeze and Cherry 1979; Briaud 2013):

$$\frac{\partial C_w}{\partial t} = -\frac{v_s}{R_d}\frac{\partial C_w}{\partial x} + \frac{D_L^*}{R_d} \frac{\partial^2 C_w}{\partial x^2} \tag{2.45}$$

CHAPTER 3: CAPILLARY BARRIER SYSTEM

3.1 General Remarks

This chapter is divided into two parts, as follows. The first part gives information about the soils which were used in the research. The details of the experiment for calculating index properties, hydraulic properties, and unsaturated soil properties of soils were explained. Also, the obtained results are represented and discussed.

The second part focuses on the infiltration box test for the capillary barrier system. The objective of the infiltration box test is to experimentally investigate the applicability of the capillary barrier for the utilization of geogenic contaminated soil in the embankment. During the testing, six different cases were constructed with a slope of 26.6 degrees. They were tested under different soil configurations, rainfall rates, and rainfall durations. At the end of the chapter, the obtained results are represented, and an overall conclusion is summed up.

3.2 Materials and Methods

3.2.1 Soils Used in the Experiments

In the experiment, three different soils were used. They were named and nominated as: poorly graded medium sand (MS), poorly graded coarse silica sand (SS), and poorly graded gravel (GP). Figure 3 -1 shows photos of the soils which were used in the research. Although this research is conducted for the utilization of geogenic contaminated soils, at the experimental stage, uncontaminated soils were used. Since the study focuses on water interception performance rather than contaminant transport. It is aimed to control the amount of water that may contact the geogenic contaminated soil with suitable design considerations.

3.2.2 Geotechnical Properties of Soil

Investigation of basic geotechnical properties involves grain-size distributions, specific gravity tests, compaction tests, relative density tests, and saturated permeability tests. The grain-size distributions were performed according to ASTM D422. The measurements of soil specific gravity were performed following JGS 0111. The soils were classified based on the unified soil classification system (USCS) following ASTM D2487. The particle size distribution of used soils was shown in Figure 3 - 2.

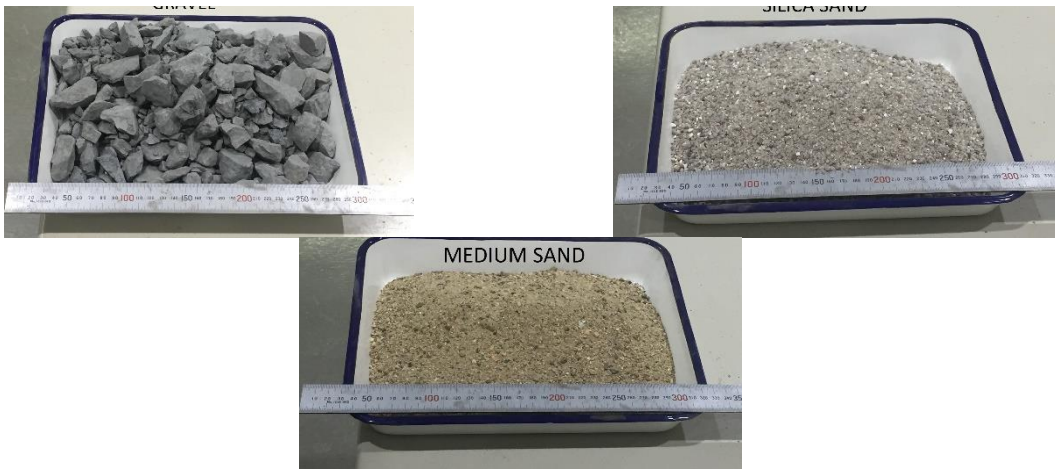

Figure 3 - 1 Soil used in the experiments

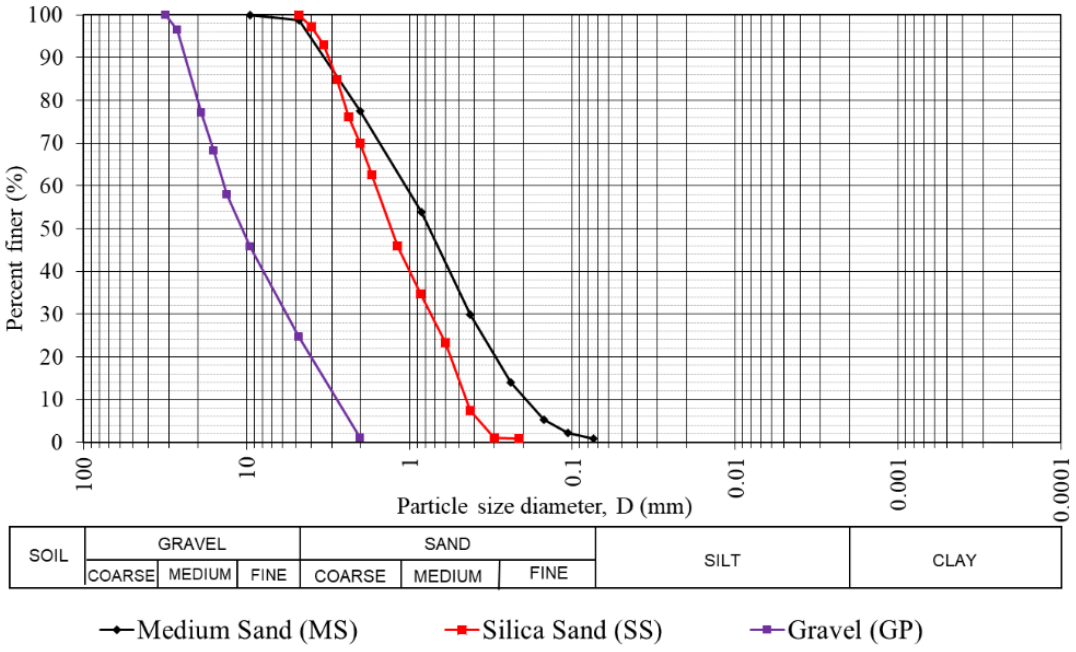

Figure 3 - 2 Grain size distribution curves for soils

The soils used in this study were classified as poorly graded medium sand (MS), poorly graded coarse silica sand (SS), and poorly graded gravel (GP). MS, SS, and GP have approximately 1% passing the #200 sieve. These properties indicate that MS nominates as “SP”, SS nominates as “SP”, and GP nominates as “GP” according to the Unified Soil Classification System (USCS). The specific gravity of MS, SS, and GP were determined to be 2.65, 2.66, and 2.76, respectively. Table 3 - 1 shows the geotechnical properties of used soils.

The compaction curve for medium soil (MS) was obtained using standard Proctor compaction effort, with procedures described in ASTM D 698. The standard Proctor

compaction curve is shown in Figure 3 -3. The optimum gravimetric water content at compaction is referred to as (w_{opt}), and it is approximately 15%, and the maximum dry density (γ_{dmax}) is 18 kN/m^3.

The saturated hydraulic conductivities of the soils were determined by applying a constant head in a sample of saturated soil and measuring the consequent rate of flow following JGS 0311. This method is applicable to coarse-grained soils, and it is used to measure one-dimensional flow. Once the soil specimen was saturated, a hydraulic gradient was applied. The gradient initiated water flow from the bottom of the specimen. The water could drain until a steady-state water flow was achieved, after which the outflow was measured over an interval of time. The test was conducted under at least three different trials, and the saturated hydraulic conductivities of the soil determined as an average value. The obtained saturated hydraulic conductivities are illustrated in Table 3 - 1.

Table 3 - 1 Geotechnical properties of soils used in the research

Parameter	**Medium Sand (MS)**	**Silica Sand (SS)**	**Gravel (GP)**
Gravel (%)	1	2	75
Sand (%)	98	97	24
Silt &Clay (%)	1	1	1
C_u	5.8	3.6	4.4
C_c	0.8	0.7	0.7
USCS	SP	SP	GP
Solid unit weight (kN/m^3)	26.5	26.6	27.6
Saturated hydraulic conductivity (m/sec)	1.14 x 10^{-4}	4.08 x 10^{-4}	1.17 x 10^{-2}
Preparation unit weight (kN/m^3)	18.0	16.5	16.75
Optimum water con. (%)	15.0	-	
Max. dry unit weight (kN/m^3)	18.0	-	
Maximum void ratio (e_{max})	-	0.823	
Minimum void ratio (e_{min})	-	0.557	

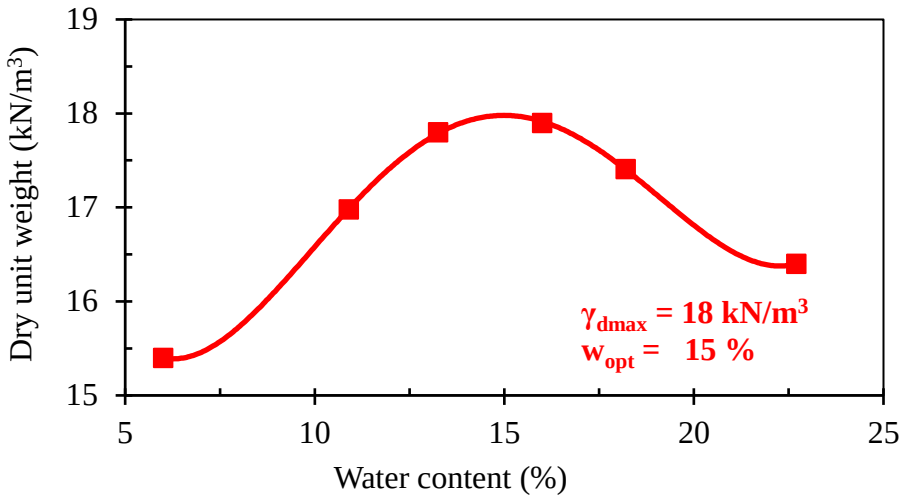

Figure 3 - 3 Compaction curve for medium sand (MS)

3.2.3 Drying Soil Water Characteristic Curve (SWCC) Measurement

In the present research, the axis-translation technique was used for the direct measurement of SWCC. The axis translation technique relies on the use of high-air entry (HAE) materials to measure matric suction. HAE materials consist of relatively uniform microscopic pores (Hilf, 1956). Once these pores are filled with water and the ceramic material is saturated, contractile skin, which is a phase between air and water, is formed due to the influence of surface tension. This phase separates the air and water phases and resists the flow of air but allows free movement of water through the pores if the HAE materials pores are saturated. The maximum pressure that can be resisted by the surface tension offering resistance for air to pass through the saturated pores is referred to as the air-entry value of the HAE material. The air-entry value is inversely proportional to the pore size and can be estimated using the principle of capillary forces equation. The axis-translation technique is generally performed by using a high air entry ceramic disk. The procedure has been accepted in unsaturated soil mechanics, agriculture-related disciplines, soil science, and soil physics (Yano et al. 2010; Nishiumura et al. 2011).

However, in this research, microporous membranes are used instead of ceramic disks for reducing the testing time. Measurements of the SWCC were conducted using a modified pressure chamber apparatus with a microporous membrane. The microporous membranes used in this study were manufactured by Toyo Roshi Corporation. It is a mixed cellulose ester, and the grade number is A100A142C.

The modified SWCC apparatus is shown in Figure 3 - 4. It consists of a pedestal, a steel mold, a pressure chamber, and a water collector that is connected to a data logger system. Both the pedestal and the steel mold are placed in a chamber. A water compartment is located below the porous stone. The drained water from the sample is collected in the compartment and

directed to the water collector with a tube system. A differential pressure transducer was attached to the chamber. During the testing period, the reading of drained water and the applied pressure are recorded with the data logger system.

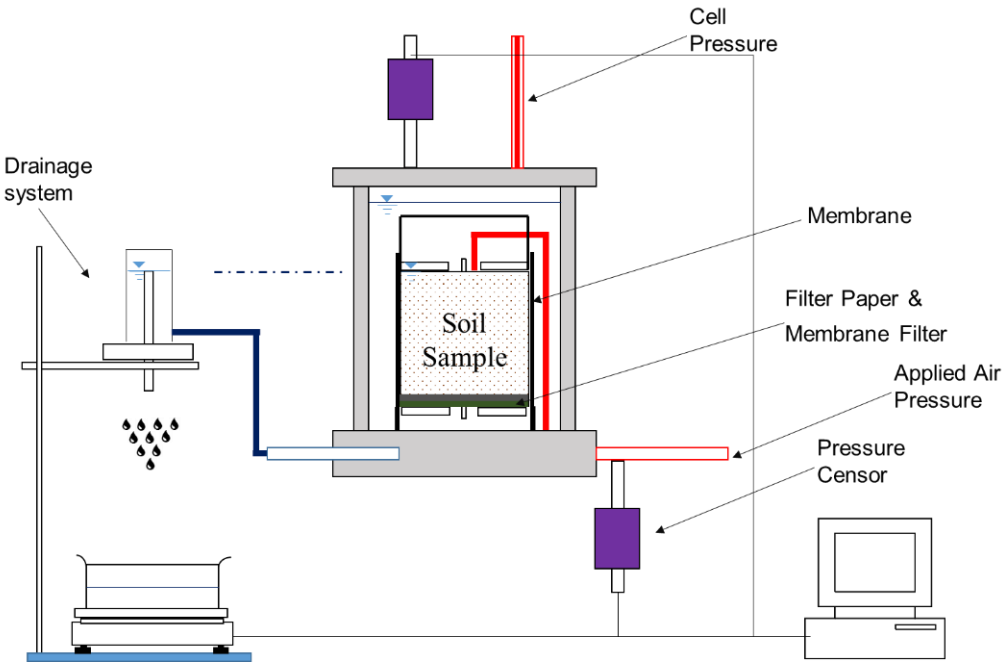

Figure 3 - 4 Illustration of the modified pressure chamber test

The drying SWCC of the soils was determined using the modified pressure chamber test. During the testing period, a required amount of oven-dried soil was placed on the testing mold and compacted with a target density that was the same with other experiments. The GP soil specimen was prepared with a diameter of 150 mm and 150 mm in height. However, the MS and SS samples were prepared 150 mm diameter and 100 mm in height. Different specimen height is selected to shorten the experiment duration. Moreover, long specimen height is considered to generate a high suction difference at the top and bottom of the sample, especially for sandy soils. The prepared specimen was connected to a suction pump inside a chamber for making sample saturated (Figure 3 - 5). After saturation, the specimen was frozen. The frozen sample was in the experiment chamber. Filter papers were placed at the top and bottom of the specimen. The HAE microporous membrane was placed only at the bottom of the specimen to resists the flow of air but allowed the free flow of water. The sample was then enclosed in a rubber membrane, which is slid over the specimen. The membrane was sealed to the specimen with O-rings. The chamber was placed over the base and fixed to it by tightening the nuts. Then, it was then filled with water. The pressure was applied to the water as a cell pressure (20 kPa) in order not to dispense of the sample. After that, without opening any valves, the free melting of the specimen was being waited (more than one day). As soon as the valves are opened, the consolidation of the specimen started. The specimen is connected to the water collector for the

measurement of volume changes. The consolidation is complete when there is no more volume change (no more drained water). When the consolidation is complete, the specimen is ready for applying negative water pressure (matric suction). At the beginning of the test, the matric suction was applied by decreasing the outlet exit head. This method is applied for obtaining the exact air-entry value of the specimen. After the air-entry value, higher matric suction pressure was applied using a pressure system. During the testing period, the cell pressure, the applied matric suction, and the amount of the drained water were continuously recorded with a data logger (Yano et al. 2010). The on-going experiment of the modified pressure chamber test is shown in Figure 3 – 5.

3.2.3.1 Estimation Soil Water Characteristic Curves

Several equations have been proposed to establish the SWCC functions. One of the equations that have been widely used was offered by van Genuchten (1980). It has an empirical relationship between matric suction and volumetric water content. The equation was used to fit the experimentally obtained data and estimated the drying SWCC (Figure 3 – 6, Figure 3 – 7, and 3 – 8). The van Genuchten (1980) equation is selected for its differentiable features (without sharp curves) even in the vicinity of the air-entry suction. It is given by:

$$\Theta = \frac{\theta - \theta_r}{\theta_s - \theta_r} = \frac{1}{\left[1+\left(\frac{\psi}{a}\right)^n\right]^m} \tag{3.1}$$

where a (has units of pressure, not 1/pressure head as in some formulations of this equation), n, m are curve fitting parameters (van Genuchten 1980).

The drying water characteristic curves of materials obtained from the modified pressure chamber tests along with van Genuchten (1980) equation best fitting curve are presented in Figure 3 – 6, Figure 3 – 7, and Figure 3 – 8, for medium sand (MS), silica sand (SS) and gravel (GP), respectively. The fitting was performed using the Microsoft Excel nonlinear equation solver tool and, then, key parameters of the SWCC (θ_s, θ_r, a, and n) were obtained using the least square method. The MS, SS, and GP drying SWCC best-fit parameters are presented in Table 3-2. The slope of the SWCC for the silica sand (Figure 3 - 7) has a steeper curve compared to the other material. This is considered to depend on the poorly graded gradation curve of the material. Because of that, the transition zone of the silica sand SWCC disappeared quicker than the other soils.

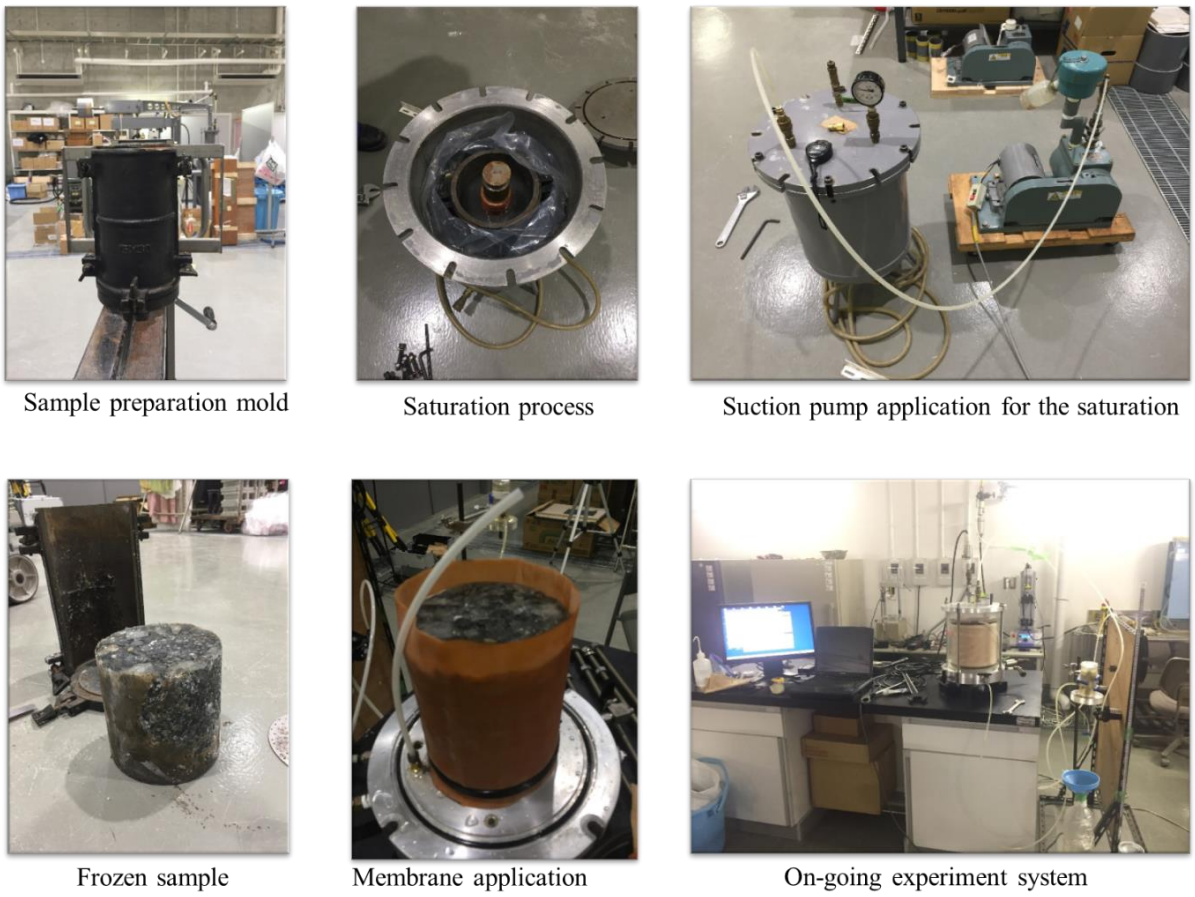

Figure 3 - 5 Experiment procedure of modified pressure chambers test

Table 3 - 2 Estimated van Genuchten parameters for soils

Parameter	Medium Sand (MS)	Silica Sand (SS)	Gravel (GP)
θ_s (m^3/m^3)	0.322	0.357	0.387
θ_r (m^3/m^3)	0.077	0.059	0.008
α (1/mm)	0.007	0.005	0.083
n	2.488	5.430	1.803
m	0.598	0.816	0.445

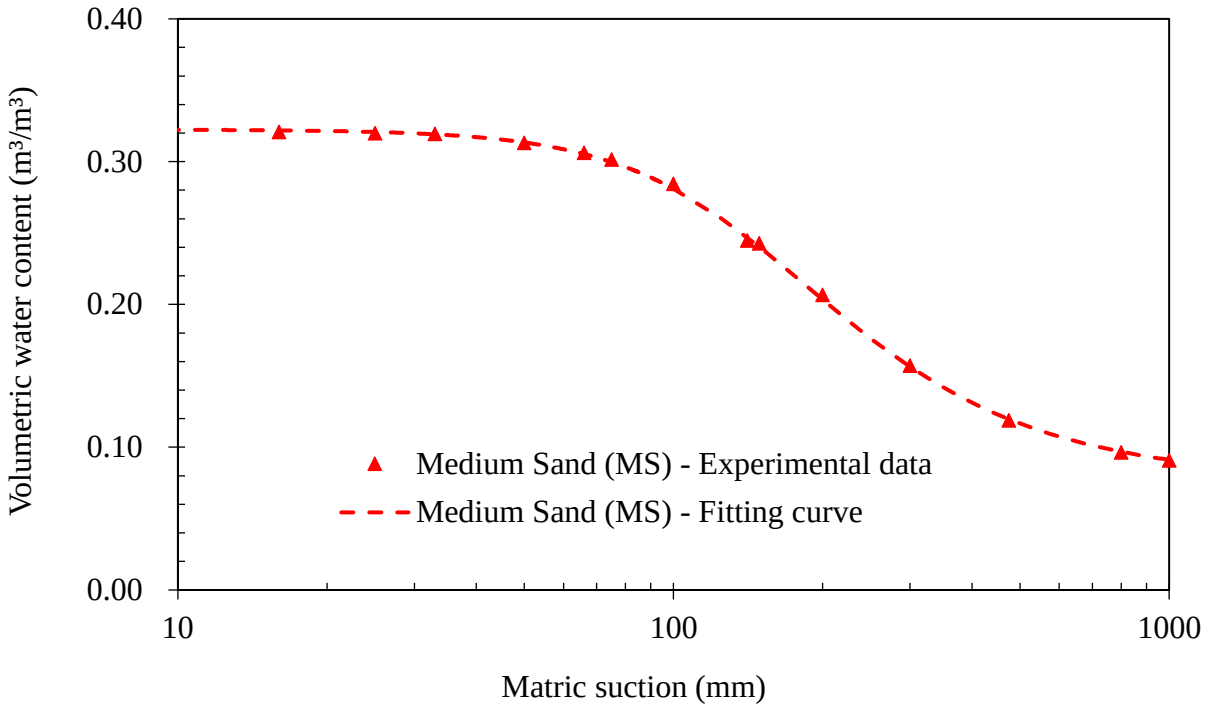

Figure 3 - 6 SWCC for medium sand (MS)

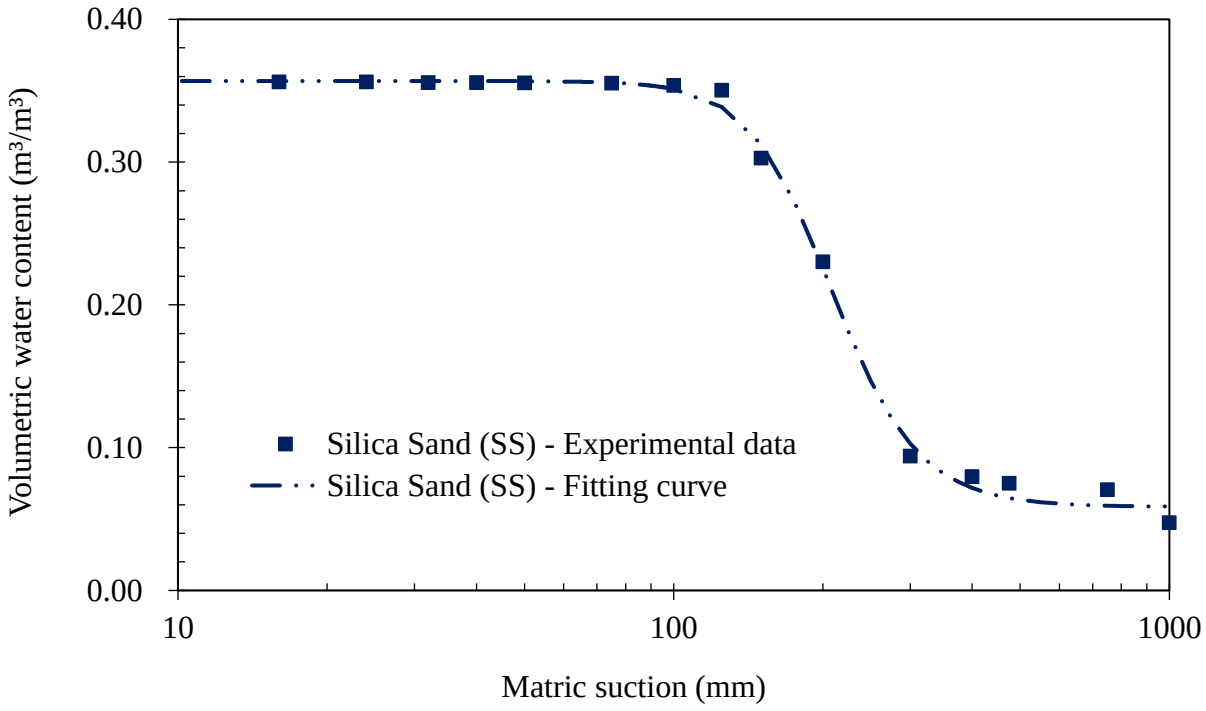

Figure 3 - 7 SWCC for silica sand (SS)

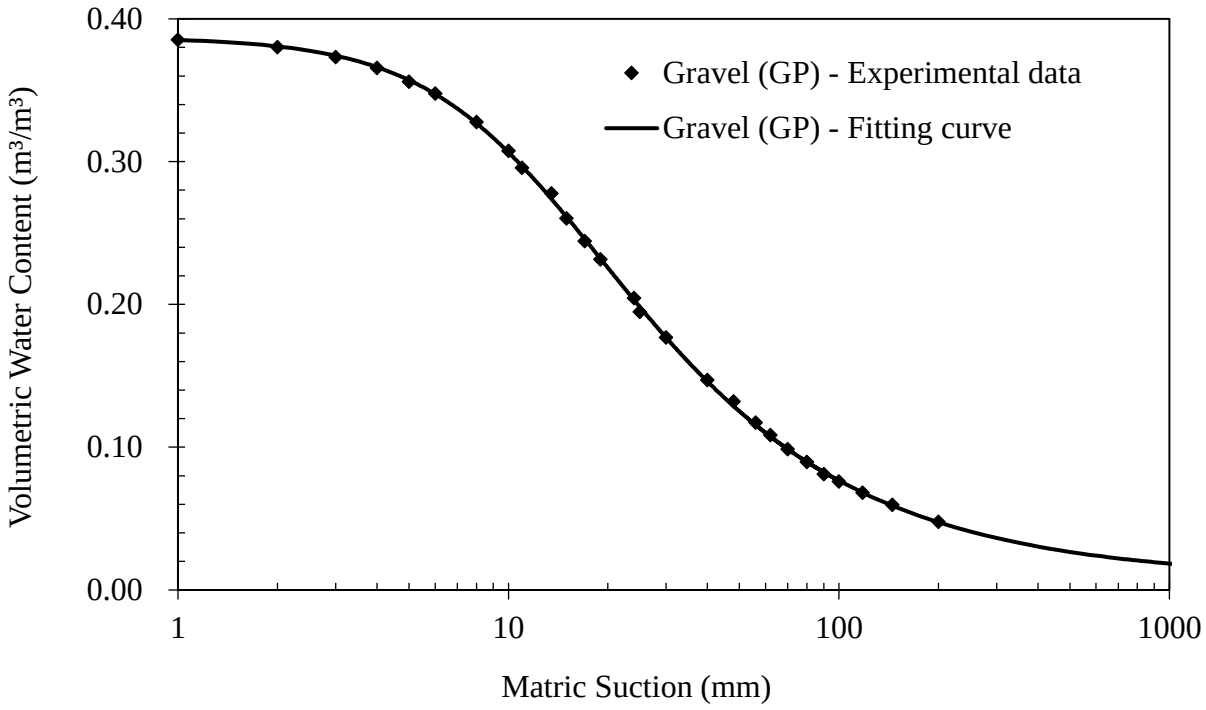

Figure 3 - 8 SWCC for gravel (GP)

3.2.3.2 Estimation of Unsaturated Hydraulic Conductivity

Unlike saturated soils, the available pathways for water flow in unsaturated soil decrease as the moisture content reduces. This is quantified by the hydraulic conductivity function $k(\theta)$, which accounts for the change in the ratio between flow rate and total hydraulic gradient with decreasing increasing suction.

The hydraulic conductivity of soil at low water content is very difficult to measure and may be equal to zero under the suctions below residual saturation. Either direct measurement or indirect measurement methods may be used for obtaining the hydraulic conductivity of unsaturated soil. Indirect measures of permeability are usually performed by establishing k-function ($k(\theta)$) based on the fact that it is a relatively unique function of the volumetric water content, which in turn, depends on the suction, i.e., either matric suction or total suction the soil.

Numerous empirical and statistical equations have been proposed to predict the permeability function for an unsaturated soil using the SWCC. In this study, the van Genuchten - Mualem permeability equation was used for predicting the k-function, shown in Figure 3 – 9. van Genuchten – Muallem model proposed the following closed-form equation to describe the hydraulic conductivity of soil as a function of matric suction shown in equation (3.2) (Mualem 1976). This equation shows that the fitting curve parameters can be estimated graphically based on the volumetric water content function of the soil. According to van Genuchten (1980), the

best point to evaluate the fitting curve parameters is the halfway point between the residual and saturated water content of the volumetric water content function.

$$\frac{k(\theta)}{k_{sat}} = \Theta^{1/2}(1-(1-\Theta^{n})^{m})^{2} \tag{3.2}$$

where Θ is the dimensionless water content, a, n, and m is the fitting parameters k_{sat} is the saturated hydraulic conductivity of the soil.

According to k-functions, near saturation, the coarser material (gavel, silica sand) have high hydraulic conductivity, while the finer material (medium sand) has low hydraulic conductivity. This can be explained using the shapes of the SWCC for these materials. The shapes of the k-functions are similar to their SWCC. The saturated permeability decreases after the air-entry value of the materials and becomes very small when the material becomes drier.

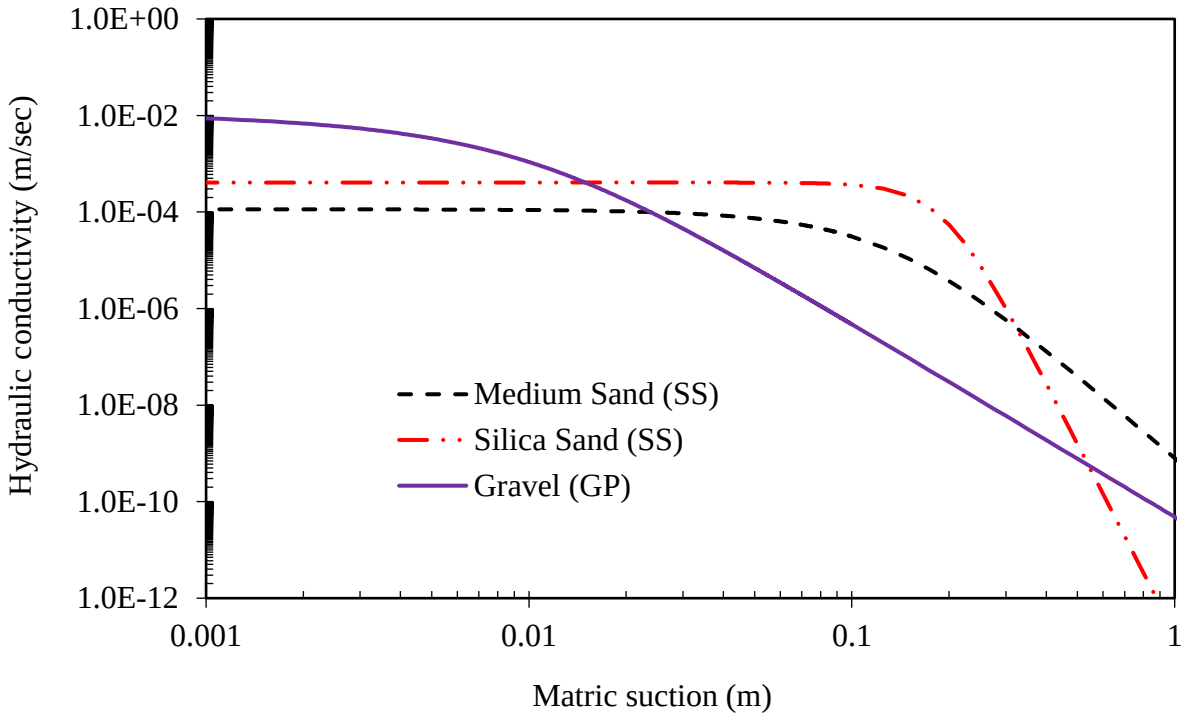

Figure 3 - 9 Hydraulic conductivity functions (k-functions) for soils

3.3 Laboratory Infiltration Box Test

An infiltration box test was designed to investigate the utilization of the naturally contaminated soils in the embankments using a capillary barrier system in a controlled environment. The apparatus was instrumented to capture the process of water flow in the capillary barrier system. The general setup of the model is presented in Figure 3 - 10. The main components of the physical model are the infiltration box, the rainfall system, the measuring devices, and the water

collection system. The box dimensions were 110 cm in length, 12 cm in width, and 60 m in height.

The infiltration box was fabricated in two parts: the acrylic box and the steel frame. Acrylic was chosen as the material for the box to be able to view the flow of water in the capillary barriers. The box was equipped with a suitable jacking system that could lift one side of the stainless-steel frame (high side) up to a height of 60 cm, which is equivalent to a 26.6°inclination angle (Figure 3 - 10).

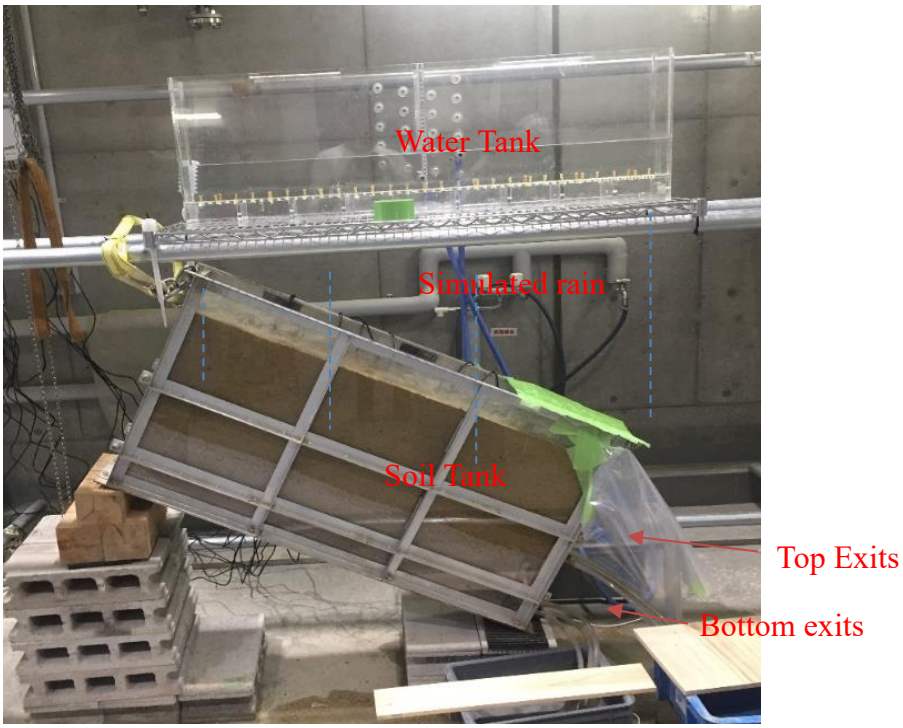

Figure 3 - 10 General view of the capillary barrier test system

3.3.1 Measuring devices and data acquisition system

Decagon Device-EC-5 was used to measure the saturation degrees of the soil. EC-5 determines the velocity of the electromagnetic pulse of energy transmitted into the soil through the transmission line, which consists of a coaxial cable and waveguides inserted into the soil. The velocity of the microwave pulse traveling in the soil is a measure of the apparent dielectric constant. The EC-5 in contact with surrounding material brings out a higher the dielectric constant readings and slower the velocity. Due to the great difference between the dielectric constant of water and other soil components, the travel velocity of the microwave pulse is highly dependent on the water content of the soil. By knowing the relationship of with dielectric constant to the volumetric water percentage, obtained values can then be converted to the volumetric water content of the soil. The EC-5 sensor has a length of 8.9 cm, and it is connected to a data logger (Decagon Device Em-50) for continuous reading.

Calibrations for sensors (EC-5) were conducted before starting the experiment for all soils used in the experiments. During the calibration, a standard procedure was followed. Firstly, dry soil was prepared. The necessary amount of soil was weighted according to the intended bulk density with water. Then, soil and water are mixed with a mixer (Figure 3 - 11). The prepared sample is placed in a container with a specific bulk density, and sensor reading is taken with the data acquisition system (Figure 3 - 11). After the sensor readings, the soil sample was dried, and the exact preparation saturation degree was calculated. These procedures were followed at the different saturation degrees, and changing of sensor readings were obtained. A simple scatter plot was made with the sensor output on the x-axis and the calculated saturation degrees on the y-axis. Then the curve fitting function was used to construct a mathematical relationship. This relationship is the calibration curve of the sensor. During this research, sensor, and soil specific calibration was obtained. This means that for nine different sensors, 27 different calibration curves were evaluated due to three different soil types. A typical sensor calibration equation is shown in Figure 3 - 12.

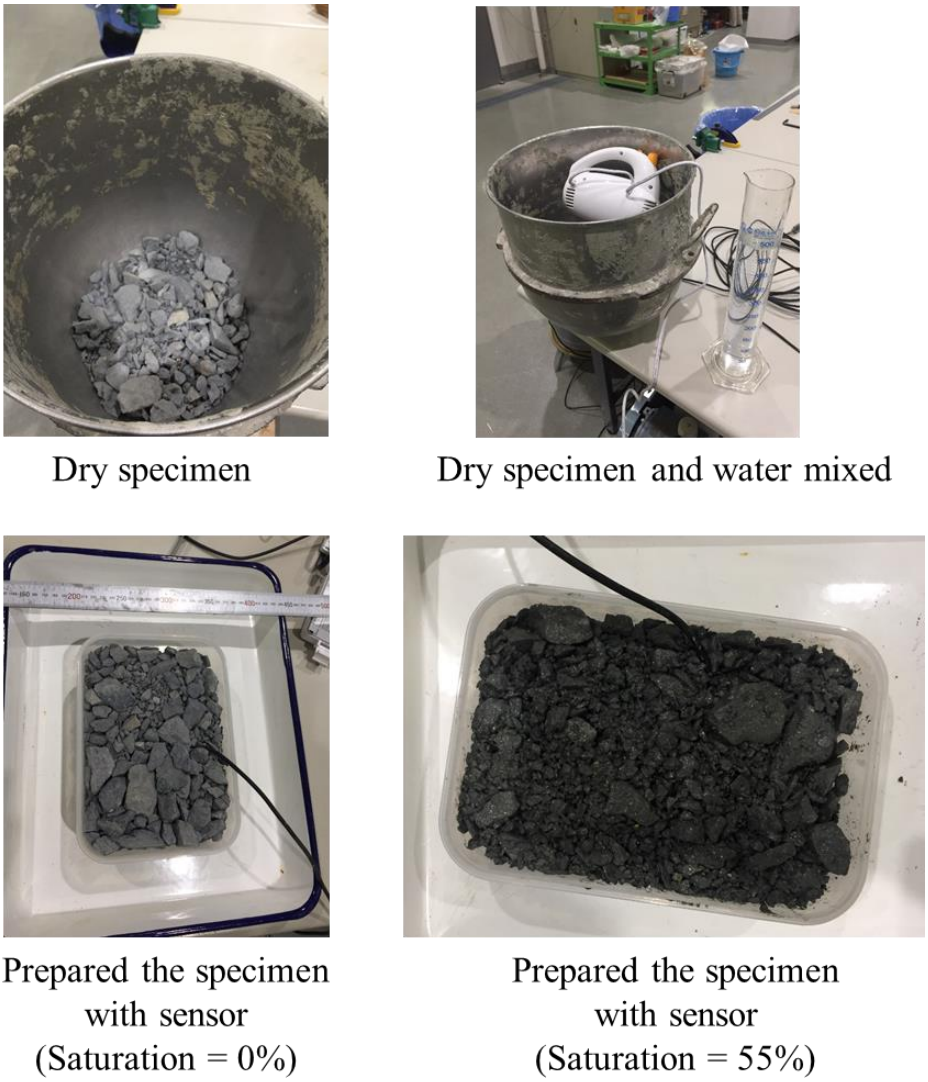

Figure 3 - 11 EC-5 moisture sensors calibration

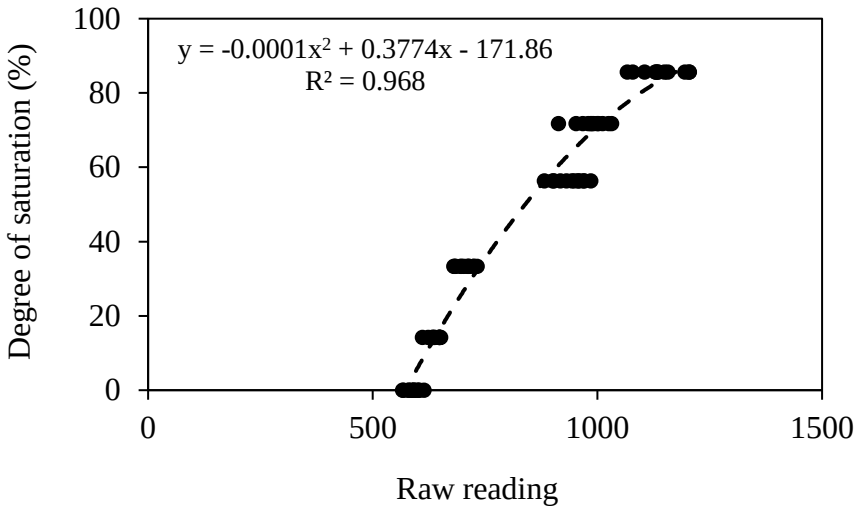

Figure 3 - 12 Typical moisture sensor calibration curve

3.3.2 Rainfall Application System

The rainfall application system consisted of inflow control, overflow discharge, and electronic weighing balance. The inflow control included a water storage tank, a constant head water tank, a pressure pump regulator, and a rainfall distribution system. The rainfall water was stored inside a tank. The stored water was directed to the constant head tank with a pump (MITSUGIRON BP-42). Water in the constant head tank steadily flowed into a rainfall distributor system. The rainfall distributor system was made of a needle arrangement (Figure 3 - 13). The needless were selected with a try before the experiment to obtain the intended rainfall rate.

Overflow discharge included a constant head water tank. Before starting the experiment, the rainfall rate calibration was conducted. During the calibration, the constant head tank height and rainfall rate relation were obtained, which is shown in Figure 3 – 14. During the tests, the rainfall was applied with a constant head height as 81 mm water. Above this height, overflow water was directed to the storage tank with a tube system. The desired rainfall was applied by changing the constant head tank height and the needle arrangement. The flow rate was calibrated before the tests. Although constant head tank and needle arrangements, the trials showed that the applied flow rates are changing with time. This problem might be caused by the temperature changing in the testing environment. The applied rainfall intensity was calculated as an average rainfall rate during the one-day duration before the test.

Figure 3 - 13 Arrangement of needle system for the rainfall application

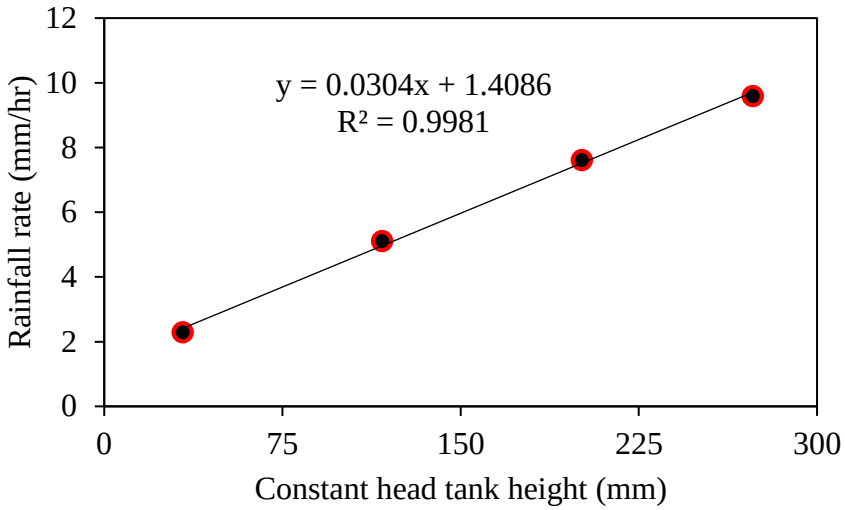

Figure 3 - 14 Calibration line for constant head tank height and rainfall rate

Two electronic weighing balance was used to measure the mass of percolated water from the box. The electronic weighing balance used in this study manufactured by AND model EK-12KGV with a capacity of 12 kg with a 1 g resolution. A digital data logger indicator model AD-1688 was connected to each weighing balance. The stored data were transfer to a personal computer.

The applied rainfall intensity was decided according to 72-hour cumulative precipitation amounts averaged over Japan's land. A rainfall intensity, which is higher than the maximum event, was selected. The maximum event occurred on 7th July 2018 with an amount of 173 mm per 72-hour (2.403 mm/hr), which was the highest since April 1988 (Figure 3 - 15) (Shimpo et al. 2019).

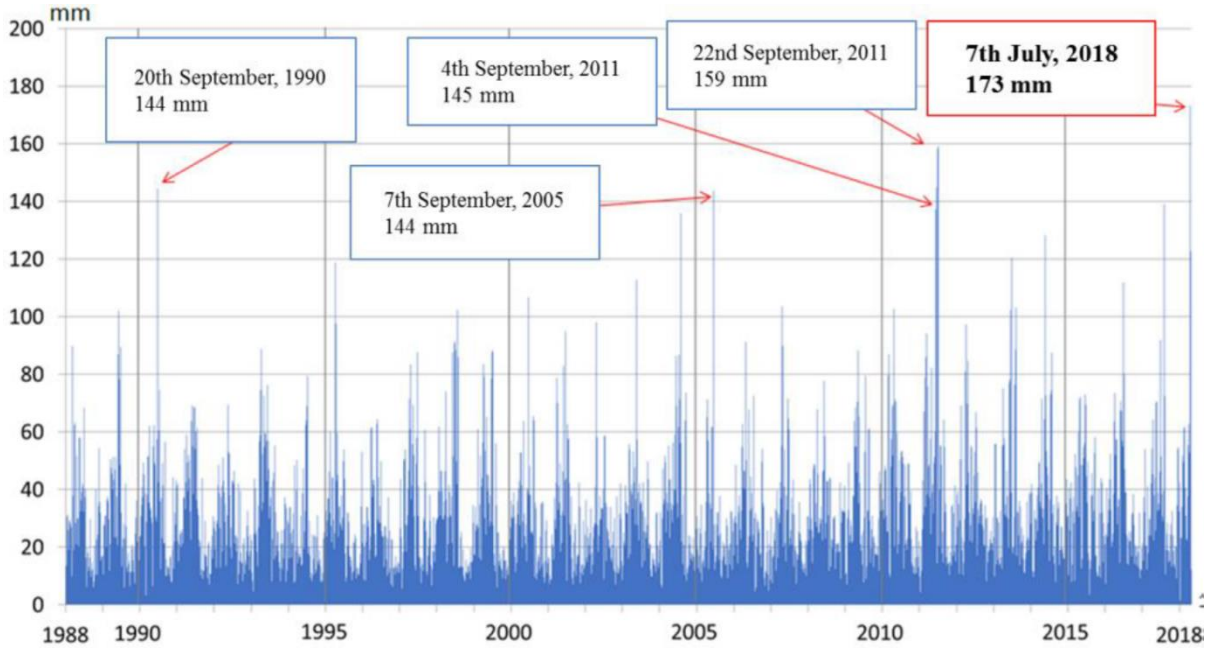

Figure 3 - 15 Cumulative 72-hour precipitation averaged over Japan grid points (Japan Meteorological Agency 2018)

3.3.3 Material and Measuring Device Installation

Layer by layer placement of the soil was performed to obtain a homogenous and uniform soil inside the tank. The target density of the compacted materials was carefully checked with specified weight and volume. Firstly, the required amount of air-dried (gravimetric moisture content of 1 to 2%) material was calculated based on the preparation of dry density. The dry densities for MS, SS, and GP were 1.80, 1.65, and 1.675 g/cm^3, respectively. Afterward, the soil was placed in a 50 mm lift (Figure 3 - 16). For every lift, the soil was compacted using a hammer. A rough surface is made between each lift for making a decent connection between two layers (Figure 3 - 16). After the compaction of a 200 mm height bottom coarser layer, a layer of woven geotextile was placed above it (Figure 3 - 16). This was followed by the compaction of the fine layer over the coarse one. This compaction method was applied considering the strength of the tank, which was made from acrylic glass, and the problem associated with the difficulty in preparing a large amount of soil with uniformly in a narrow environment (12 cm).

Totally nine moisture sensors are used in the capillary barrier tests. The sensors were also installed during the placement of the materials. That is because of ensuring good contact between the materials and the sensors. After compaction and sensor initialization was completed, the infiltration box tilted was tilted to a specified angle, which is 26.6 degrees (Figure 3 - 16).

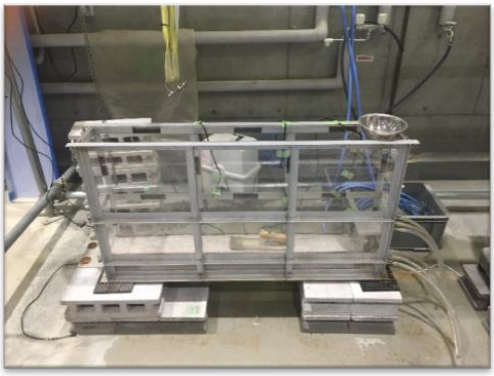

Sample is prepared with 50 mm layer

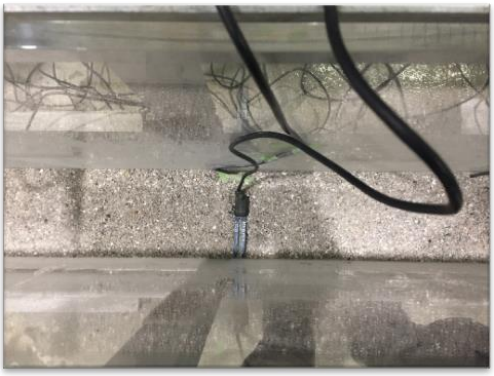

Installation of moisture sensor

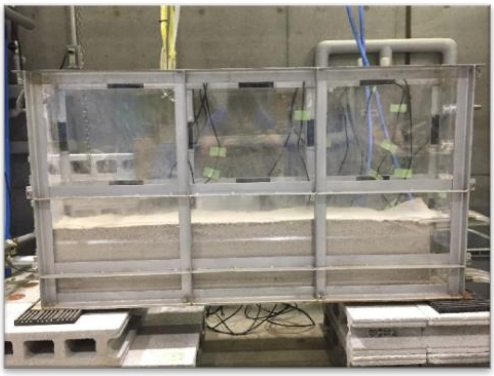

Using of a GeoNet for separation

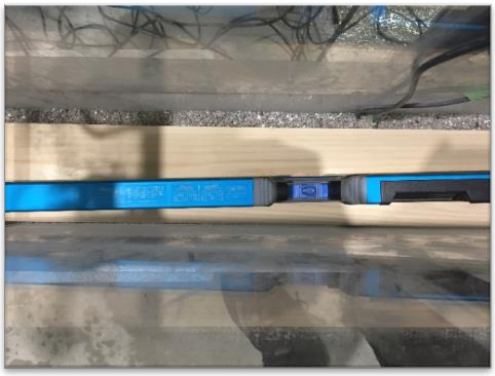

Checking the gradient

Layer connection application

Entire test system

Figure 3 - 16 Preparation of infiltration tank test

3.4 Experimental Program for Capillary Barrier Models

In the experimental works, two different capillary barrier models were investigated with varying soil combinations. Two coarser materials (poorly graded coarse silica sand (SS) and poorly graded gravel (GP)) was used for the bottom layer, and a finer material (poorly graded medium sand (MS)) was used for the top layer. The first capillary barrier model is constructed with 10 cm thick medium sand (MS) overlying 20 cm thick, coarse silica sand (SS), and it is

named as Capillary Barrier Model – I (CB_MS-SS). The second model consists of 10 cm of the medium sand (MS) overlying 20 cm thick gravel (GP), and it is named as Capillary Barrier Model – II (CB_MS-GP). These two different capillary barrier models are shown in Figure 3 - 17. The reason for using two different coarser materials is to compare the effectiveness of soil configuration for the utilization of different naturally contaminated soil inside the embankment with the capillary barrier approach.

Each model was tested according to three different initial preparation conditions. They were initially dry, prepared with optimum moisture content, a drawdown (free drainage after the saturation) case. Drawdown condition means that the soil was prepared at optimum water content (OMC), then saturated, and drained to reach the equilibrium. The dry cases are applied to understand waterfront progress in the fully dry media and the effect of different initial degree of saturation of fine soil on the capillary barrier occurrence. Optimum moisture content case is applied to check a typical construction method in field applications. Drawdown cases are conducted to generate an initially stabilized equilibrium conditions of pore-water pressure before rainfall application. The experimental program is summarized in Table 3 – 3.

Table 3 - 3 Summary of the experimental program of the capillary barrier system

Case	Soil combination (Contaminated soil – cover soil)	Condition before rainfall	Saturation degree of the top layer before rainfall	Saturation degree of the bottom layer before rainfall	Rainfall intensity (mm/hr)
1	CB_Model I (Medium sand – Silica sand)	Dry	1-3%	0-1%	3.22
2	CB_Model I (Medium sand – Silica sand)	OMC	70-80%	7-35%	3.94
3	CB_Model I (Medium sand – Silica sand)	Drawdown	55-60%	10-45%	6.64
4	CB_Model II (Medium sand – Gravel)	Dry	2-3%	3-8%	2.72
5	CB_Model II (Medium sand – Gravel)	OMC	75-80%	13-25%	1.96
6	CB_Model II (Medium sand – Gravel)	Drawdown	35-60%	13-22%	2.29

"Drawdown" condition means that the soil layers were prepared at optimum water content (OMC), then saturated and drained to reach the equilibrium.

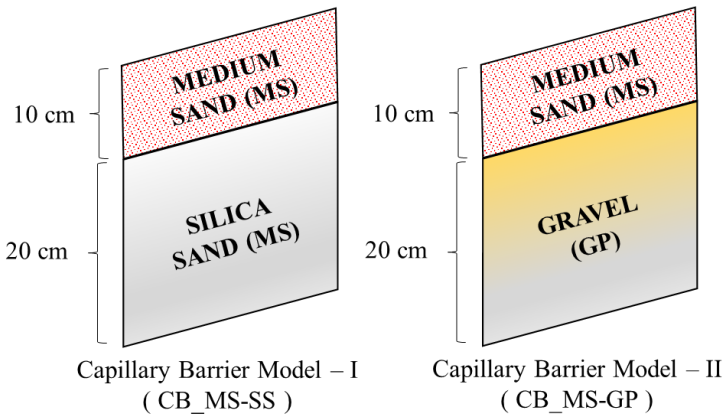

Figure 3 - 17 Two capillary barrier models tested during the research

3.5 Results of Experimental Studies on Capillary Barrier Models

This section presents the capillary barrier test results. The capillary barrier models were tested under different material configurations, rainfall rates, and rainfall durations. The results presented as saturation degree and drained water from top and bottom exits. Measurements location of saturation degrees and the location of the drains are shown in Figure 3 – 18. Three different background fills are selected for the representation of saturation degrees results in the figures. The diverse background fill is denoted for the sensor section. The blue background fill belongs to the sensor section near the exits (close the toe of the tank – sensor 1, sensor 4, and sensor 7). The yellow background fill shows the sensor section at the center of the tank (sensor 2, sensor 5, and sensor 8). The white background fill belongs to the sensor section near the rear of the tank (sensor 3, sensor 6, and sensor 9).

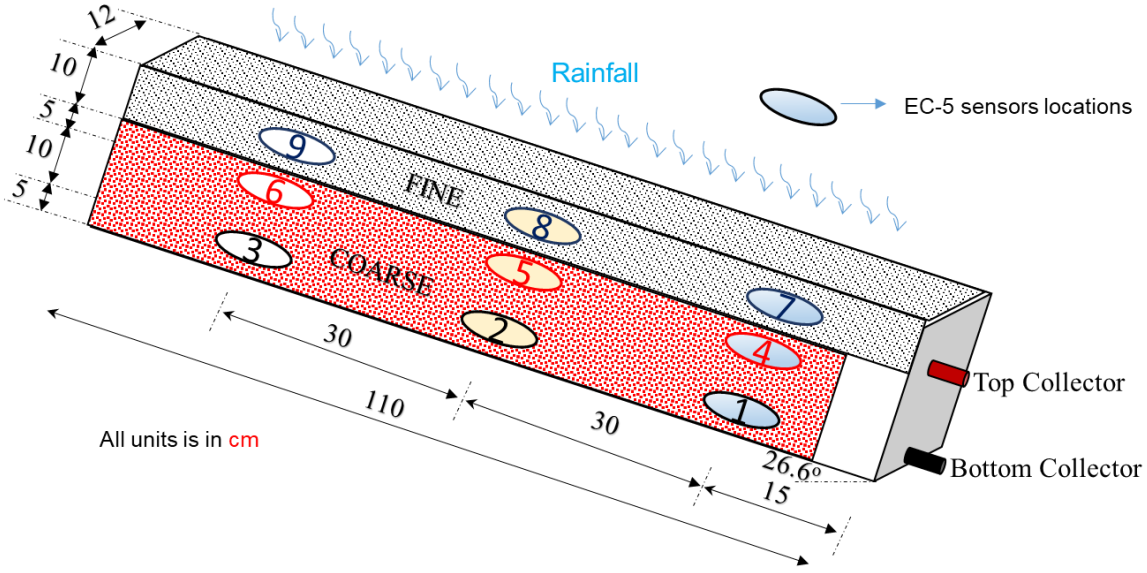

Figure 3 – 18 Position of sensors and exits in the infiltration box test

3.5.1 Capillary Barrier Model – I (CB_MS-SS) Results

Results of the capillary barrier model – I (CB_MS-SS), which was constructed with 10 cm thick medium sand (MS) overlying 20 cm thick coarse silica sand (SS) (CB_MS-SS), are presented in this section. The CB_MS-SS models were tested under three different initial conditions: a dry case – Case 1, an optimum moisture content case – Case 2, and a drawback case – Case 3.

Case 1 – Dry Case – (CB_MS-SS DRY)

Case 1 – CB_MS-SS DRY model was subjected to a rainfall of 3.22 mm/hr for 2880 minutes (48 hours). At the beginning of the experiment, the materials were almost dry conditions. The initial saturation degrees were around 1% and 3% for the medium sand (MS) and gravel (GP). The tank was tried to fill with dry target densities, which were the same all the experiments. The dry preparation densities were roughly 1.80 g/cm^3 and 1.65 g/cm^3 for the MS and GP, respectively. After the preparation of the tank, it was tilted to achieve a slope of 26.6°, and the adjusted rainfall intensity was applied.

During the infiltration box test, time histories of top and bottom exits are obtained separately. The locations of the exits are shown in Figure 3 – 18. With the use of exits time histories, and the occurrence of capillary barrier effect is checked.

Figure 3 – 19 shows the time histories of top and bottom exits. According to time histories, all the water drained from the bottom exit. That means there are no capillary barrier effects on this soil configuration. Although there is a hydraulic conductivity difference between the coarser layer (ss) and the finer layer (MS), the capillary barrier effect doesn't occur. It is considered that during the test, the suction equilibrium primarily occurs inside the tank. At this equilibrium value, the hydraulic conductivity of SS becomes higher than the MS. Therefore, a capillary barrier effect does not take place. Consequently, no lateral flow was observed for the Case - 1, although both top and the bottom layer was prepared initially fully dry condition.

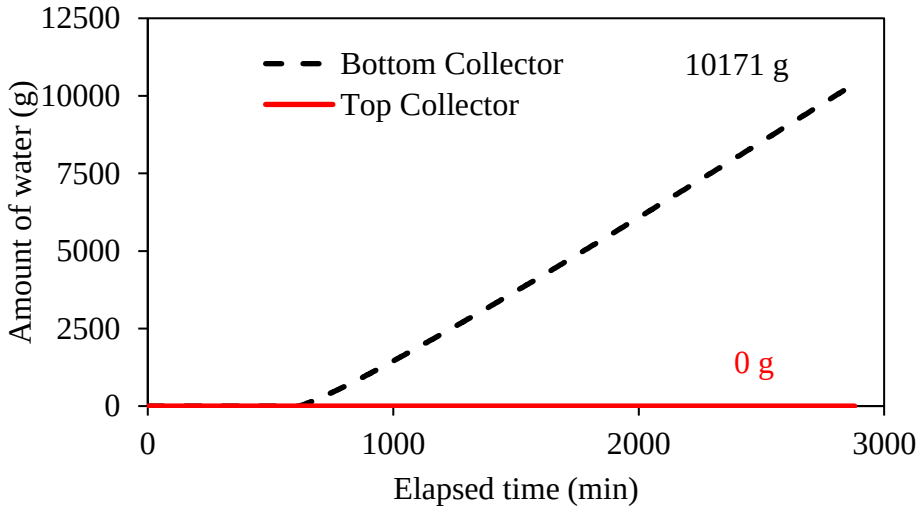

Figure 3 - 19 Time history of the drainage water for Case 1

The changes in the sensor degree of saturation during the testing period are shown in Figure 3 – 20, Figure 3 – 21, and Figure 3 – 22. An increase in the degree of saturation was observed during the rainfall stage at all sensors. However, after a time, the sensor readings become constant until the end of the experiment. It can also be seen that the degree of saturation values for the sensors 3-6-9 had lower saturation values because of their locations. The applied rainfall doesn't directly reach this region.

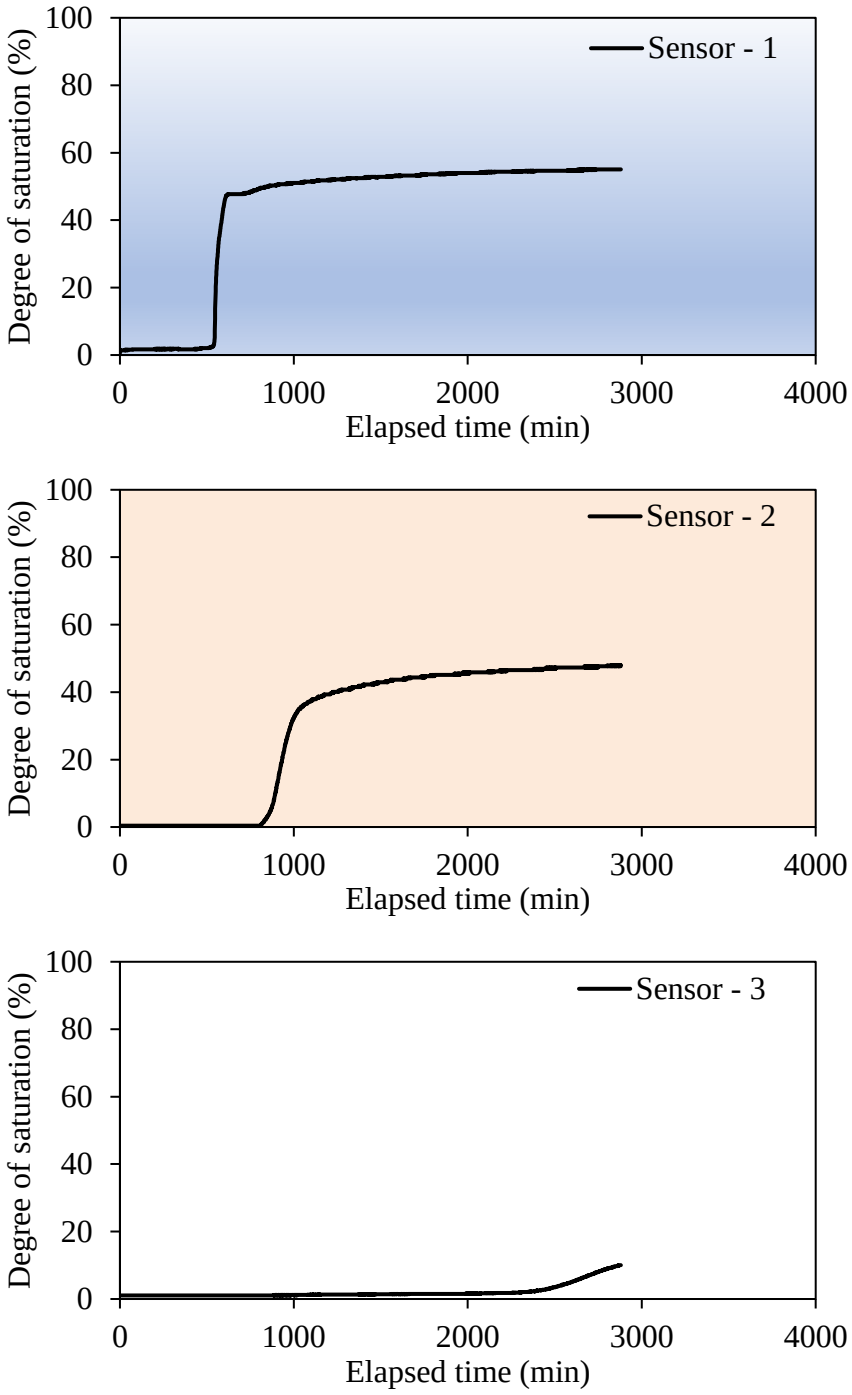

Figure 3 - 20 Saturation degrees of sensors 1, 2, and 3 for Case 1

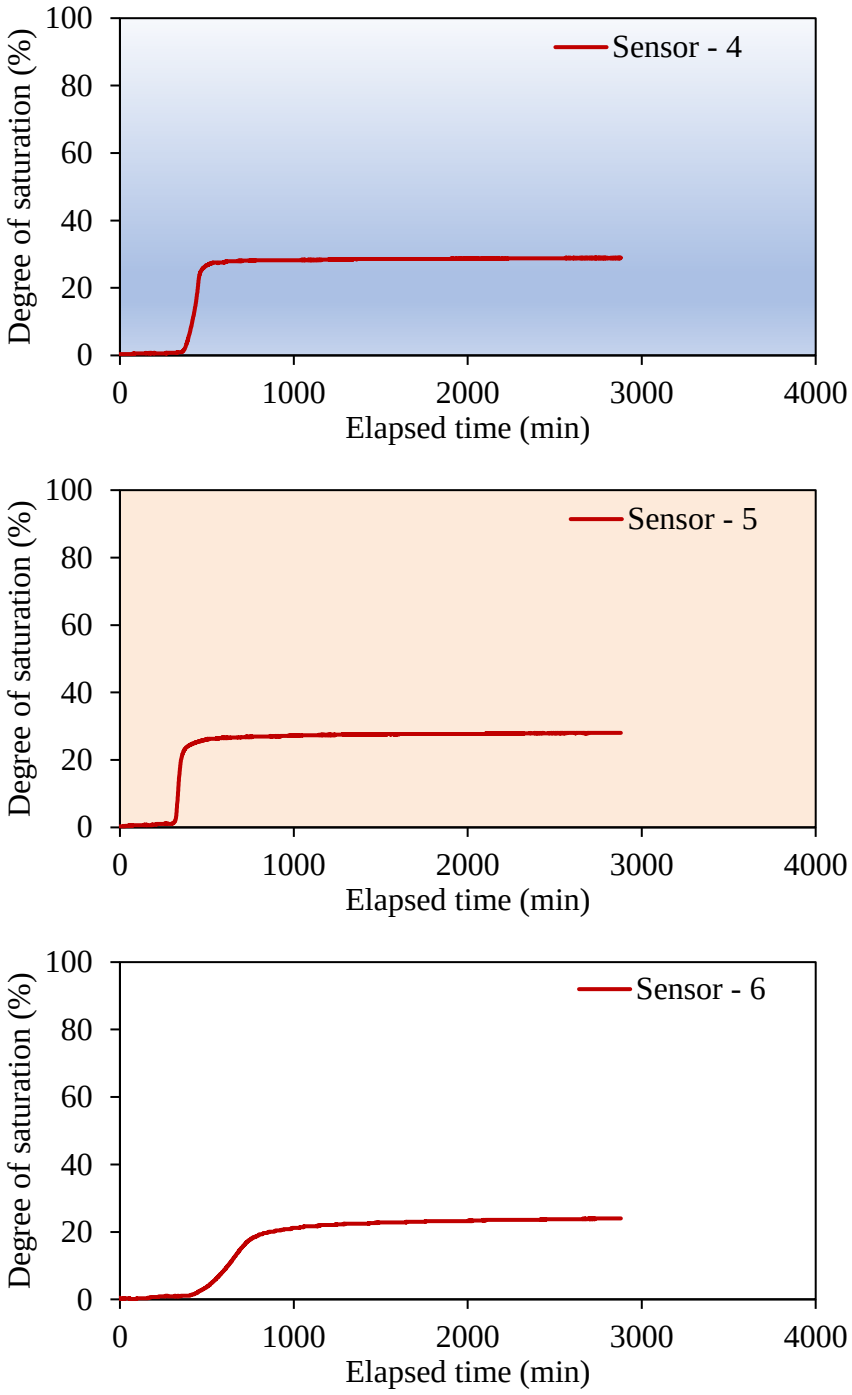

Figure 3 - 21 Saturation degrees of sensors 4, 5, and 6 for Case 1

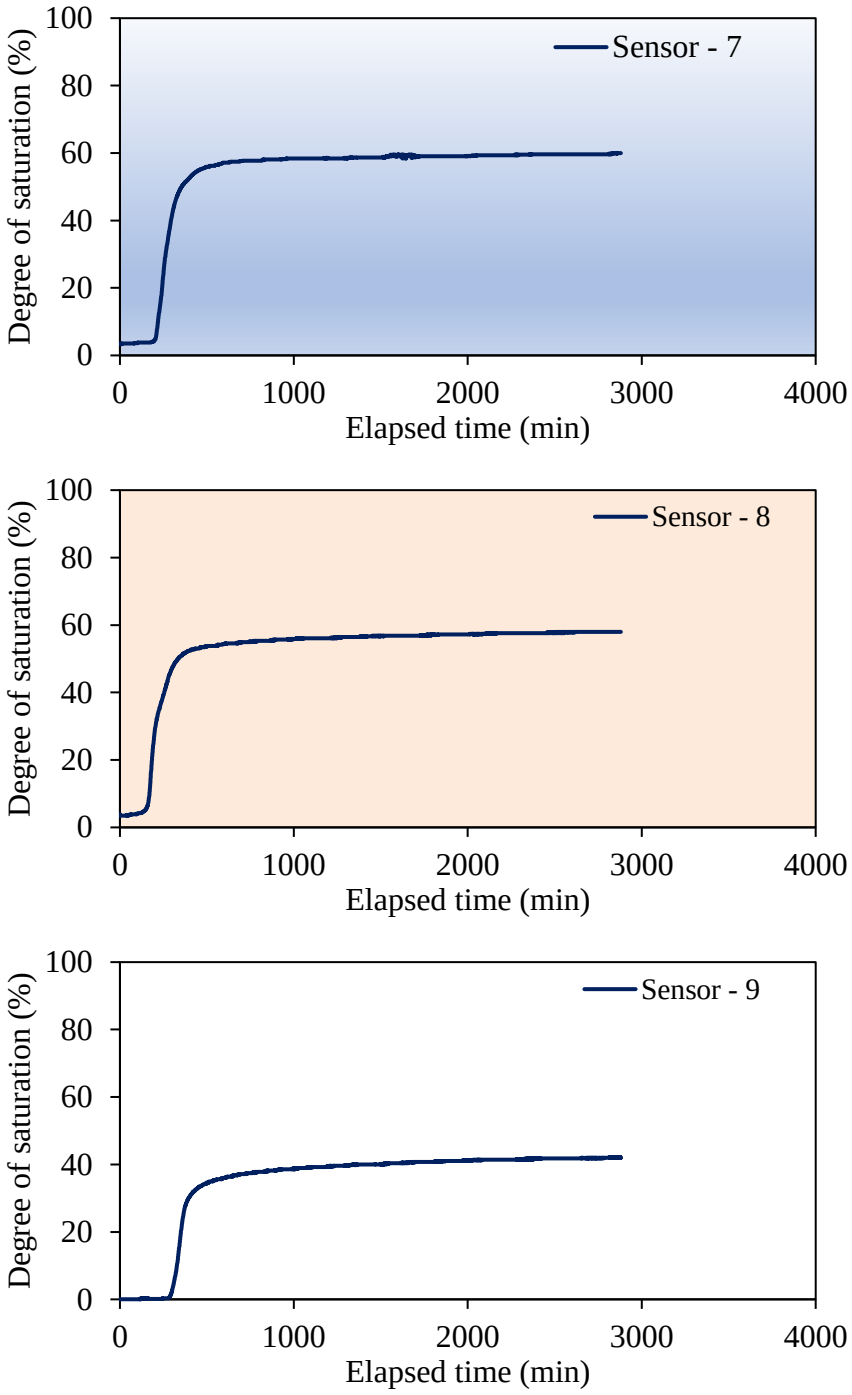

Figure 3 - 22 Saturation degrees of sensors 7, 8, and 9 for Case 1

Case 2 - Optimum Moisture Content Case - (CB_MS-SS OMC)

Case 2 - The CB_MS-SS OMC model was initially prepared with optimum moisture content for the fine layer (medium sand-MS). The fine layer was prepared with 15% gravimetric water

content concerning the standard Proctor test result. The initial saturation degrees (before rainfall application) were around 70% to 80% for the top layer (MS) and 7% to 35% bottom layer (SS). The dry preparation densities were 1.80 g/cm^3 and 1.65 g/cm^3 for the fine and the coarse layer, respectively. After the preparation of the tank, it was then tilted to achieve a slope of 26.6°, and the adjusted rainfall intensity was applied. The model tested with a rainfall of 3.94 mm/hr for 1440 minutes (24 hours). During the testing period, the total amount of water that goes out from each exit is separately logged. Figure 3 - 23 shows the time histories of top and bottom exits. According to the time histories, all the water drained from the bottom exit, which means that capillary barrier effects do not occur at the Case 2, too. Even though initially, air-dried coarse material was placed during the experiment due to the high moisture content of the top layer (MS), an increase of saturation degrees of the bottom layer (SS) occurred before rainfall application (shown in Figure 3 – 24, Figure 3 – 25, and Figure 3 - 26).

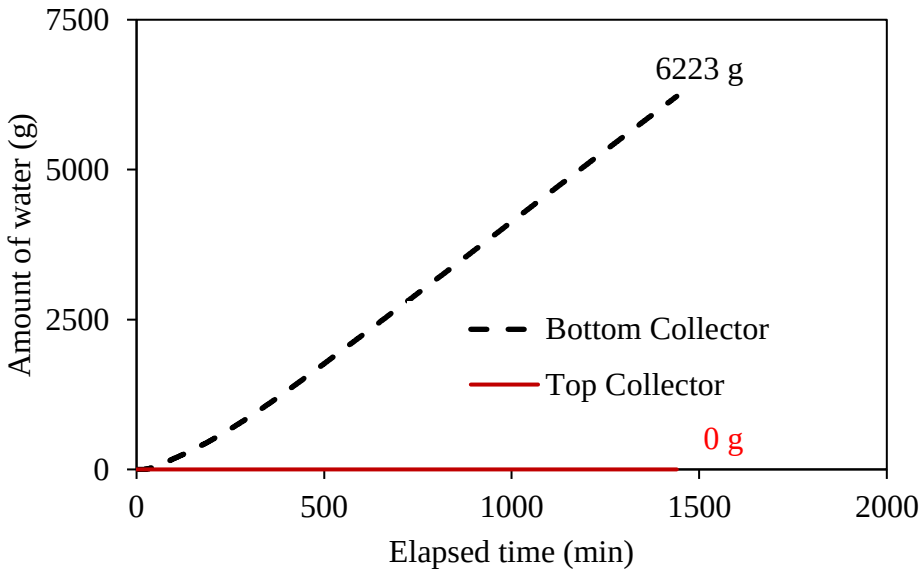

Figure 3 - 23 Time history of the drainage water for Case 2

The degree of saturation versus time are presented in Figure 3 – 24, Figure 3 – 25, and Figure 3 - 26. It can be seen results that a slight increase occurs nearly all the sensors. However, the increment is not severe. It might be explained that initial water content is higher than the storage capacity of the materials under the testing condition.

Moreover, during the filling and compaction process of the tank, the waterfront has already reached the coarse layer. Therefore, just after 35 minutes from rainfall starts, a water flow recorded from the bottom exits of the model (Figure 3 - 23). On the other hand, sensors 2 and 3 had an increment in terms of saturation degree because sensors 2 and 3 did not reach

storage capacity during the tank preparation period. This increment is also related to the locations of sensors that are far from the exits.

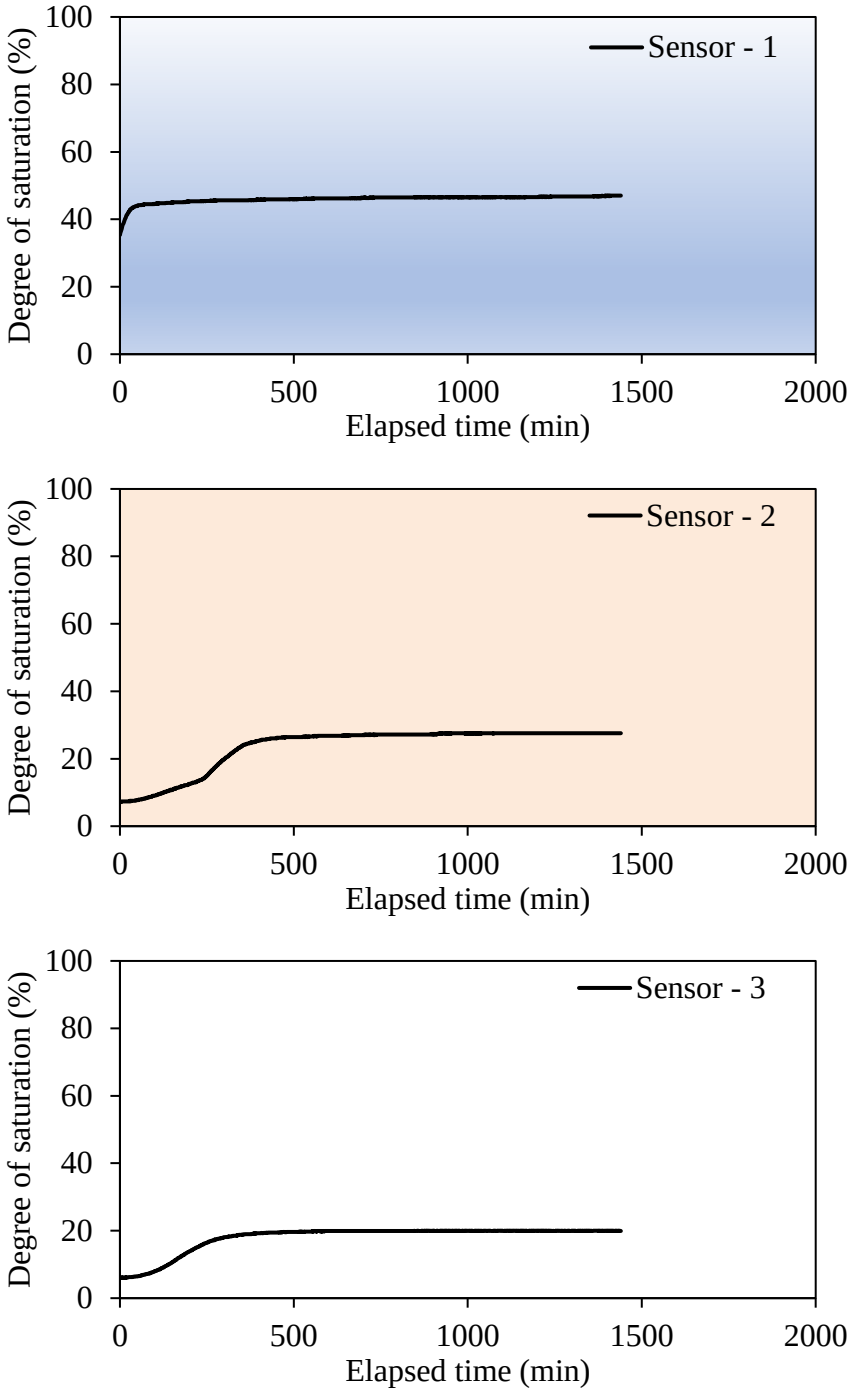

Figure 3 - 24 Saturation degrees of sensors 1, 2, and 3 for Case 2

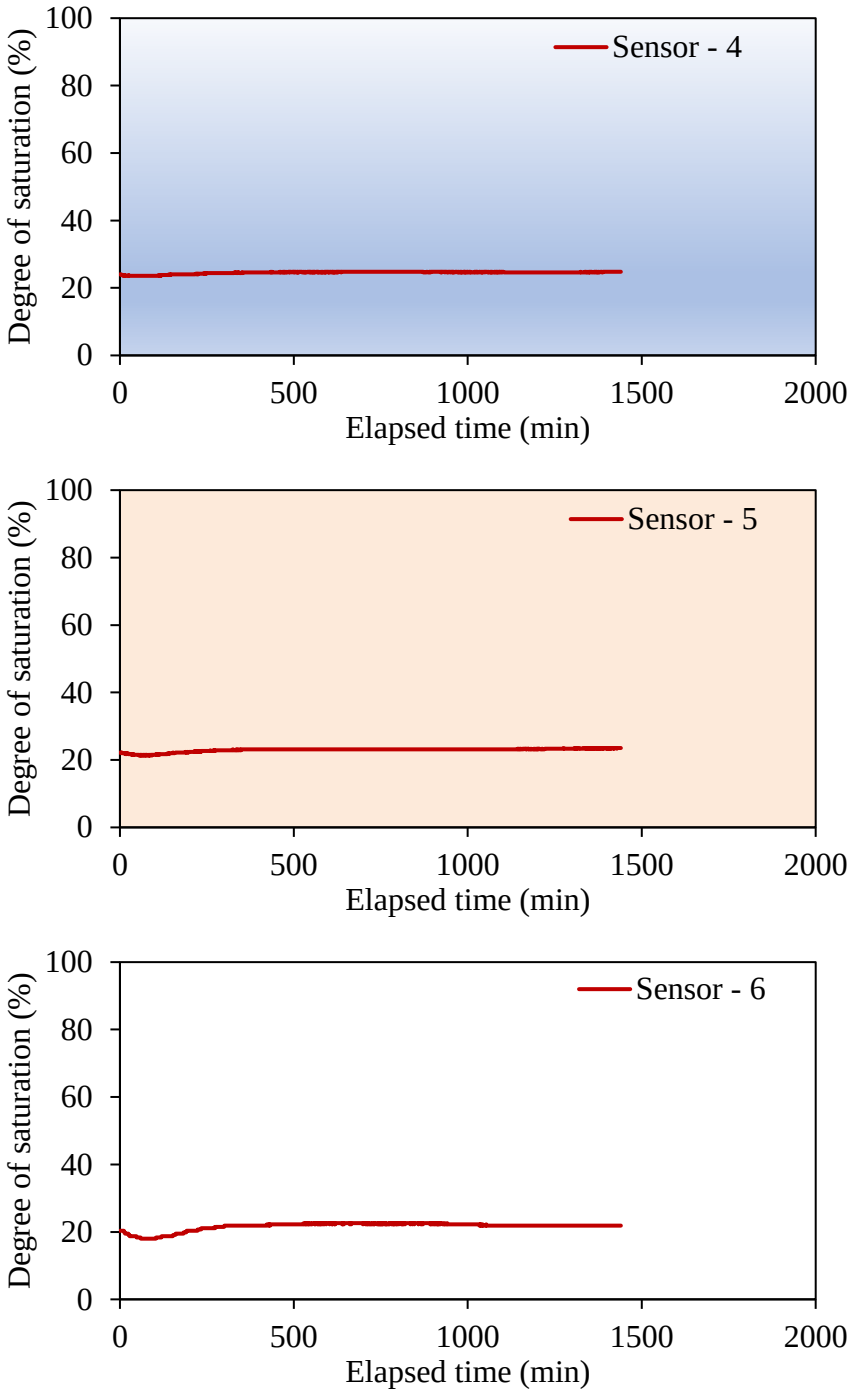

Figure 3 - 25 Saturation degrees of sensors 4, 5, and 6 for Case 2

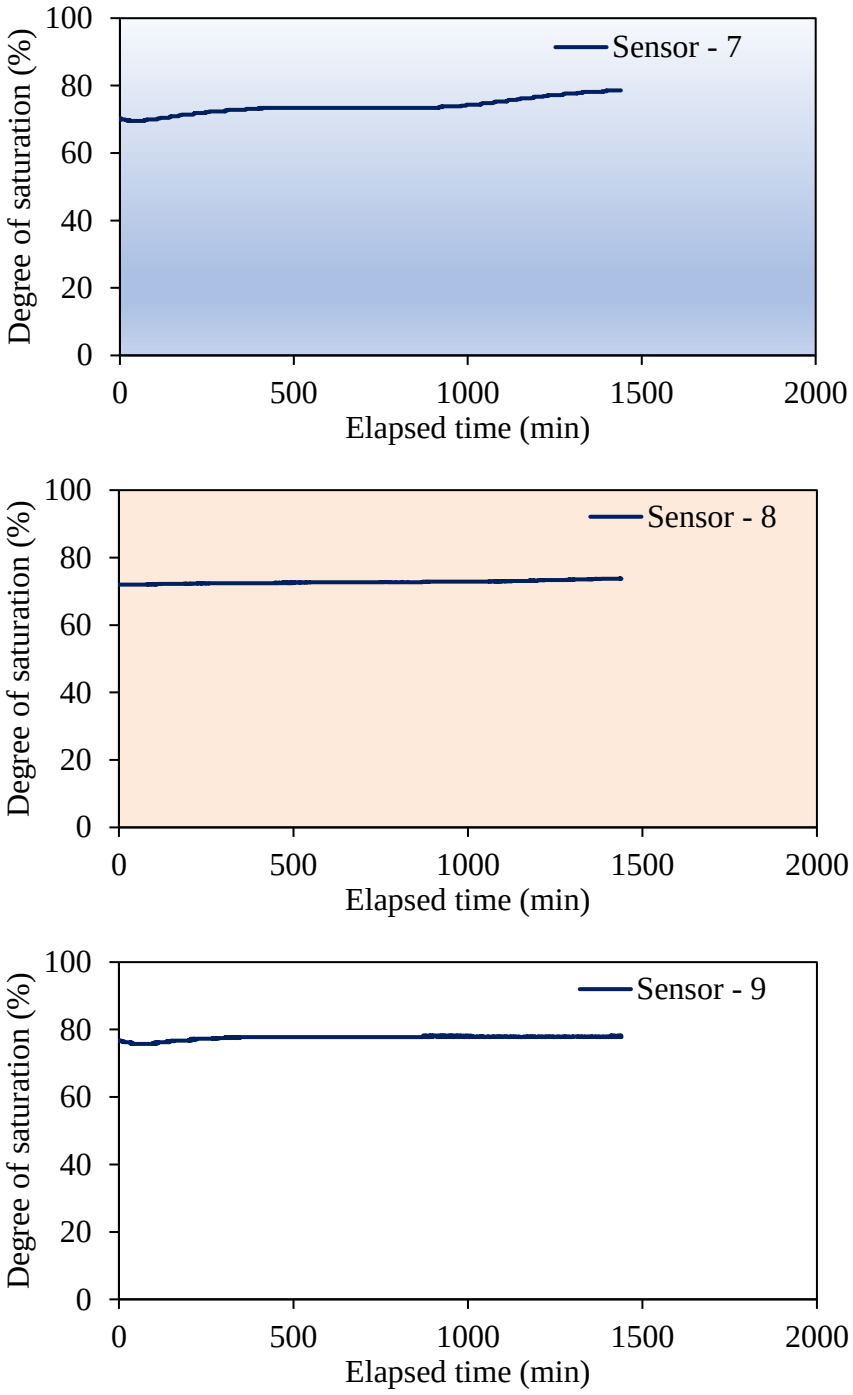

Figure 3 - 26 Saturation degrees of sensors 7, 8, and 9 for Case 2

Case 3 - Drawdown Case (CB_MS-SS DD)

Case 3 - CB_MS-SS DD model was tested after the drawdown period. The model was initially prepared with optimum water content for the top layer (medium sand - MS) and nearly dry with the bottom layer (coarse silica sand - SS). The dry preparation densities are 1.80 g/cm^3 and 1.65 g/cm^3 for the MS and the SS layers, relatively. After the compaction, a saturation or nearly saturation condition was achieved by closing the valves. Then, the drainage valves were opened, and free drainage of water was supplied from the tank with a tilting position. Before starting the rainfall, the exits outlets were checked until there is no more water drainage. After the drawdown period, the adjusted rainfall was applied. Case 3 tested with a rainfall of 6.64 mm/hr for 2500 minutes (41.7 hours). Figure 3 - 27 shows the time histories of top and bottom exits. According to time history from exits, all the water drained from the bottom exit. The capillary barrier effect did not occur.

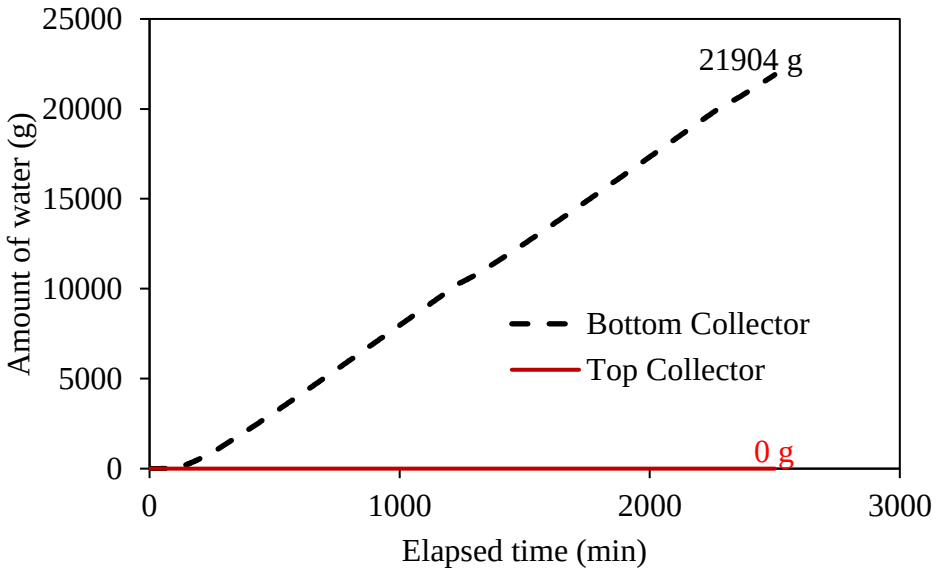

Figure 3 - 27 Time history of the drainage water for Case 3

Sensor readings from Case 3 are presented in Figure 3 – 28, Figure 3 – 29, and Figure 3 - 30. The obtained results are similar to Case 2 (optimum moisture content case). An increment was seen in the degree of saturation readings at the beginning of rainfall. After that, the sensor readings were stabilized. The sensors near the exits had higher saturation degrees readings compare to far ones. This difference is considered to occur due to the limited drainage area in the tank. It is thought that it is a limitation of laboratory testing system.

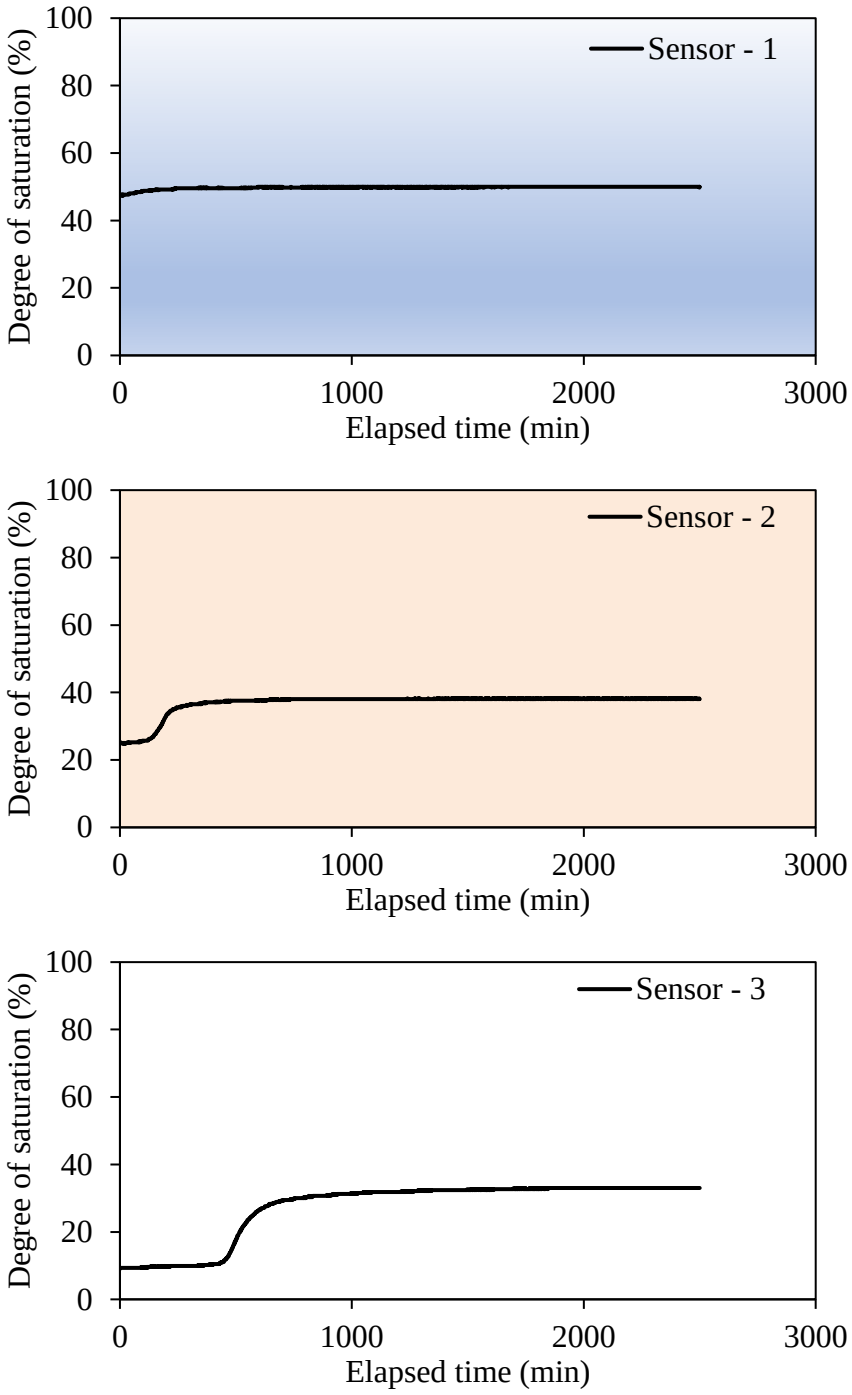

Figure 3 - 28 Saturation degrees of sensors 1, 2, and 3 for Case 3

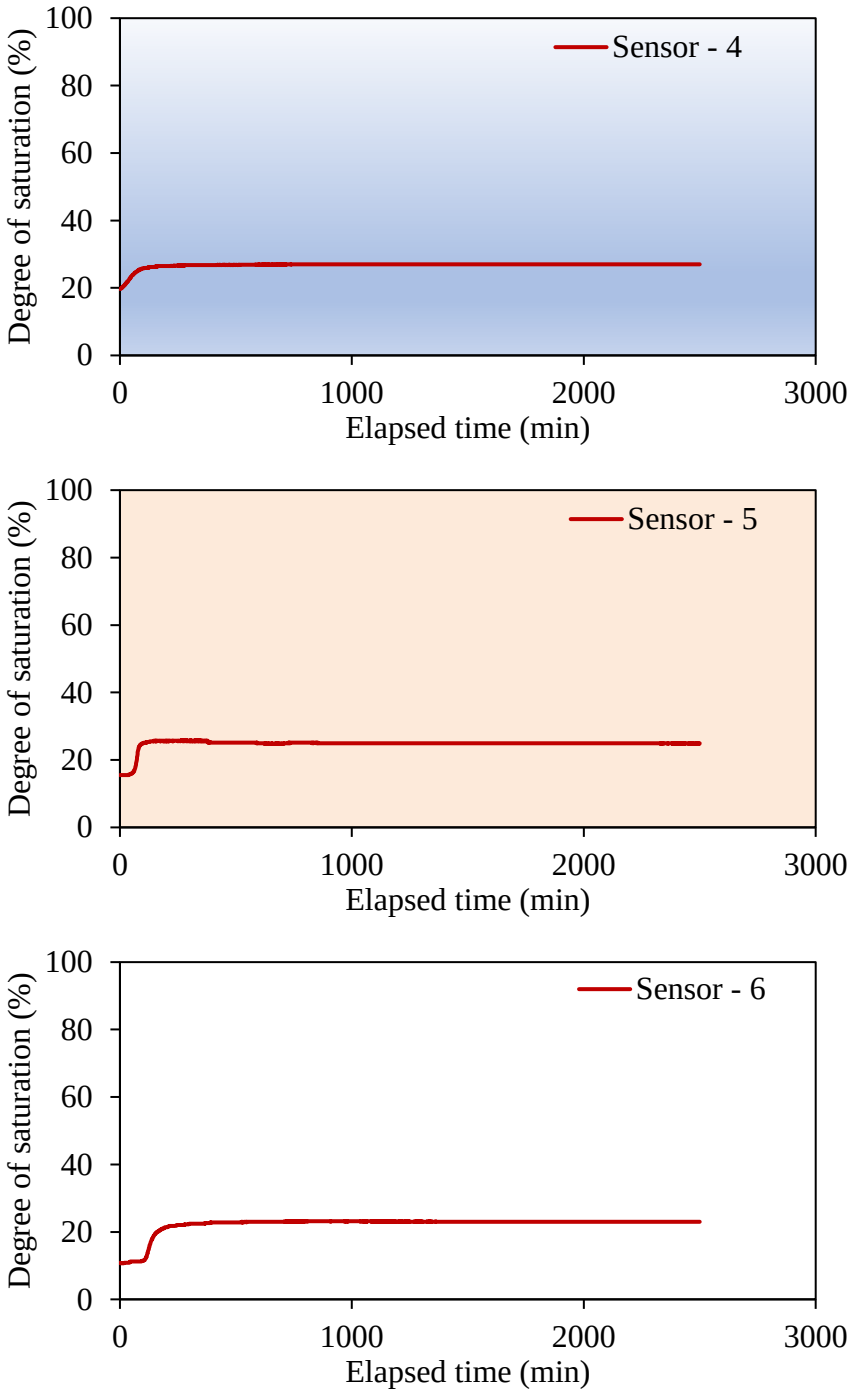

Figure 3 - 29 Saturation degrees of sensors 4, 5, and 6 for Case 3

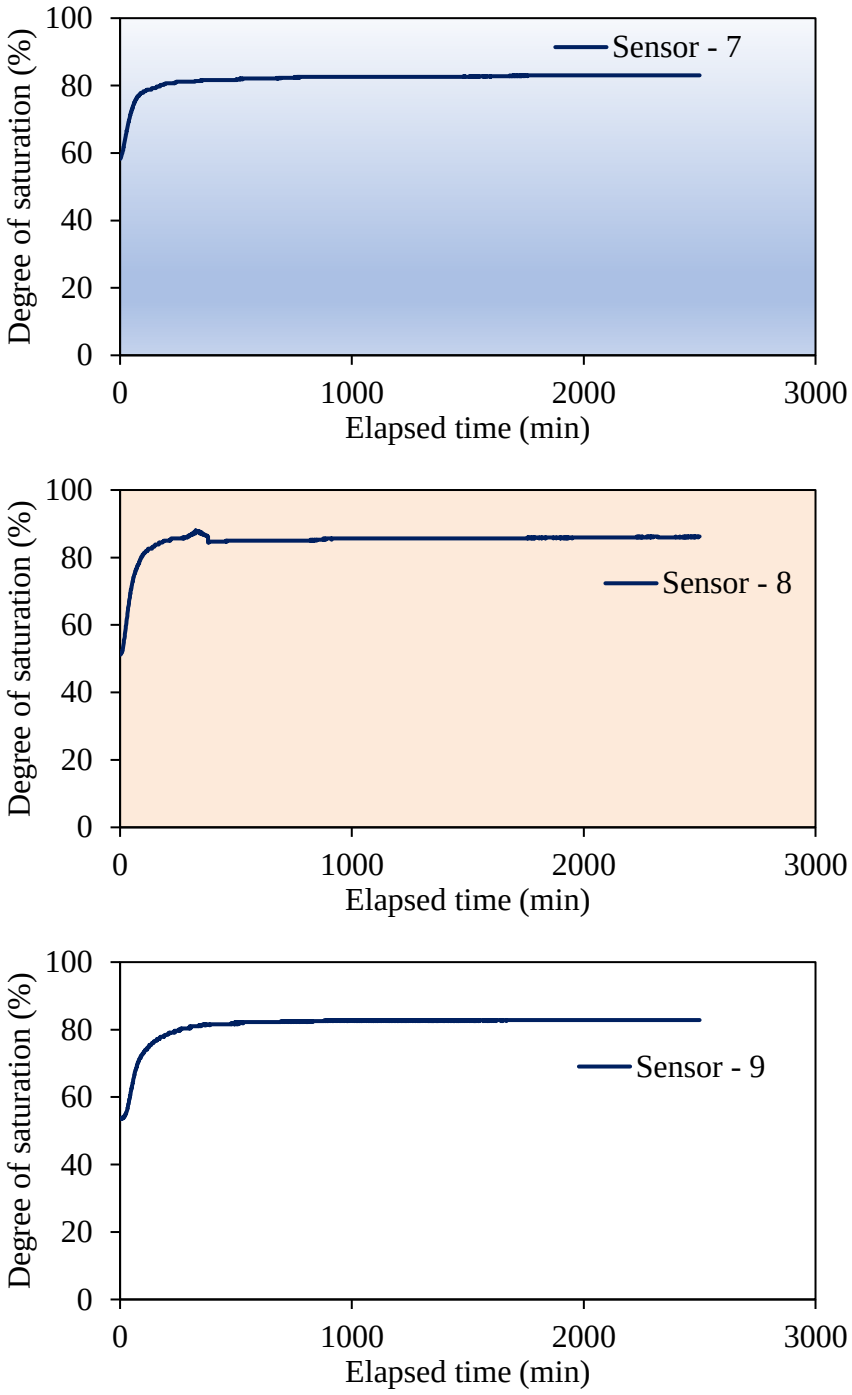

Figure 3 - 30 Saturation degrees of sensors 7, 8, and 9 for Case 3

3.5.2 Capillary Barrier Model - II (CB_MS-GP) Results

Results of the capillary barrier model – II (CB_MS-GP), which built with 10 cm thick medium sand (MS) overlying 20 cm thick poorly graded gravel (GP) (CB_MS-GP) are illustrated in this section. The CB_MS- GP models were tested under three different initial cases: a dry case – Case 4, an optimum moisture content case – Case 5, and a drawback case – Case 6.

Case 4 - Dry Case - (CB_MS-GP DRY)

The Case - 4 was subjected to a rainfall of 2.72 mm/hr for 4980 minutes (83 hours). At the beginning of the experiment, both layers were approximately dry conditions (air-dried soils were used). The initial saturation degrees for the finer layer were around 2.0% - 3.0%, while the coarser layer was about 3.0% - 8.0%. Figure 3 - 31 shows the time histories of top and bottom exits. According to results, all the water drained from the top exit. The lateral flow was observed for the Case - 4. The results indicate that the capillary barrier effects continue until the end of the test (nearly 3.5 days). Due to the hydraulic conductivities difference between the GP and MS layer, the capillary barrier effect did not break with 2.72 mm/hr rainfall and 26.6 degrees slope.

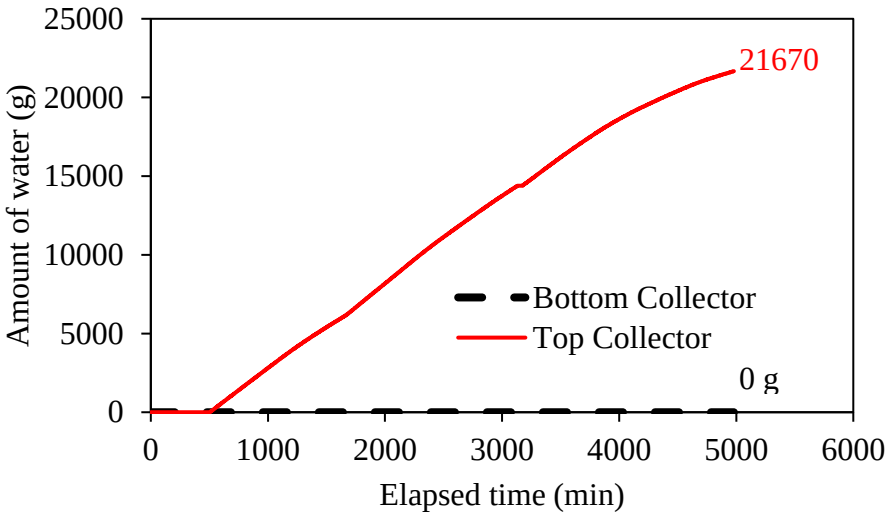

Figure 3 - 31 Time history of the drainage water for Case 4

During the test, nine moisture sensors were used, and sensors readings recorded every two minutes. The degrees of saturation versus time is displayed in Figure 3 – 32, Figure 3 – 33, and Figure 3 - 34. According to results, the saturation degrees inside the coarse layer (sensors 1, 2, 3, 4, 5, and 6) did not reach more than 16%, because of lateral diverted water (Figure 3 - 31). However, sensors inside the fine layer (sensors 6, 7, and 8), the saturation degree reading had been increased after the starting the rainfall. Then they became constant. After the stable saturation degrees, soil combinations reached an equilibrium state according to the applied

rainfall intensity and preparation slope. Therefore, there was no water flow from the bottom exit.

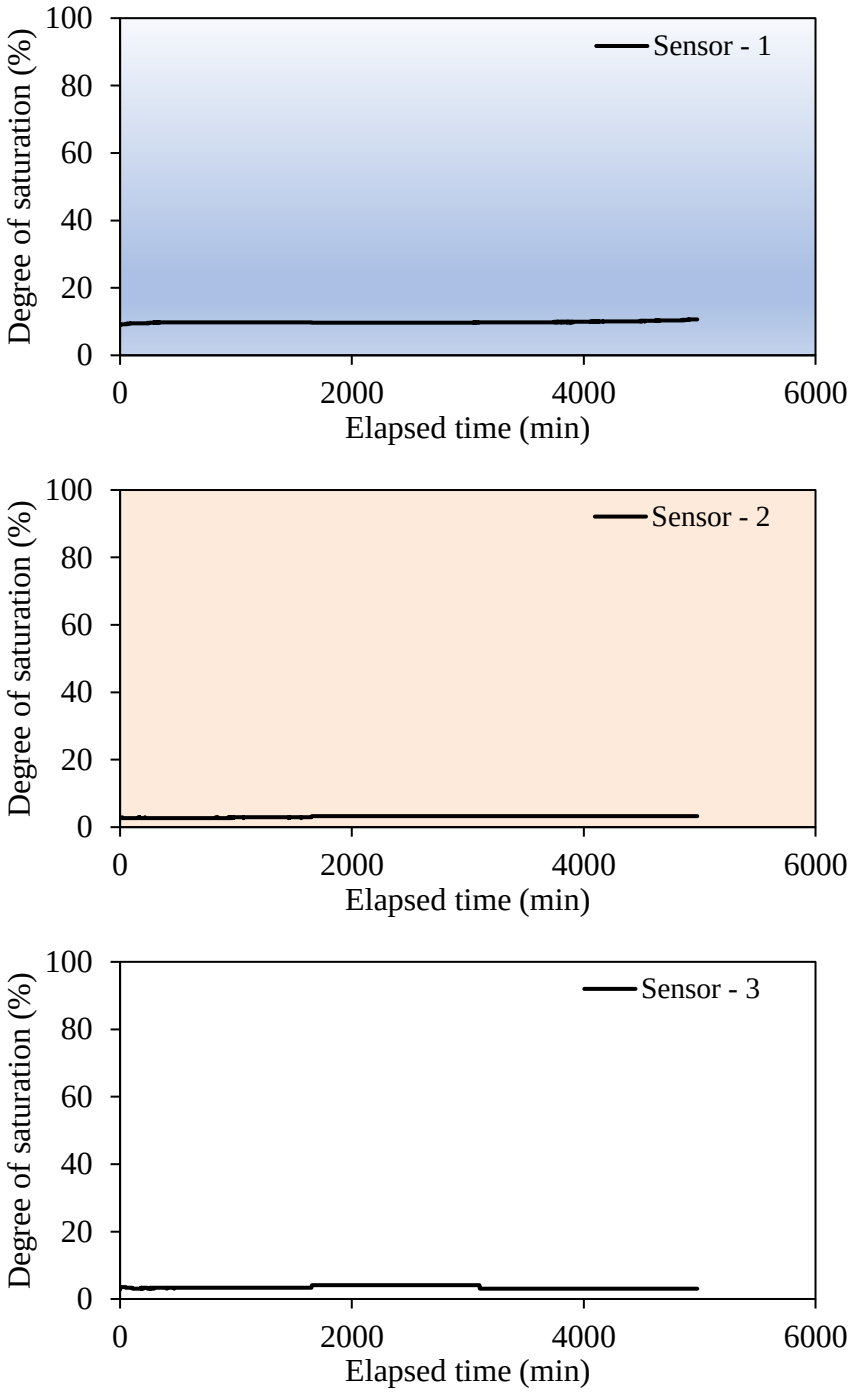

Figure 3 - 32 Saturation degrees of sensors 1, 2, and 3 for Case 4

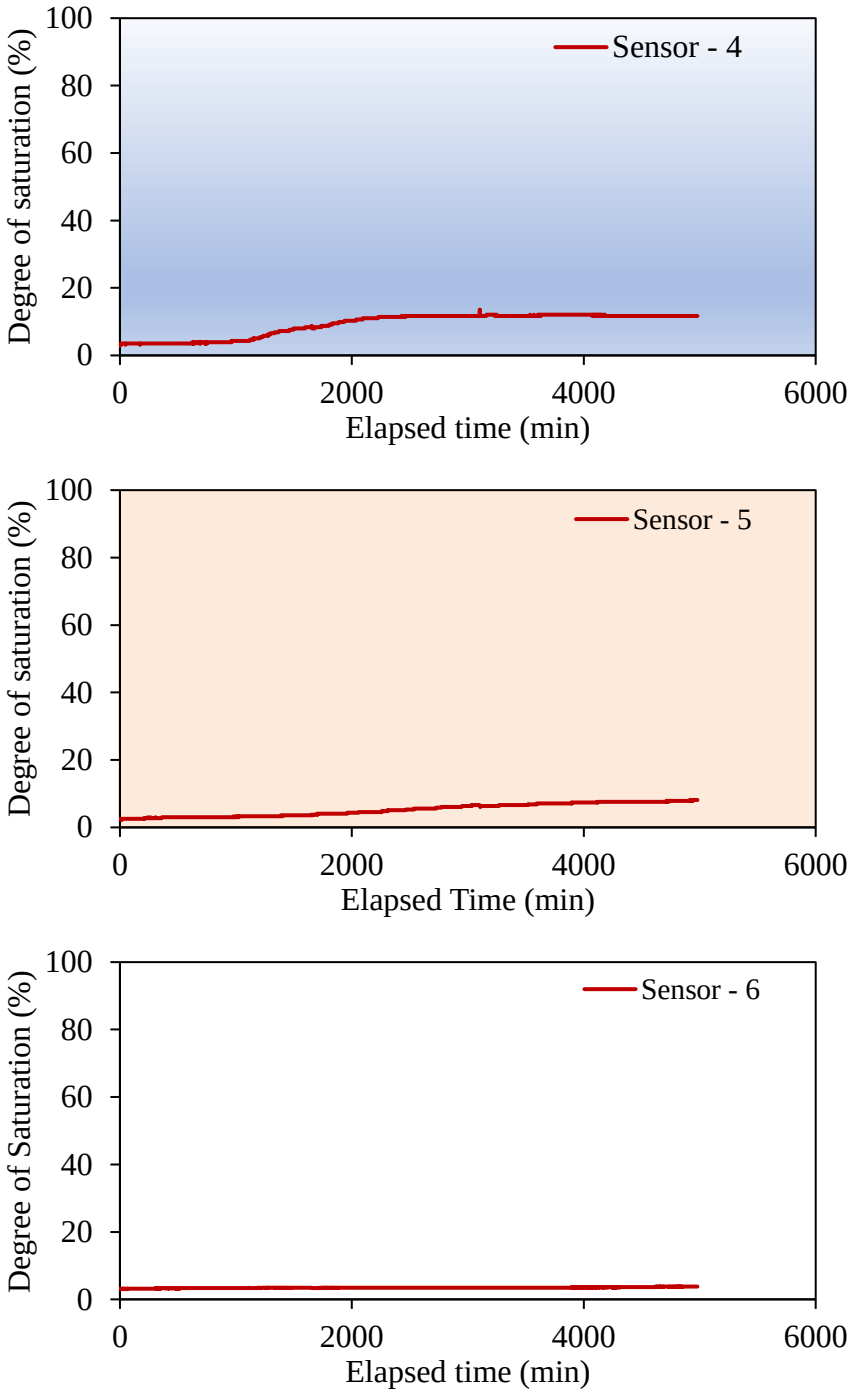

Figure 3 - 33 Saturation degrees of sensors 4, 5, and 6 for Case 4

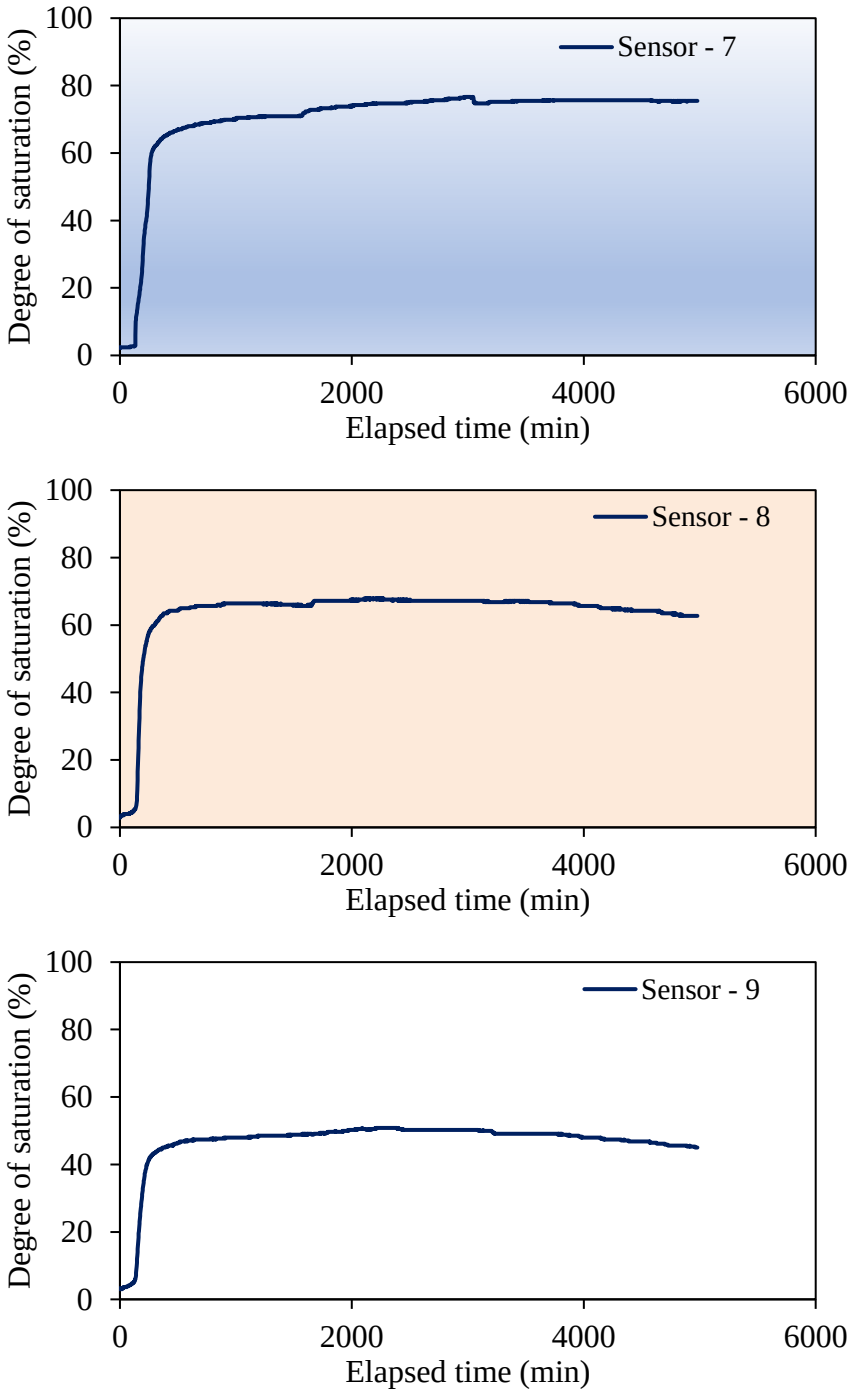

Figure 3 - 34 Saturation degrees of sensors 7, 8, and 9 for Case 4

Case 5 - Optimum Moisture Content Case - (CB_MS-GP OMC)

The CB_MS-GP OMC model was initially prepared with optimum moisture content for the top layer (MS). The bottom layer (GP) was approximately dry at the preparation. The initial saturation degrees were around 75% to 80% inside the MS layer and 15% to 25% inside the GP layer, respectively. Although an air-dried GP material was used for the bottom layer before the rainfall application, during the preparation period of the top layer (MS) degree of saturation had already increased a constant level for the GP layer. This saturation increase inside the bottom layer was considered due to water flow from the top layer. The model tested with a rainfall of 1.96 mm/hr for 1430 minutes (nearly one day).

The time histories for the top and bottom exits are illustrated in Figure 3 – 35. It shows that the water started to drain from the bottom exit (from just after the rainfall application); however, the lateral water flow also occurred. Therefore, the capillary barrier effect also generated. After the suction equilibrium achieved, the water follow had started to go out from the top exit (Figure 3 – 35). The water drainages from top and bottom exits continued with the same trend until the ending of the test. At the end of Case 5, nearly 75% percent of water drained from the top exit. It is considered that the storage capacity of the top layer cannot capture the water, which was added during the preparation of the tank. Therefore, the released water from the fine layer had already started to dip in the bottom layer until the suction equilibrium occurs. As a result, the water movement stated from the bottom exits before the rainfall application.

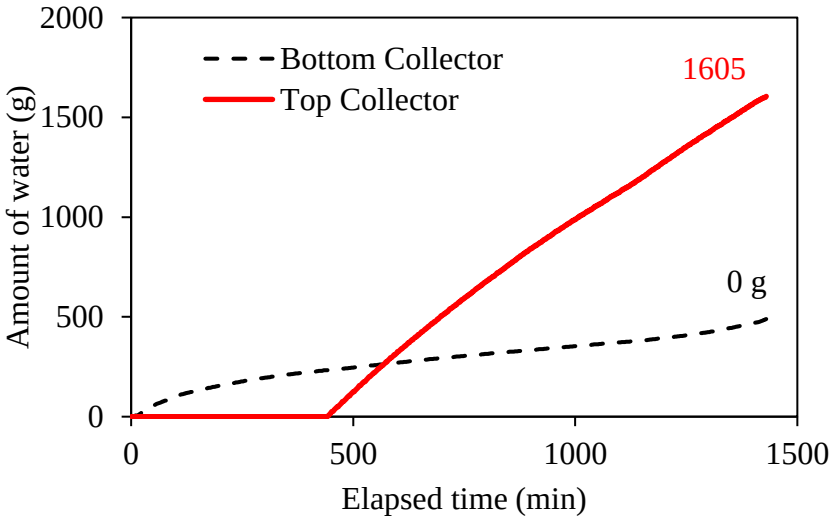

Figure 3 - 35 Time history of the drainage water for Case 5

The degree of saturation versus time is presented in Figure 3 – 36, 3 – 37, and 3 – 38. There is no change at the saturation inside the tank. It might be explained that the preparation water content of the MS layer is already higher than the storage capacity of the materials. Although the SS layer was filled with a dry condition, it also reached a specific saturation degree

during the filling process. Therefore, the degree of saturation for all the sensors became constant from the beginning of the test.

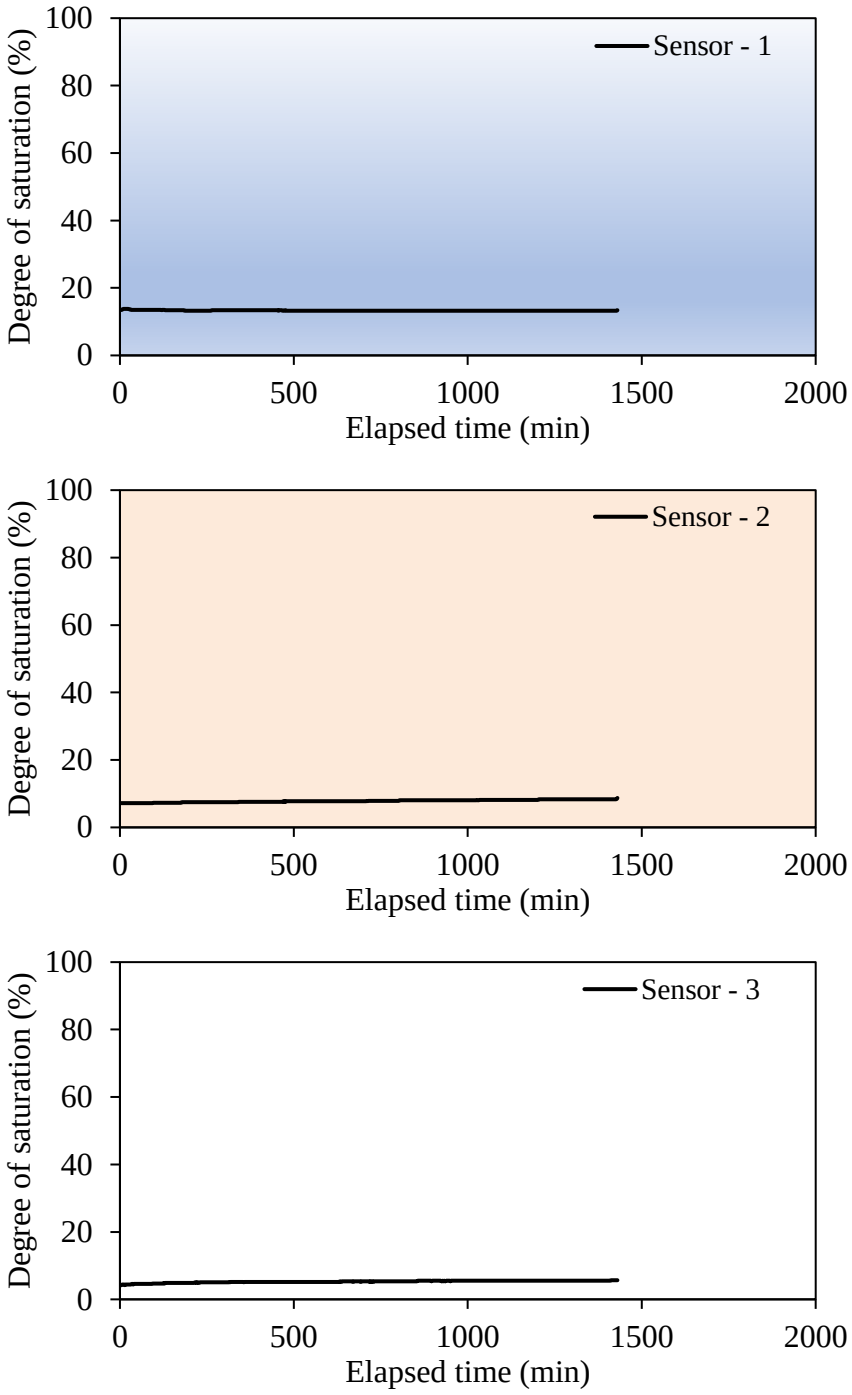

Figure 3 - 36 Saturation degrees of sensors 1, 2, and 3 for Case 5

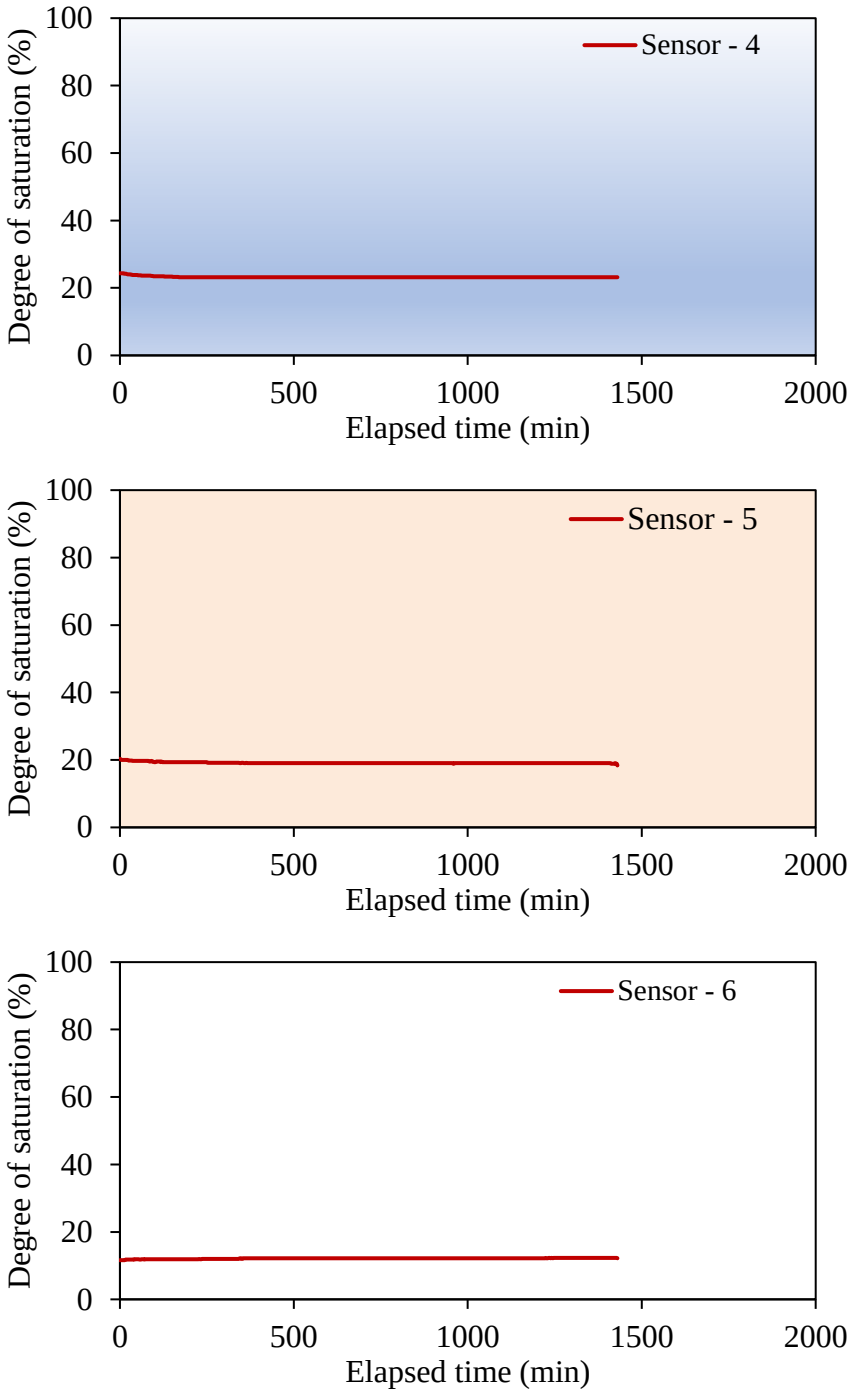

Figure 3 - 37 Saturation degrees of sensors 4, 5, and 6 for Case 5

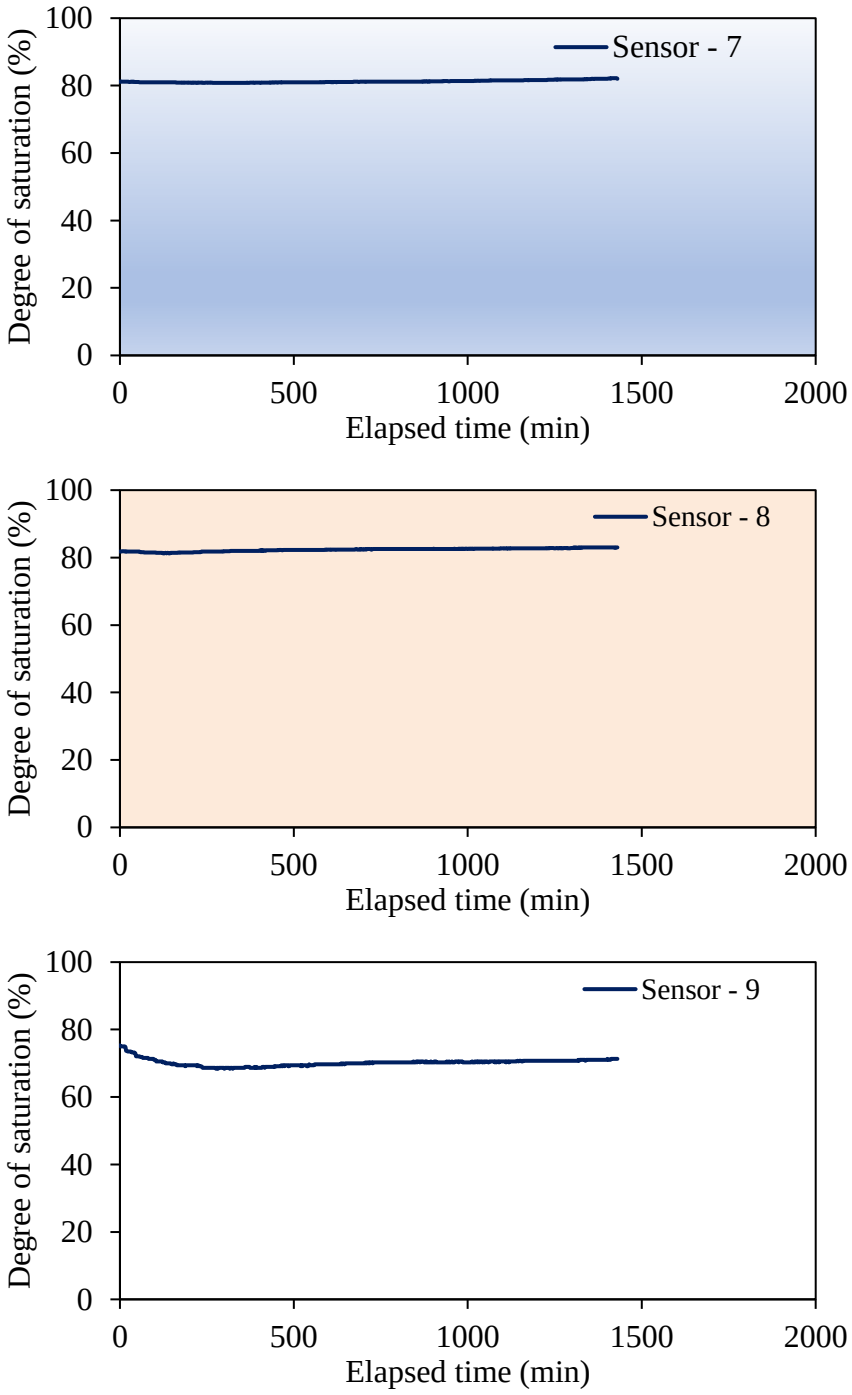

Figure 3 - 38 Saturation degrees of sensors 7, 8, and 9 for Case 5

Case 6 - Drawdown Case (CB_MS-GP DD)

Case 6 - CB_MS-GP DD model was tested after the drawdown period. It tested with a rainfall of 2.29 mm/hr for 5520 minutes (92 hours). Figure 3 - 39 shows the time histories of top and bottom exits. According to time histories of exits, nearly all the water drained from the top exit, which means that the capillary barrier effect occurred at Case 6. There is no water flow from the exits until 250 minutes. After 250 minutes, the water started to flow out the top exit, and it continued during the test. As can be seen from the time history results, there is no straight line. The bent behavior of the top collector time history was considered to depend on o the changing of rainfall rate during the experiment. According to Figure 3 – 39, 99% of cumulative drainage water occurred from the lateral exit. Approximately, only 258 grams of water flowed out from the bottom exit of the tank. It can be inferred that even though the model was not prepared at the dry condition, the capillary barrier effect works efficiently with the suitable soil configuration and slope angle.

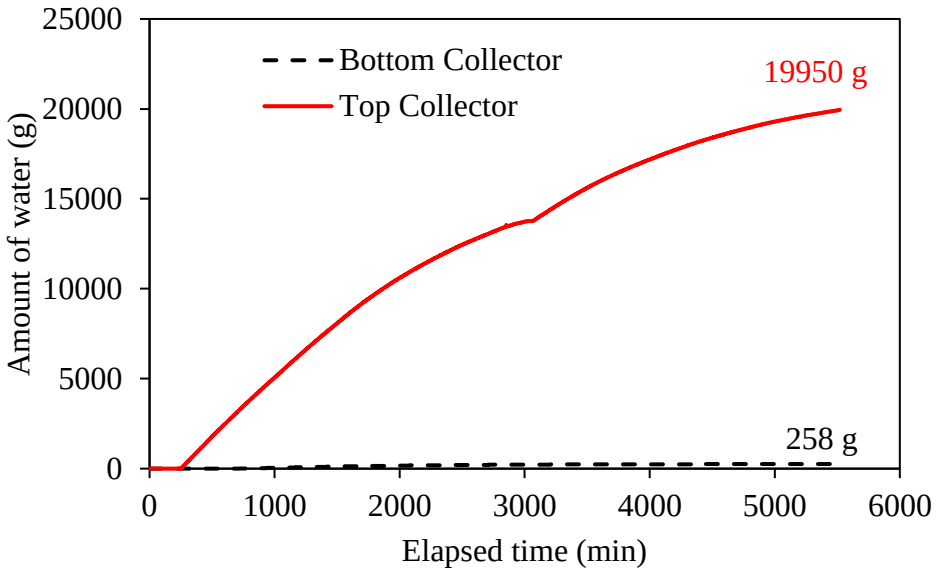

Figure 3 - 39 Time history of the drainage water for Case 6

Sensor readings are presented in Figure 3 - 40, Figure 3 – 41, and Figure 3 - 42. There were no changes in the saturation degrees inside the bottom layer (GP) due to the continuous lateral follow from the top exit. In contrast, the saturation degrees inside the top layer (MS) had an increase of nearly 10% after the rainfall applied. According to results, the capillary effect continued during the testing time. Approximately 1% of cumulative water drainage obtained from the bottom exits. This amount might be occurred due to limited lateral drainage of the experimental system.

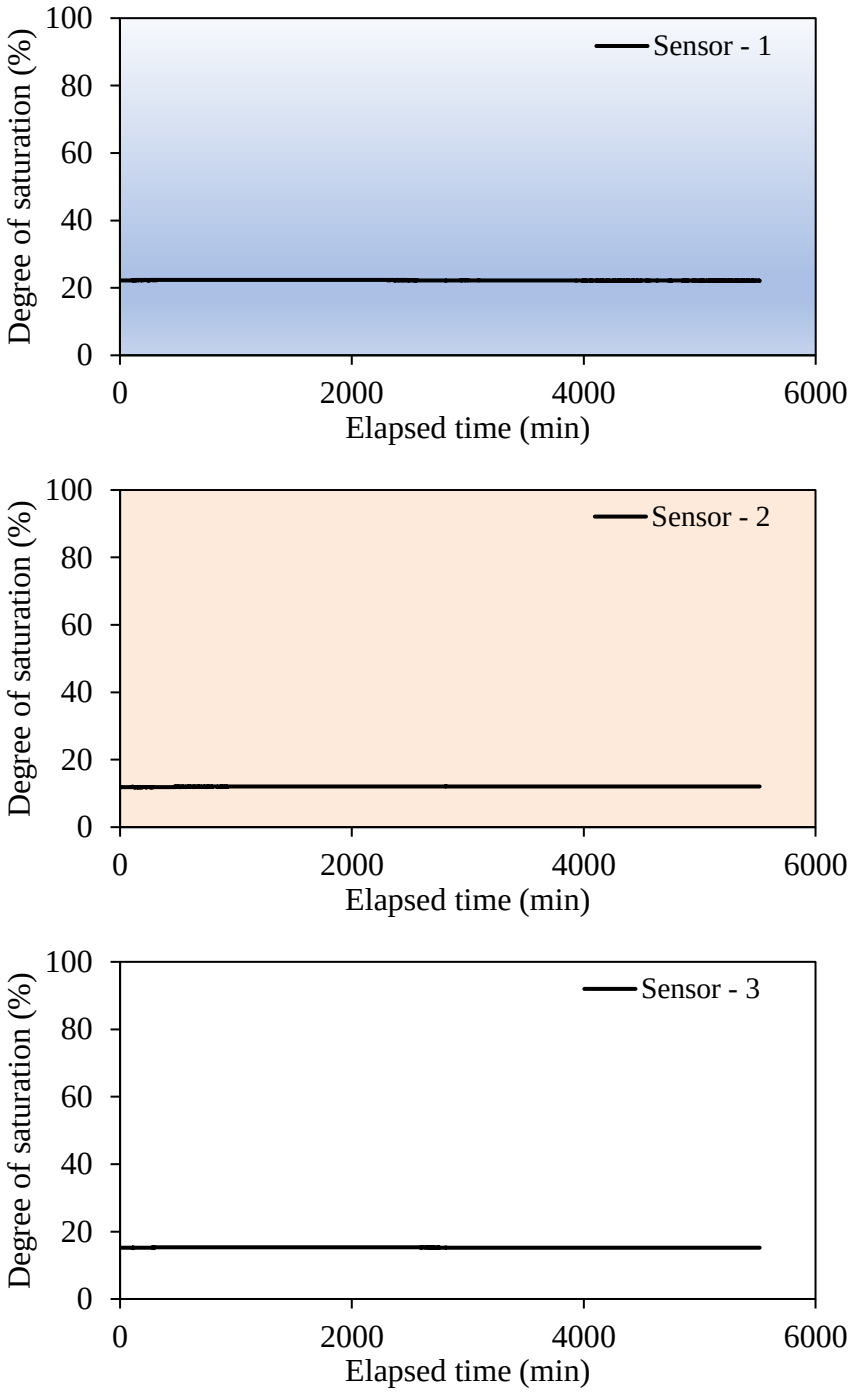

Figure 3 - 40 Saturation degrees of sensors 1, 2, and 3 for Case 6

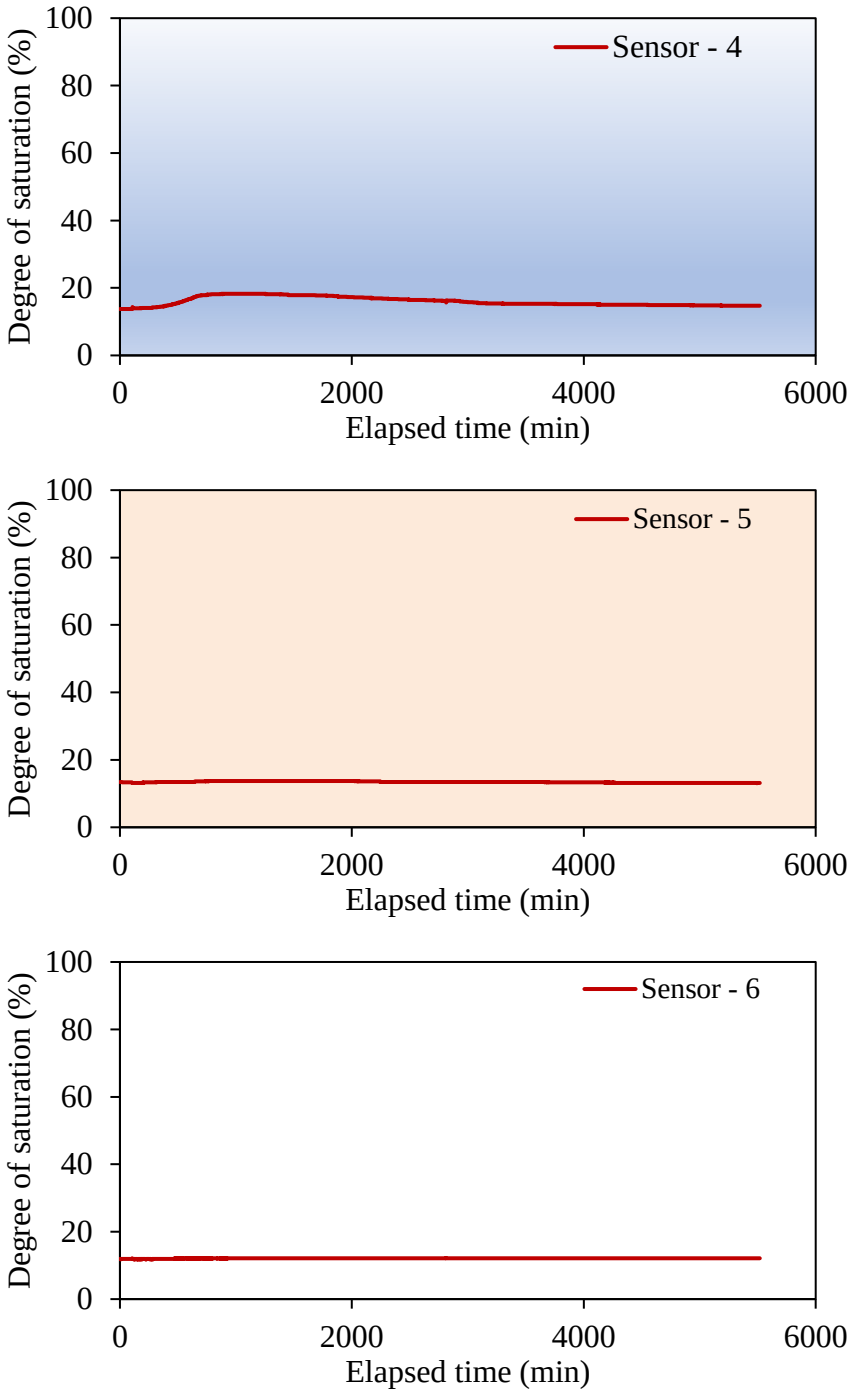

Figure 3 - 41 Saturation degrees of sensors 4, 5, and 6 for Case 6

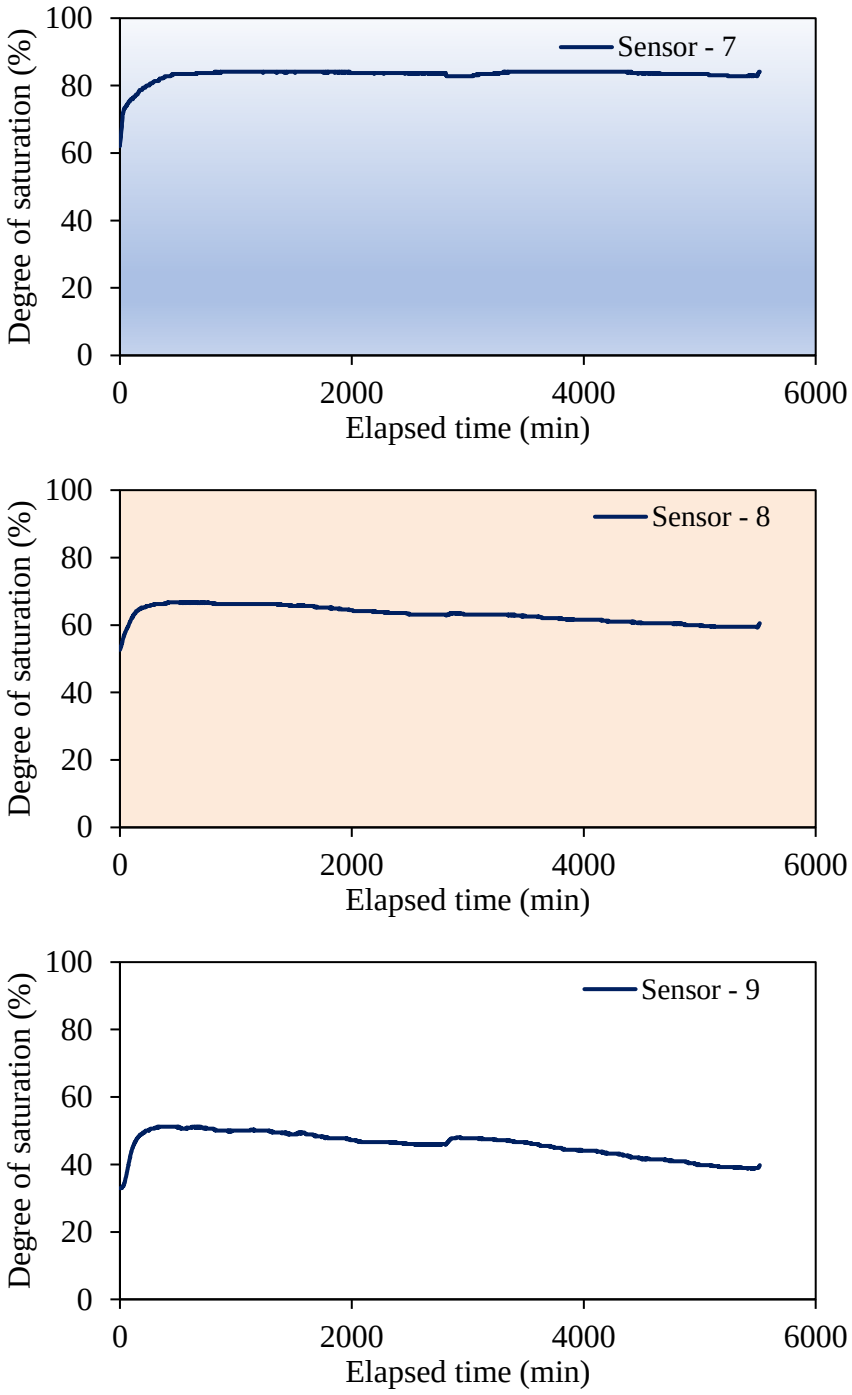

Figure 3 - 42 Saturation degrees of sensors 7, 8, and 9 for Case 6

3.5.3 Discussion on Capillary Barrier Model Results

One of the main objectives of this research is to investigate the use of geogenic contaminated soil in the embankment. For that reason, a capillary barrier system is suggested, and the efficiency of the proposed method is tested experimentally. A capillary barrier model is planned to construct with the available in-situ soil as the finer layer (top) and contaminated soil as the coarser layer (bottom). Two different soil configurations were tested with different initial moisture content and different rainfall rates. The results of the capillary barrier models are shown in Section 3.5.

The performance of models was examined according to the changing of saturation degrees in both layers and time histories of drained water. Table 3 – 4 summarizes the overall results. It can be seen that the capillary barrier model – II, which combines medium sand (MS) as a top layer and gravel (GP) as a bottom layer, gives satisfactory results. However, the capillary barrier model – I did not have any capillary barrier effects although it was tested with a slight rainfall rate and dry condition too.

Effects of soil configuration

The SWCC and hydraulic conductivity function relationships for both models were investigated to clear understanding of the occurrence of the capillary barrier effect on both models. The CB_I Model does not have any lateral flow during all the six cases. The SWCC and hydraulic conductivity function of the CB_I model is illustrated in Figure 3 – 43. The final saturation degrees range, both in the finer and coarser layers, are also shown in Figure 3 – 43. At the approximated equilibrium suction zone, which is obtained from the final saturation degrees reading from the experiments, it is seen that the related hydraulic conductivity of the bottom layer (silica sand - SS) is higher than the top layer (medium sand - MS). At that range, the capillary barrier effects have already diminished.

On the other hand, CB_II models have an equilibrium suction range where the hydraulic conductivity of the bottom layer (gravel - GP) is lower than the top layer (medium sand - MS), as shown in Figure 3 - 44. With an approximated equilibrium suction range, the hydraulic conductivity of the GP is about 1000 times lower than MS. According to these results, it can be seen that the equilibrium suction is not related to the initial preparation saturation degree. Although CB_I models were prepared at a dry condition (Case 1), the capillary barrier effect did not occur due to the equilibrium suction range where hydraulic conductivity of fine soil (MS) higher than the coarse one (SS). Therefore, the hydraulic conductivity relationship at the equilibrium suction generated the occurrence of a capillary barrier effect regardless of initial preparation saturation.

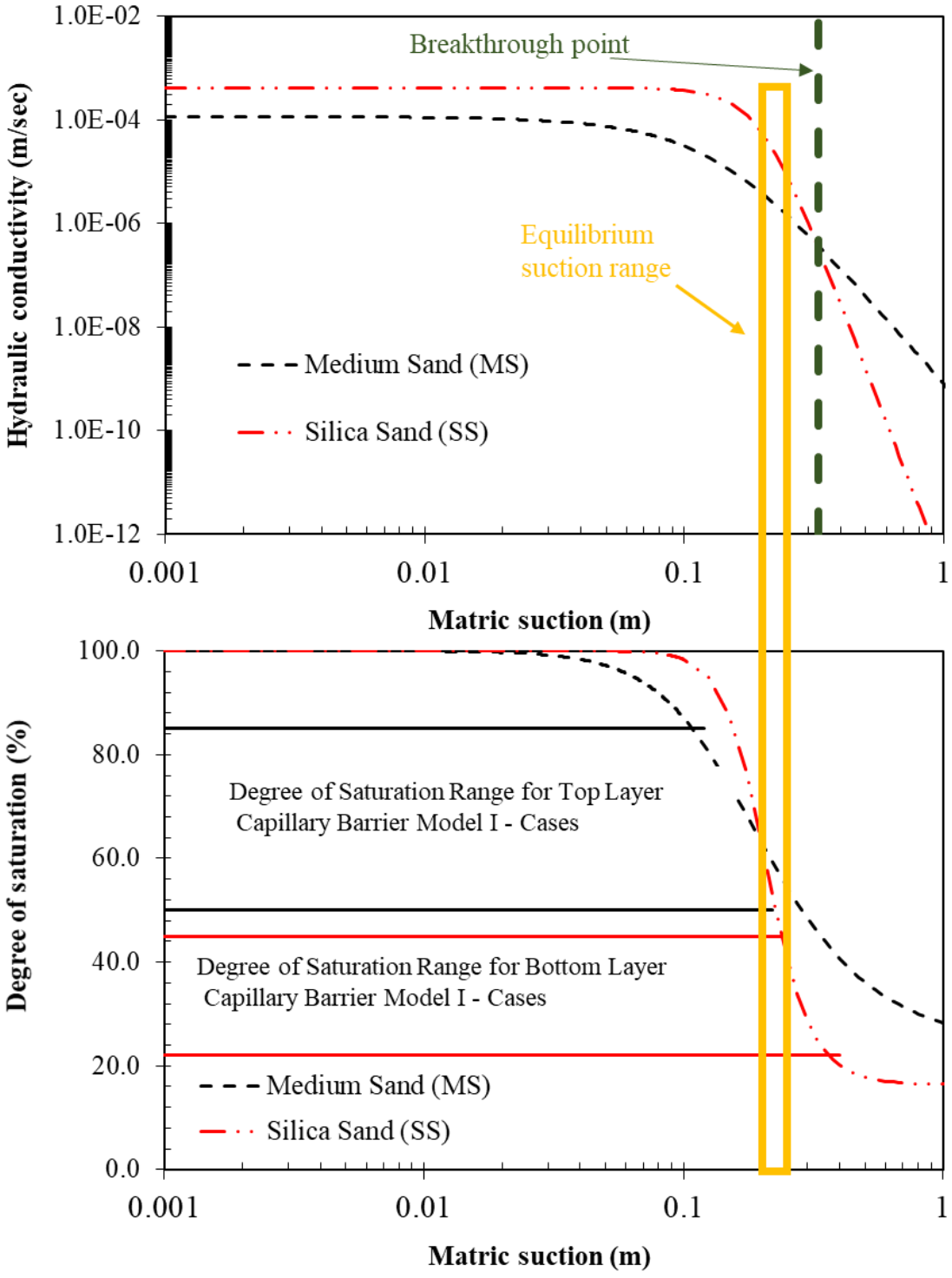

Figure 3 - 43 Representation of hydraulic conductivity relationship CB_I models

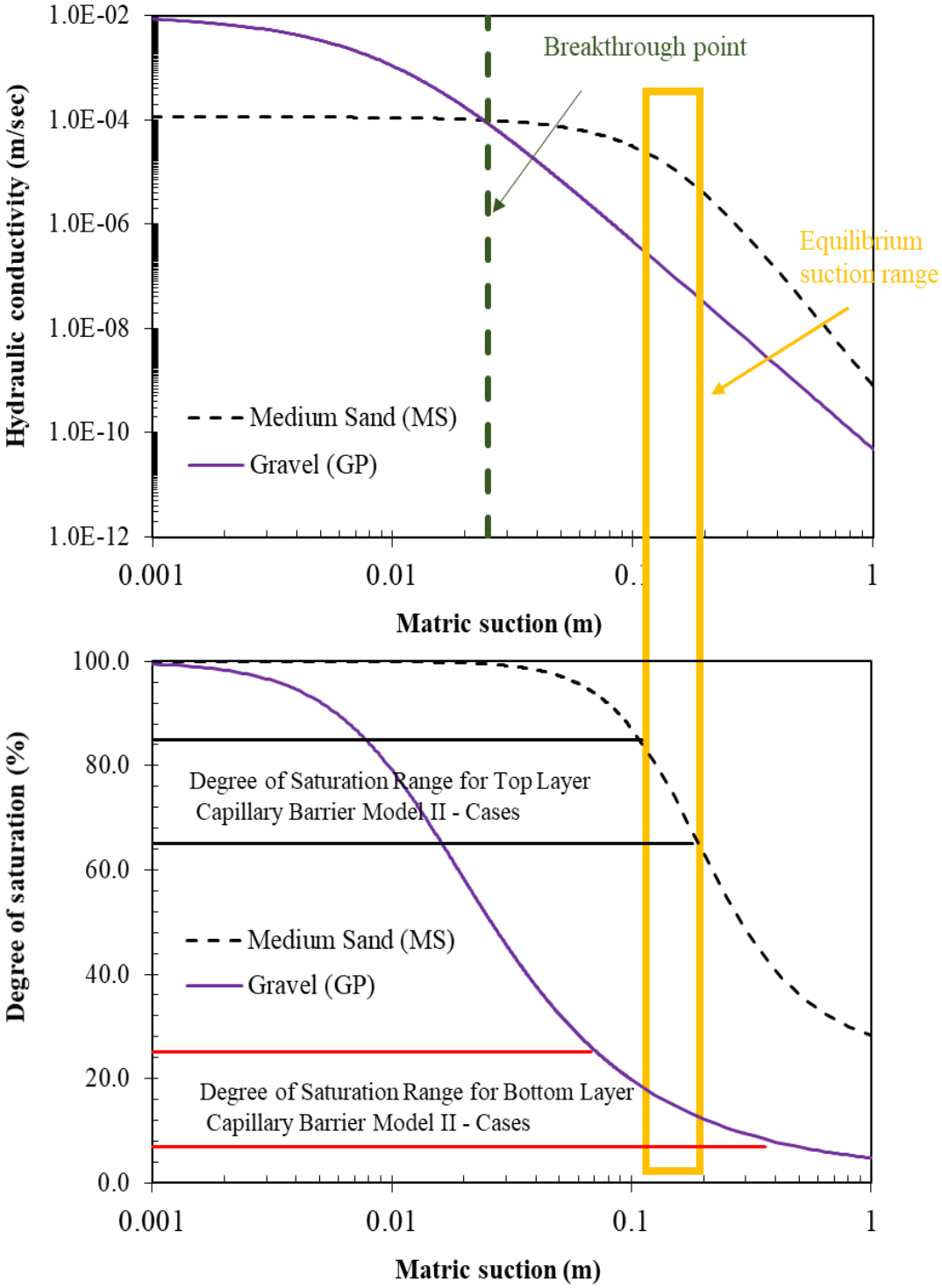

Figure 3 - 44 Representation of hydraulic conductivity relationship CB_II models

Table 3 - 4 Summary and results of the capillary barrier experiments

Case	Cover soil	Contaminated soil	Condition before rainfall	Saturation degree of the cover layer before rainfall	Saturation degree of the contaminated layer before rainfall	Rainfall intensity (mm/hr)	Rainfall duration (hr)	Barrier efficiency (%)
1	Medium sand	Silica sand	Dry	1-3%	0-1%	3.22	2880	0
2	Medium sand	Silica sand	OMC	70-80%	7-35%	3.94	1440	0
3	Medium sand	Silica sand	Drawdown	35-60%	10-45%	6.64	2500	0
4	Medium sand	Gravel	Dry	2-3%	3-8%	2.72	49830	100
5	Medium sand	Gravel	OMC	75-80%	13-25%	1.96	1430	77
6	Medium sand	Gravel	Drawdown	38-55%	13-22%	2.29	5520	99

"OMC" condition means that the cover soil (medium sand) was prepared at optimum moisture content.

"Drawdown" condition means that the soil layers were prepared at optimum water content (OMC), then saturated and drained to reach the equilibrium.

Effects of preparation moisture content

The effect of preparation moisture content was studied. In Figure 3 - 45 and Figure 3 – 46, initial preparation degrees of saturation and final degrees of saturation during the testing period are represented for the CB_I models and CB_II models, respectively. It is seen than the final degree of saturation at the boundary of investigated cases that belong to the same models are nearly equal at the top layer and the bottom layer of the capillary barrier models regardless of initial preparation condition. It is considered that, before the occurrence of the capillary barrier effect, first of a suction equilibrium comes true in soil media; after that, the capillary barrier effect occurrence might be generated at that equilibrium suction. Therefore, the initial preparation degree of saturation does not affect the existence of the capillary barrier effect.

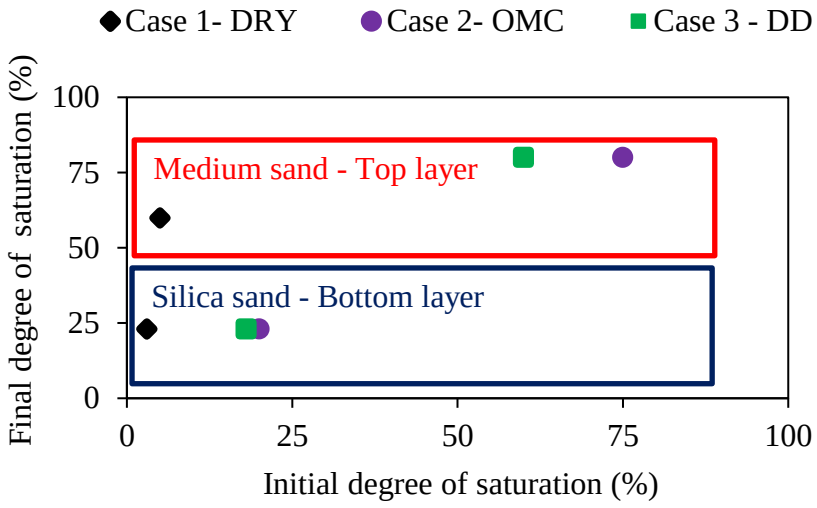

Figure 3 - 45 The effects of preparation saturation degree for CB_I Models

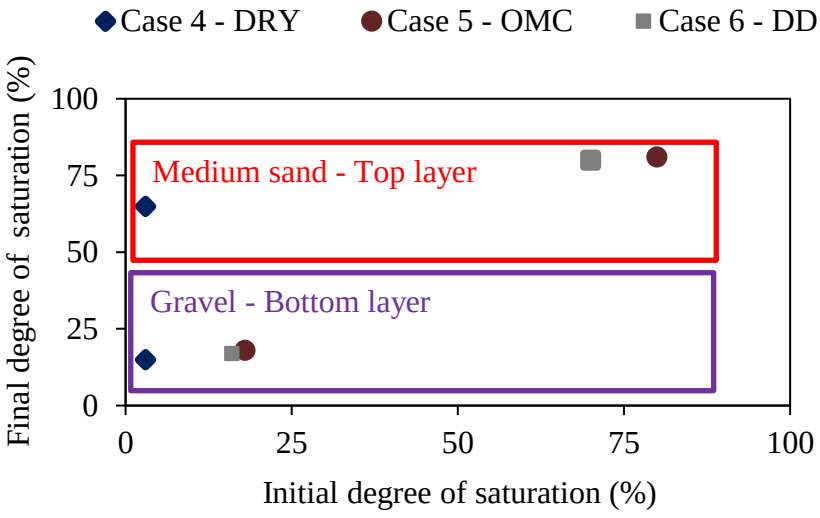

Figure 3 - 46 The effects of preparation saturation degree for CB_II Models

Time-dependent barrier performance

The time-dependent barrier performance of the capillary barrier system was investigated. Figure 3 – 47 shows the time-dependent drainage percentage from top exits and bottom exits of Case 5 (CB_II Model). Case 5 is selected due to its specific drainage results; both top and bottom collectors had drained water. However, other cases results have only flowed out from the bottom collector or top collector. The changing of cumulative drained water within 30 minutes time interval was selected for understanding the time-dependent barrier performance of Case 5. Then, the ration of drained water of each collector was calculated by their percentage (dividing the total cumulative amount). According to Figure 3 – 47, it is seen that the optimum moisture content prepared case (Case 5) has drainage from the bottom exit at the beginning of the experiment. However, after a specific time, the water started to flow out from the top exit as a lateral flow. After the equilibrium, the drainage ration of both layers becomes constant. It is considered that initial drainage water from the bottom exits is triggered by non-storable water, which comes from the preparation of the tank. Therefore 420 minutes later, starting from the experiment, this drainage characteristic changed, and water started to drain from top exits due to the capillary barrier effect. At the end of the test, a constant time-dependent barrier performance was obtained. At the end of the test, 77% of the water drained from the top exit.

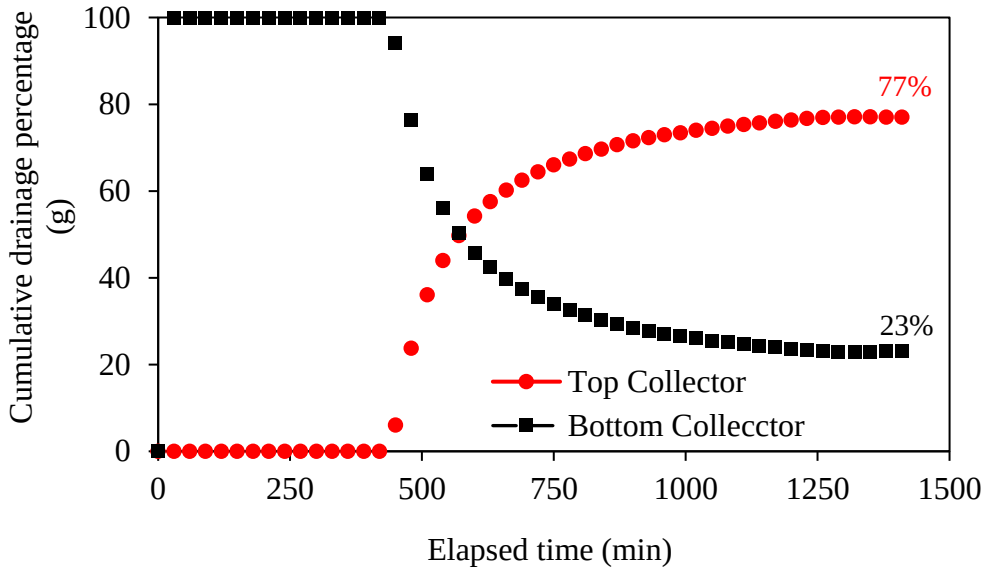

Figure 3 - 47 Time-dependent barrier performance of Case 5

Limitation of laboratory test for the capillary barrier model

A typical representation of the capillary barrier system, at the laboratory scale, and in-situ scale is illustrated in Figure 3 - 48. If an imaginary groundwater level is at the bottom of both the in-situ scale and laboratory scale, the generated negative pore water pressure values (suction) will have a different range between these two systems. At the in-situ scale, the generated boundary

suction will be higher than the laboratory scale. Due to suction difference at both systems, although the capillary barrier effect does not occur at the laboratory scale, it might arise in the in-situ scale (Figure 3 – 48).

Another limitation of the laboratory test is the limited drainage area for the lateral flow. In the laboratory, the drainage area is just three nozzle exits with a diameter of 10 mm. However, in-situ applications, more extensive drainage areas are available for the lateral flow. The wider drainage area might be more useful for the occurrence of the lateral flow inside the capillary barrier system.

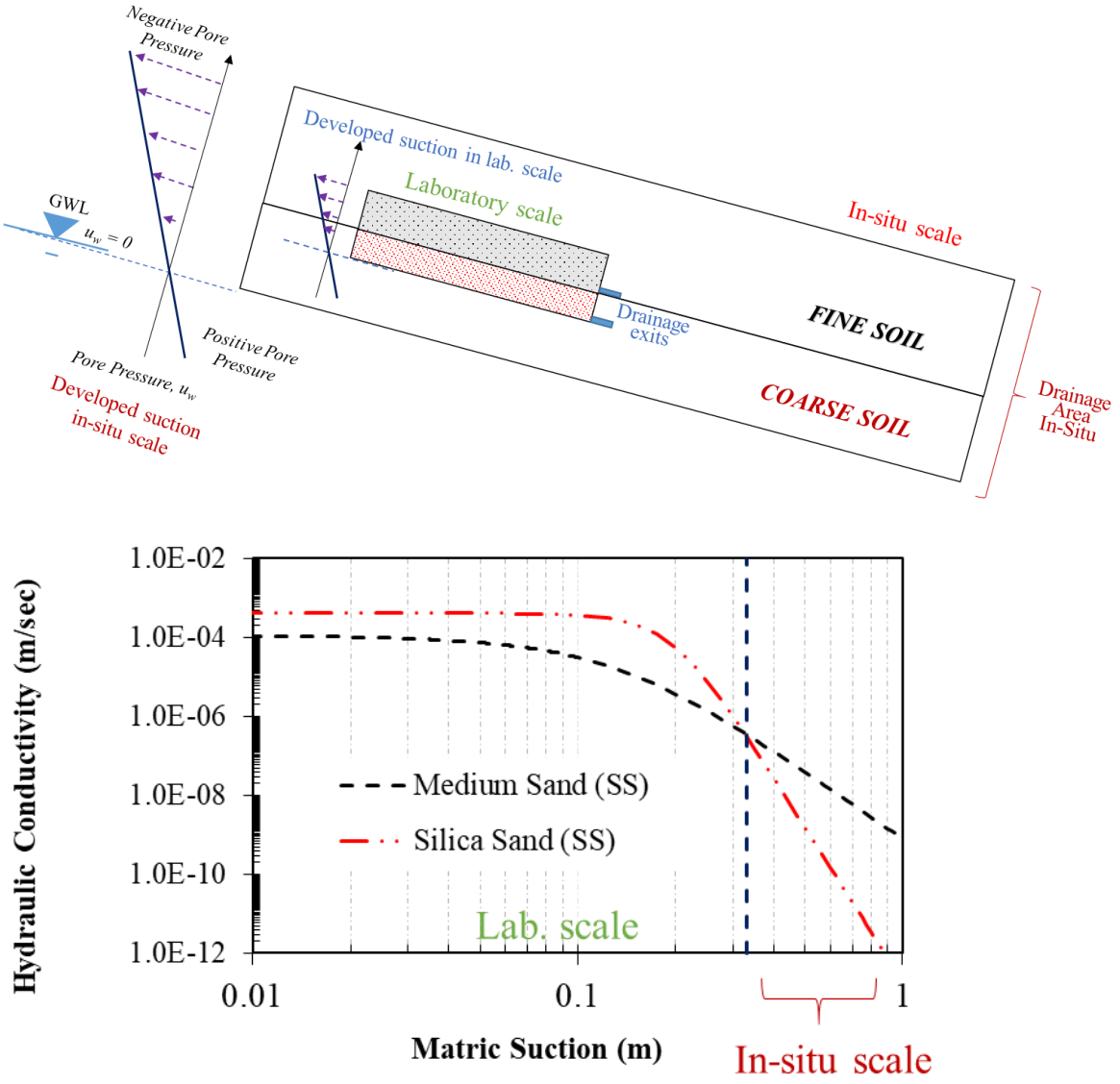

Figure 3 - 48 Comparison of laboratory scale and in-situ scale for capillary barrier systems

3.6 Summary and Conclusions

In this chapter, the materials used in the experiments and experimental program of this study are explained in detail. Methods for obtaining the unsaturated soil properties (soil-water

characteristic curves) are described, and unsaturated hydraulic conductivity function is estimated with van Genuchten equation and SWCC experimental test results.

Moreover, the setup, measuring devices, and experimental plan of the two-dimensional infiltration box test are described. In the last part of the chapter, the capillary barrier test results are presented and discussed. The main results obtained in this chapter can be summarized as follows.

A modified axis-translation technique with a microporous membrane instead of the ceramic disk was used for measuring SWCC. Using of microporous membrane instead of a ceramic disc gives an advantage for shorting the testing time.

For the gravel as a contaminated soil overlain by medium sand as a cover soil, the capillary barrier successfully works. In contrast, for the silica sand as a contaminated soil versus medium sand as a cover soil, the capillary barrier did not occur. It is understood that at the equilibrium state with the slope angle 26.6 degrees, hydraulic conductivity of gravel is smaller than hydraulic conductivity of cover soil, while hydraulic conductivity of silica sand is higher than the cover soil.

Initial water content does not affect the occurrence of a capillary barrier. That is because the capillary barrier takes place after the equilibrium matric suction came true inside the soil media regarding with preparation slope angle.

The capillary barrier effect is a reversible phenomenon. As a result of drawdown cases, it is understood that CB can recover itself after saturation and drainage periods.

The distribution of water content is higher near the outlets. In the experiments, only drainage holes were used as exits; however, in the field applications, wider drainage areas are generally available. This result may be a restriction of a laboratory tank test.

CHAPTER 4: DRAINAGE LAYER SYSTEM

4.1 General Remarks

This chapter focuses on the drainage layer system. The experiment program and results are explained. It consists of three main sections, which are details of the laboratory infiltration box test, results obtained from the experimental studies, and discussion of the results, respectively.

The drainage layer system is suggested to use geogenic contaminated soils in the embankment. The efficiency of the proposed system was checked with a laboratory infiltration box test. The experimental procedures and details of it are described in Section 4.2. The second part of the chapter includes the experimental results obtained from the laboratory studies in Section 4.3. The last part consists of the discussion of the obtained results. The effects of different utilization geometry and initial preparation moisture content are discussed in Section 4.4.

4.2 Laboratory Infiltration Box Test for Drainage Layer System

In the experimental works, three drainage layer models were investigated using two different materials. As a finer material (poorly graded medium sand (MS)) was used in the experiments. It is constituted as contaminated soil and placed in the core of embankment. On the other hand, the coarser material (poorly graded gravel (GP)) was used as a drainage layer due to its higher saturated hydraulic conductivity than medium sand (MS).

The experimental model test system is constructed as a half embankment section. The finer layer (MS) soil is assumed as slightly contaminated, and it is thought to lay out under the pavement layer in the field applications. The reason for using a fine layer as a representation of contaminated soil is to propose a method for finer contaminated soils. In this dissertation, the capillary barrier system is suggested for the utilization of coarser contaminated soil; however, the drainage layer system is recommended for the utilization of finer contaminated soil. The drainage layer experimental system is illustrated in Figure 4 – 1.

The drainage layer models tested according to three different geometric arrangements. In the first model, the contaminated soil is placed just under the pavement layer without any side slope between contaminated soil and drainage layer soil (vertically). It is named DL_I, which denotes the drainage layer (DL), the first model (I) (shown in Figure 4 - 2).

In the second model, the contaminated soil is also placed under the pavement; however, the utilization of area contaminated soil is lessened using a side slope with a 45 degrees angle.

In this model, although the contaminated area is narrow, a safer design was aimed. The second model is named as DL_II (shown in Figure 4 - 2).

In the third model, the contaminated soil is also located under the pavement; however, the investigated area is expanded towards the side slope with an angle of 45 degrees. In this model, the deposited region is considered the widest of the models as a utilization volume of contaminated soil. However, the contaminated area is not only located under the pavement. Therefore, rainfall is also applied to the contaminated soil. The third model is named as DL_III (shown in Figure 4 - 2).

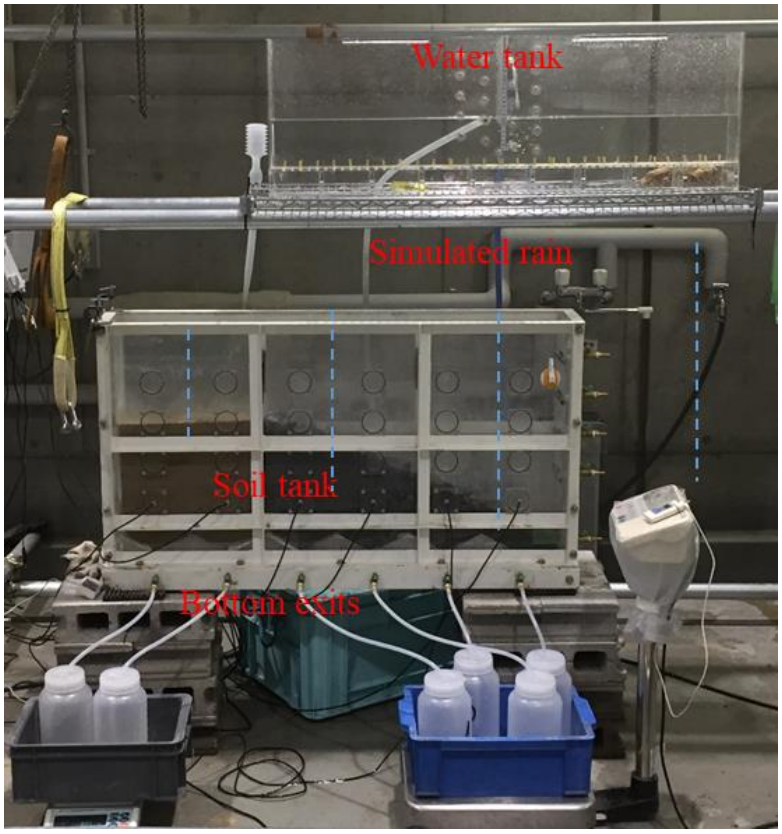

Figure 4 - 1 Experimental system for the drainage layer models

During the experiments, all three models are tested with two different initial preparation conditions: optimum moisture content preparation case and drawdown case (free drainage after the saturation). Optimum moisture content cases may show the typical construction method of an embankment. Thus, in the experiment system, this condition tried to be tested. The finer layer (medium sand) was placed according to optimum moisture content before applying the rainfall. Drawdown cases are conducted to generate an equilibrium condition of pore-water pressure and volumetric water content before rainfall infiltration. The drawdown case is created as follows: first, the contaminated fine-grained soil (medium sand) is prepared at optimum moisture content, then the tank is saturated by closing the exit valves. After that, free drainage was applied to reach the pore water pressure equilibrium between soils until there is no more

water flow from the exits. Then, adjusted rainfall was implemented just over the side slope. Details of the infiltration box tests for all cases are shown in Table 4 – 1.

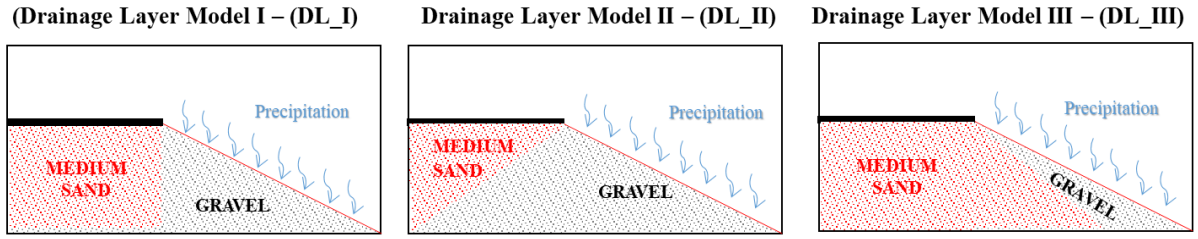

Figure 4 - 2 Investigated model geometries

Table 4 - 1 Testing details of the drainage layer models

Case	Soil combination (Drainage layer – Contaminated soil)	Condition before rainfall	Saturation degrees of the contaminated layer before rainfall	Saturation degrees of the drainage layer before rainfall	Rainfall intensity (mm/hr)
1	DL_ I (Medium sand – Gravel)	OMC	75-80%	2-4%	2.93
2	DL_ I (Medium sand – Gravel)	Drawdown	58-70%	15-20%	2.98
3	DL_ II (Medium sand – Gravel)	OMC	85%	2-5%	2.76
4	DL_ II (Medium sand – Gravel)	Drawdown	85%	15-20%	3.72
5	DL_ III (Medium sand – Gravel)	OMC	75-80%	12-20%	2.79
6	DL_ III (Medium sand – Gravel)	Drawdown	70-85%	15-22%	3.02

4.3 Results of Experimental Studies on Drainage Layer Models

This section presents the results of drainage layer models. The drainage layer models are tested under different rainfall rates, rainfall duration, and utilization geometries. The results presented as changing of the saturation degree inside soil and time histories of the drained water from separated exits.

4.3.1 Drainage Layer Model Results for the DL_I

The DL_I model was tested under two different cases: optimum moisture content case and drawdown case. The geometry of the prepared model and the sensor locations are presented in Figure 4 – 3. Two different background fills are selected for the figures which represent the saturation degree. The altered background fill is denoted sensor section. The yellow background fill shows the sensor inside the contaminated layer (medium sand) (sensor 5 and sensor 6). The white background fill represents the sensor inside the drainage layer (sensor 1, sensor 2, sensor 3, and sensor 4).

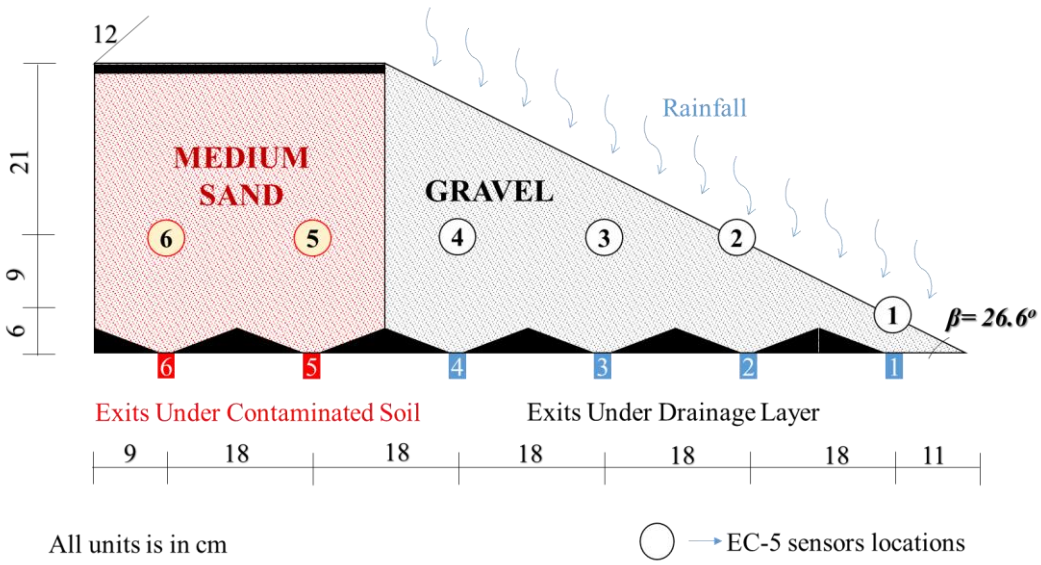

Figure 4 - 3 General schematic of the DL_I models

Case 1 - Optimum Moisture Content Case - DL_I OMC

The DL_I OMC – Case 1 model was subjected to a rainfall of 2.93 mm/hr for 4320 minutes (72 hours). At the beginning of the experiment, the contaminated layer (medium sand-MS) was tried to compact at optimum moisture content and standard Proctor relative density. The side slope (drainage layer) was constituted with gravel (GP) according to the target dry density, which is the same value of the all experimental studies of GP. The dry preparation densities are 1.80 gr/cm^3 and 1.675 g/cm^3 for the MS and GP, respectively. The initial saturation degrees (before rainfall application) were around 75% to 80% for the contaminated layer (MS) and 2% to 4% for the drainage layer (GP). After the preparation of the tank, the adjusted rainfall intensity was applied only over the side slope (in Figure 4 - 3).

During the infiltration box test, the water comes from the bottom exits under the contaminated layer (MS), and the drainage layer (GP) are recorded separately. Exits 1 – 2 – 3, and 4 located under the drainage layer (GP); and exits 5 and 6 situated under the contaminated soil (MS). The time histories for two different exits regions were separately logged. The

locations of the exits are shown in Figure 4 – 3. With the use of exits time histories, the effectiveness of the drainage layer is checked. Figure 4 – 4 shows the time histories of exits under the contaminated soil and drainage layer. Also, Table 4 - 2 shows the percentage of the drainage amount from different exits. According to obtained results, a large amount of water flows out under the drainage layer (nearly 10932 grams at the end of the test). Although there is water drainage under the contaminated layer, almost 88% of drained water goes out from the drainage layer.

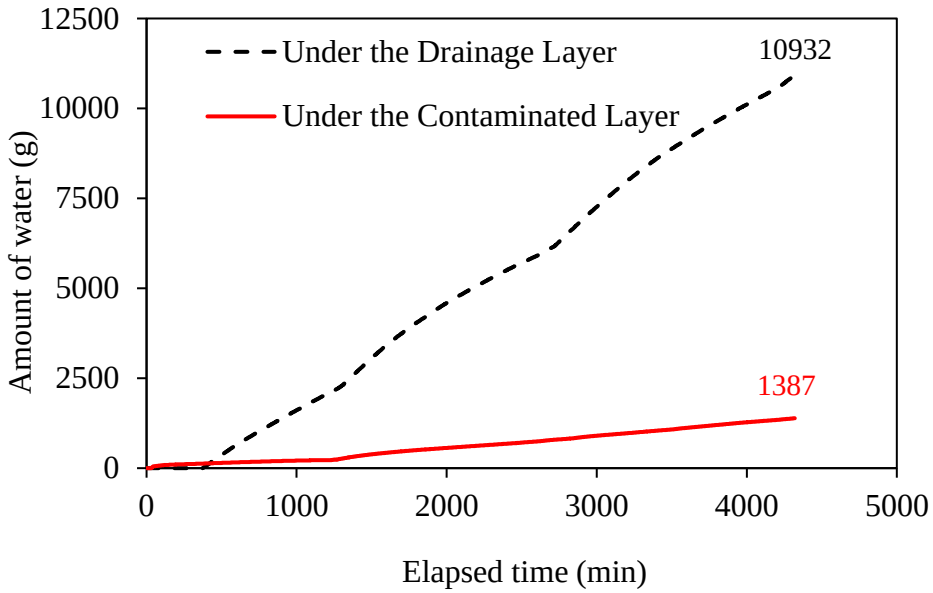

Figure 4 - 4 Time history of the drainage water for Case 1

Table 4 - 2 Total drained water from exits for Case 1

Exit	Exit location	Amount of water (g)	Percentage (%)	Amount of water each layer (g)
1	Under the drainage layer	3340	27	10931
2	Under the drainage layer	3087	25	
3	Under the drainage layer	3155	26	
4	Under the drainage layer	1350	11	
5	Under the contaminated layer	673	5	1387
6	Under the contaminated layer	652	6	

During the test, the changing of the degree of saturation recorded with six EC-5 volumetric moisture content sensors. They logged readings every two minutes. The degree of saturation versus time is presented in Figure 4 – 5, and 4 – 6. According to the results, a slight decrease was seen in sensors inside the contaminated layer (sensor 5 – 6) and a slight increase

under the drainage layer sensors. It might be explained that the rainfall did not apply over the contaminated layer (Figure 4 - 3).

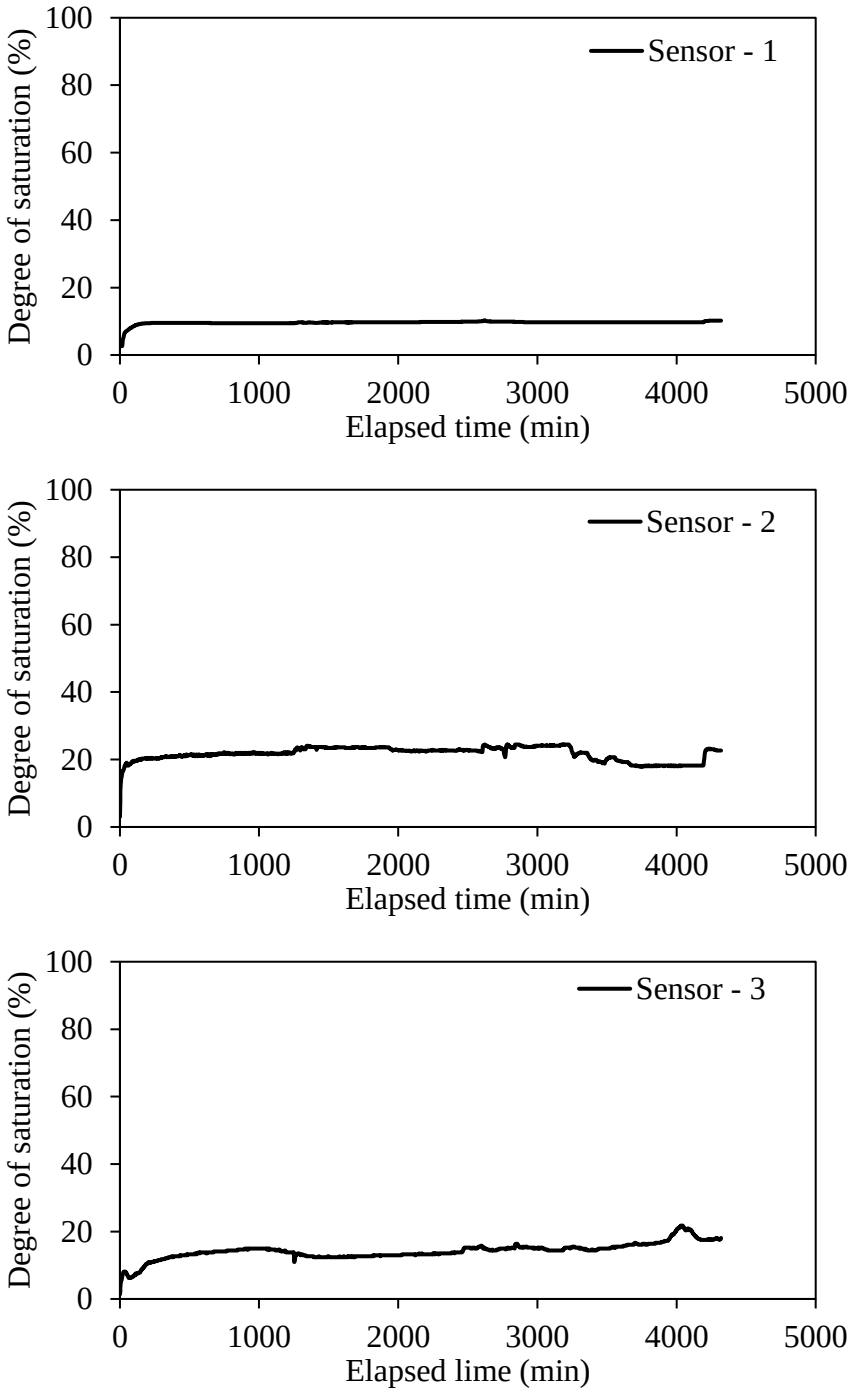

Figure 4 - 5 Saturation degrees of sensors 1, 2, and 3 for Case 1

Therefore, sensors 5 and 6, which are inside the contaminated layer, had a decreasing trend at saturation during the test. The water flow under the drainage layer started after the 374 minutes later from the rainfall application. Until 374 minutes, the drainage layer absorbed the water and then started to release. Although there is water drainage under the contaminated layer (1387 grams at the end of the test), a large amount of water flowed out the drainage layer (10932 grams at the end of the test). According to cumulative drainage water, only 11% percent of the

drained water collected under the contaminated layer. It might occur that the optimum moisture content prepared contaminated layer (medium sand - MS) did not storage all initially added water during the preparation case. Therefore, leftover water inside the medium sand flowed out from the exits 5 and 6, although the applied rainfall did not reach this region. The quick starting of the drainage under the contaminated layer is also a proof of it.

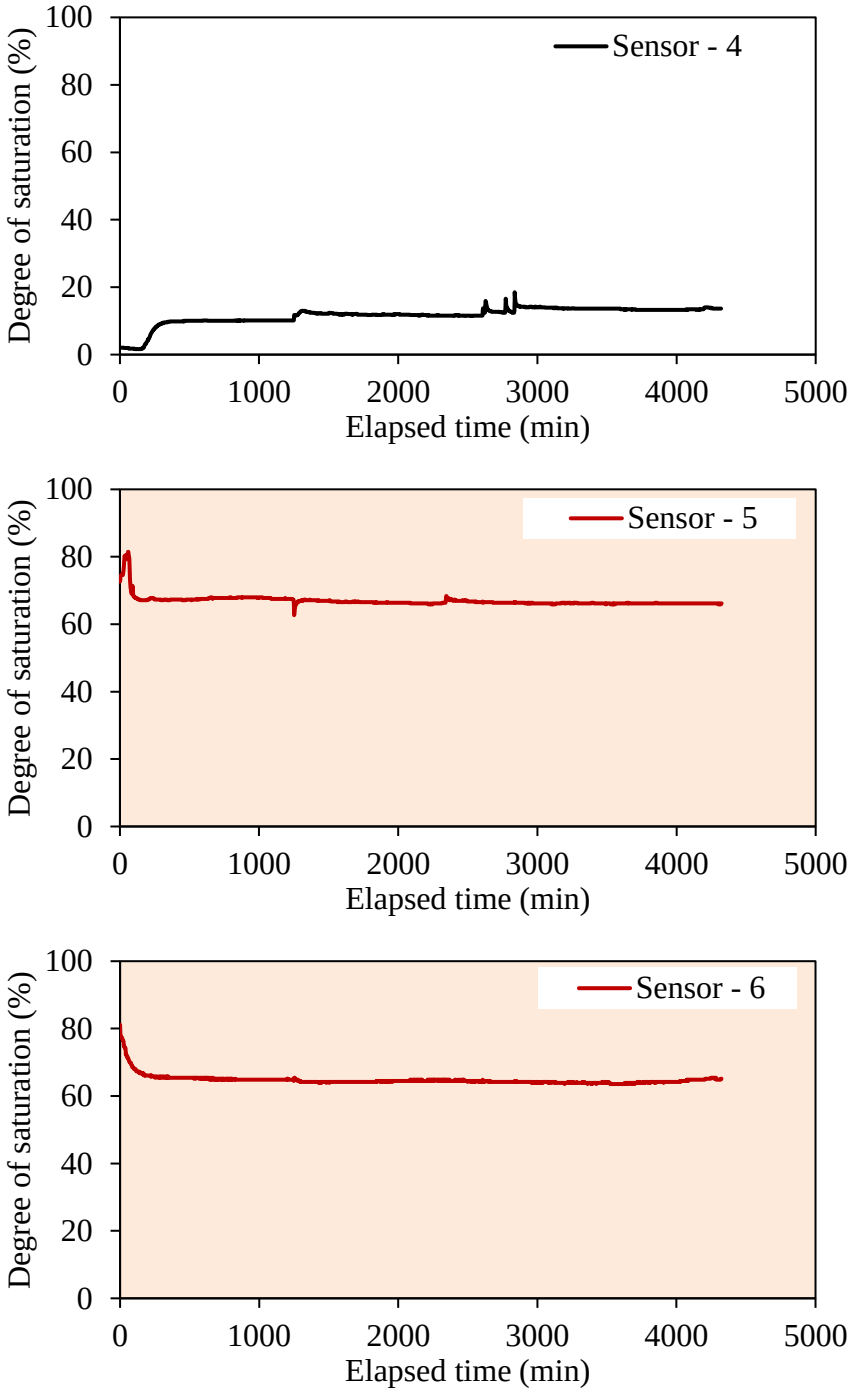

Figure 4 - 6 Saturation degrees of sensors 4, 5, and 6 for Case 1

Case 2 - Drawdown Case - DL_I DD

Case 2 (DL_I DD) model is tested after the drawdown period. The model was initially prepared with optimum water content for the contaminated layer (medium sand-MS) and nearly dry with

the drainage layer (gravel-GP). The preparation densities are 1.80 g/cm^3 and 1.65 g/cm^3 for the MS and GP, relatively. After the compaction of the tank, a saturation or nearly saturation condition was applied by closing the valves. Then, the drainage valves were opened. Before starting the rainfall, the exits outlets were checked until there is no extra water drainage. At the end of a drawdown period, the adjusted rainfall was applied. Case 2 tested with a rainfall of 2.98 mm/hr for 3960 minutes (66 hours). Figure 4 - 7 shows the time histories exit under the contaminated layer and drainage layer. Also, Table 4 - 3 shows the percentage of the drainage amount from different exits at the end of the test. According to cumulative drainage water, 98% percent of the drained water collected under the drainage layer. Nearly 8% difference occurs between the results of optimum moisture content case (Case 1) and drawdown case (Case 2). This difference is considered to cause non-storable water during Case 1.

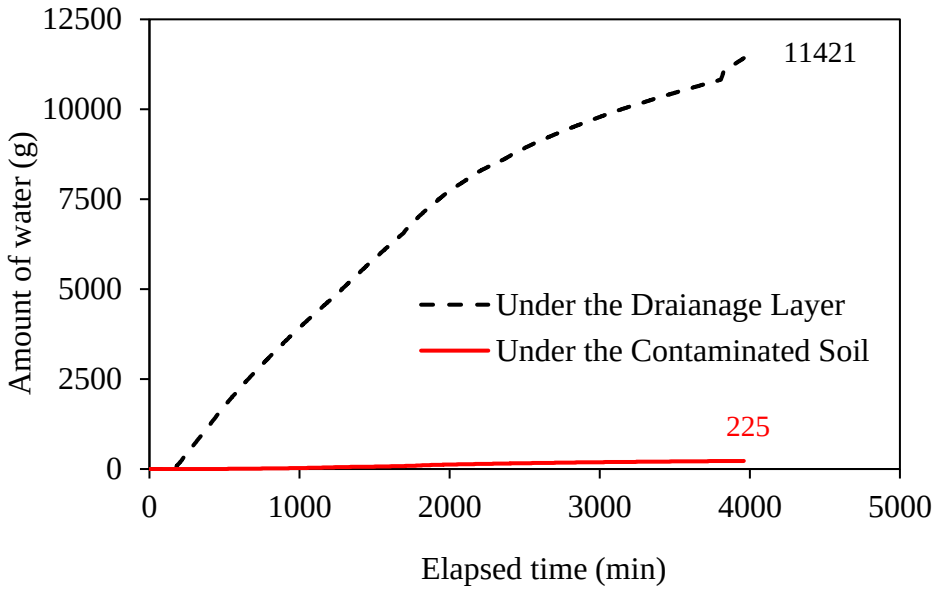

Figure 4 - 7 Time history of the drainage water for Case 2

Table 4 - 3 Total drained water from exits for Case 2

Exit	Exit location	Amount of water (g)	Percentage (%)	Amount of water each layer (g)
1	Under the drainage layer	2508	22	11421
2	Under the drainage layer	4104	35	
3	Under the drainage layer	2374	21	
4	Under the drainage layer	2436	21	
5	Under the contaminated layer	124	1	225
6	Under the contaminated layer	100	1	

The degree of saturations recorded from six sensors is presented in Figure 4 – 8, and Figure 4 - 9. The saturation degree near the rainfall applied area had higher values than the far ones. Thus, sensor - 5 has a higher saturation degree than sensor - 6. The sensors inside the drainage layer had relatively lower saturation concerning the contaminated layer due to its limited water storage capacity.

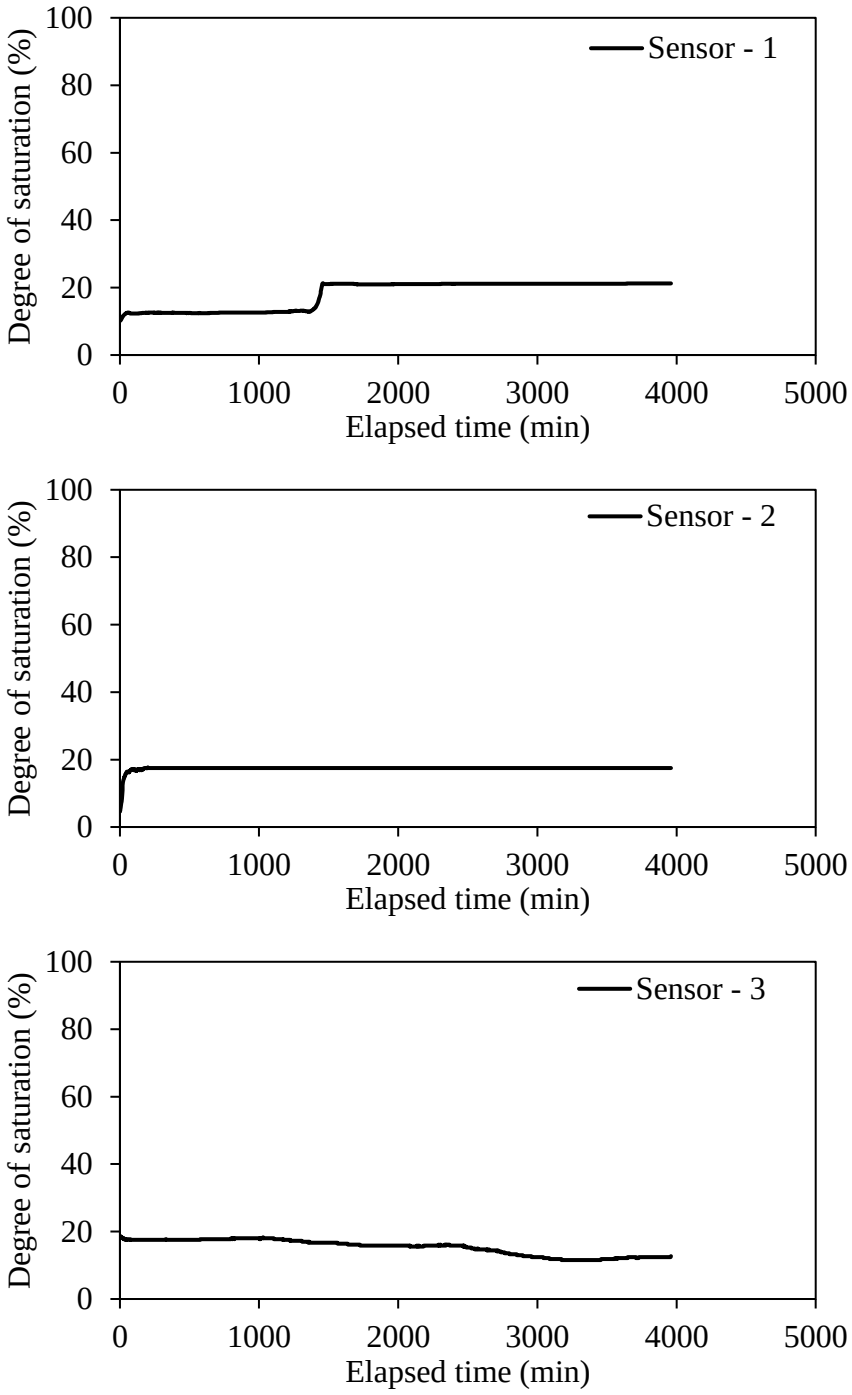

Figure 4 - 8 Saturation degrees of sensors 1, 2, and 3 for Case 2

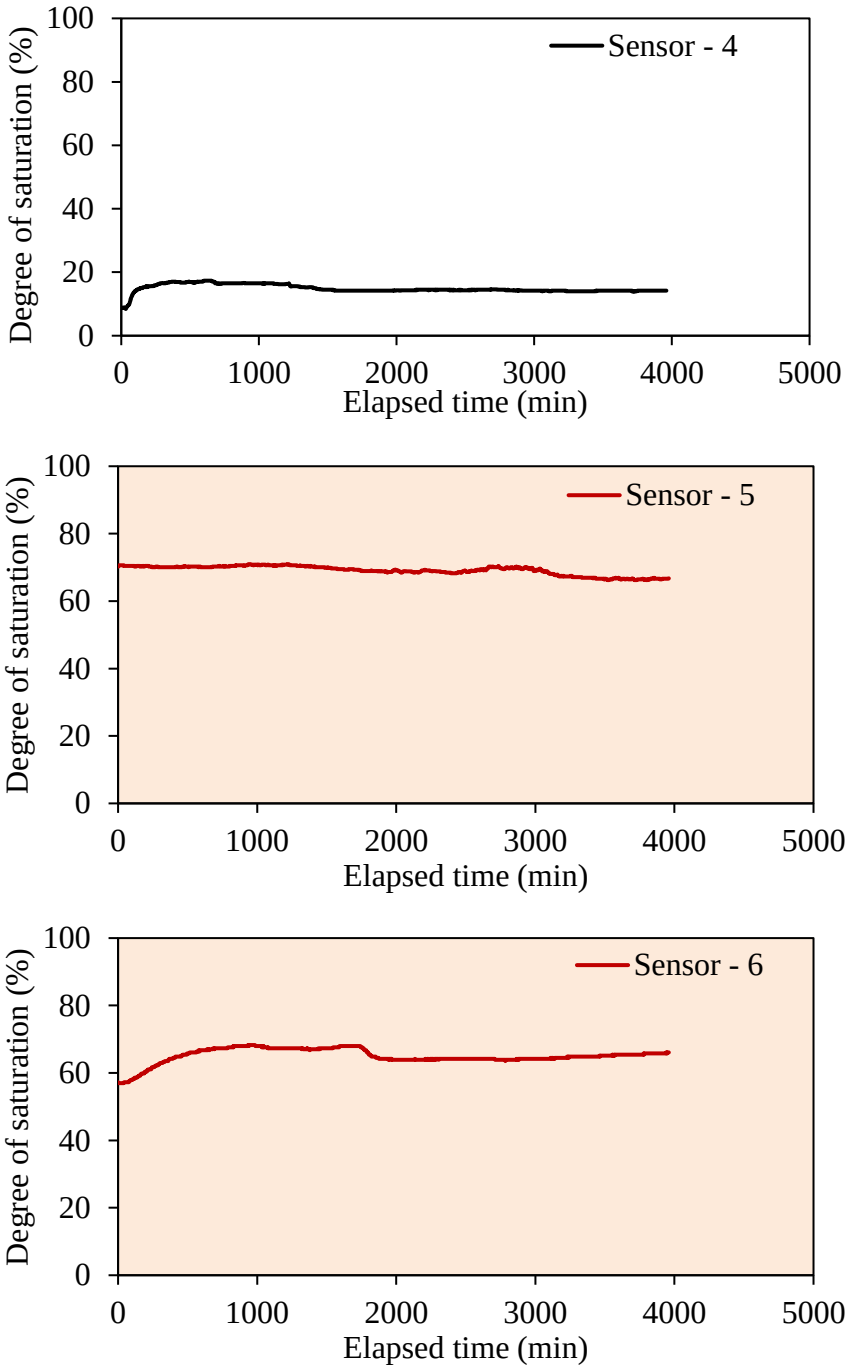

Figure 4 - 9 Saturation degrees of sensors 4, 5, and 6 for Case 2

4.3.2 Drainage Layer Model Results for the DL_II

The DL_II models was tested under two different cases: optimum moisture content case and drawdown case. The prepared model geometry and the location of the sensors are presented in Figure 4 – 10. Totally six sensors were used in the experiments. A sensor inside the

contaminated layer (sensor 6), and five sensors inside the drainage layer (sensor 1, sensor 2, sensor, sensor 4, and sensor 5).

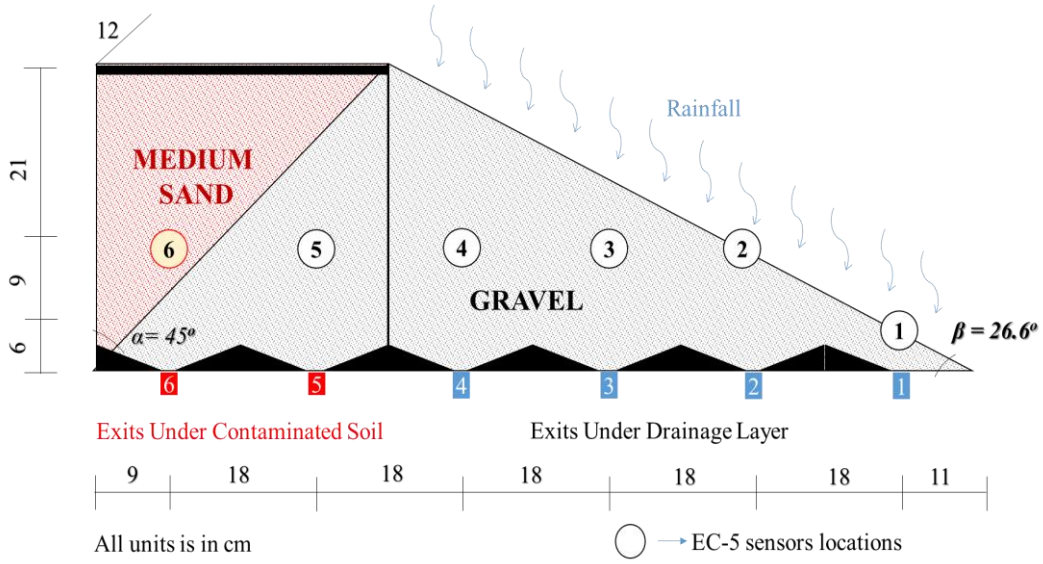

Figure 4 - 10 General schematic of the DL_II models

Case 3 - Optimum Moisture Content Case - DL_II OMC

The DL_II OMC – Case 3 model was subjected to a rainfall of 2.76 mm/hr for 3810 minutes (63.5 hours). The initial saturation degrees (before rainfall application) were around 85% for the medium sand (contaminated layer) and 2% to 5% gravel (drainage layer). The dry preparation densities are 1.80 g/cm^3 and 1.675 g/cm^3 for the medium sand and gravel, respectively. After the preparation of the tank, the adjusted rainfall intensity was applied.

The time histories for two different exits regions were separately recorded. The locations of the exits are shown in Figure 4 – 10. With the use of time histories of the two different layers, the effectiveness of the proposed model is checked. Figure 4 – 11 shows the time histories of exits under the contaminated soil and drainage layer soil. Also, Table 4 - 4 shows the percentage of the drainage amount from different exits. According to Figure 4 – 11 and Table 4 - 4, a large amount of drained water flows out under the drainage layer (nearly 9370 grams at the end of the test).

Even though there is water drainage under the contaminated layer (1037 grams at the end of the test), most of the water flowed out the drainage layer. According to results, only 9% percent of the drained water collected under the contaminated region. That amount of water might come from the preparation moisture of the contaminated layer. It can be understood from the drainage time histories. Although there is no drainage under the drainage layer, initially, water started to drain from exits 6.

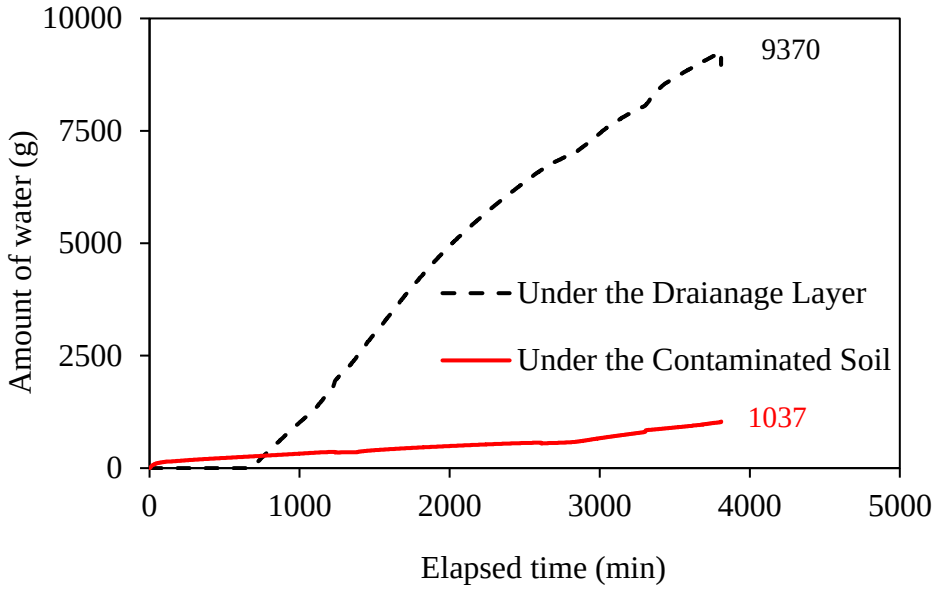

Figure 4 - 11 Time history of the drainage water for Case 3

Table 4 - 4 Total drained water from exits for Case 3

Exit	Exit location	Amount of water (g)	Percentage (%)	Amount of water each layer (g)
1	Under the drainage layer	1704	16	9370
2	Under the drainage layer	3490	34	
3	Under the drainage layer	2411	23	
4	Under the drainage layer	1766	17	
5	Under the contaminated layer	575	5	1037
6	Under the contaminated layer	462	4	

The saturation degrees of sensors versus timer is presented in Figure 4 – 12, and 4 – 13. Sensor – 6 inside the contaminated layer did not show a significant change during the experiment. It is nearly constant. However, the sensors inside the drainage layer had a slight increase after the starting of the rainfall. It might be explained that the applied rainfall flows out from the drainage layer. Because of that, the sensors inside the drainage layer had an increment at saturation reading.

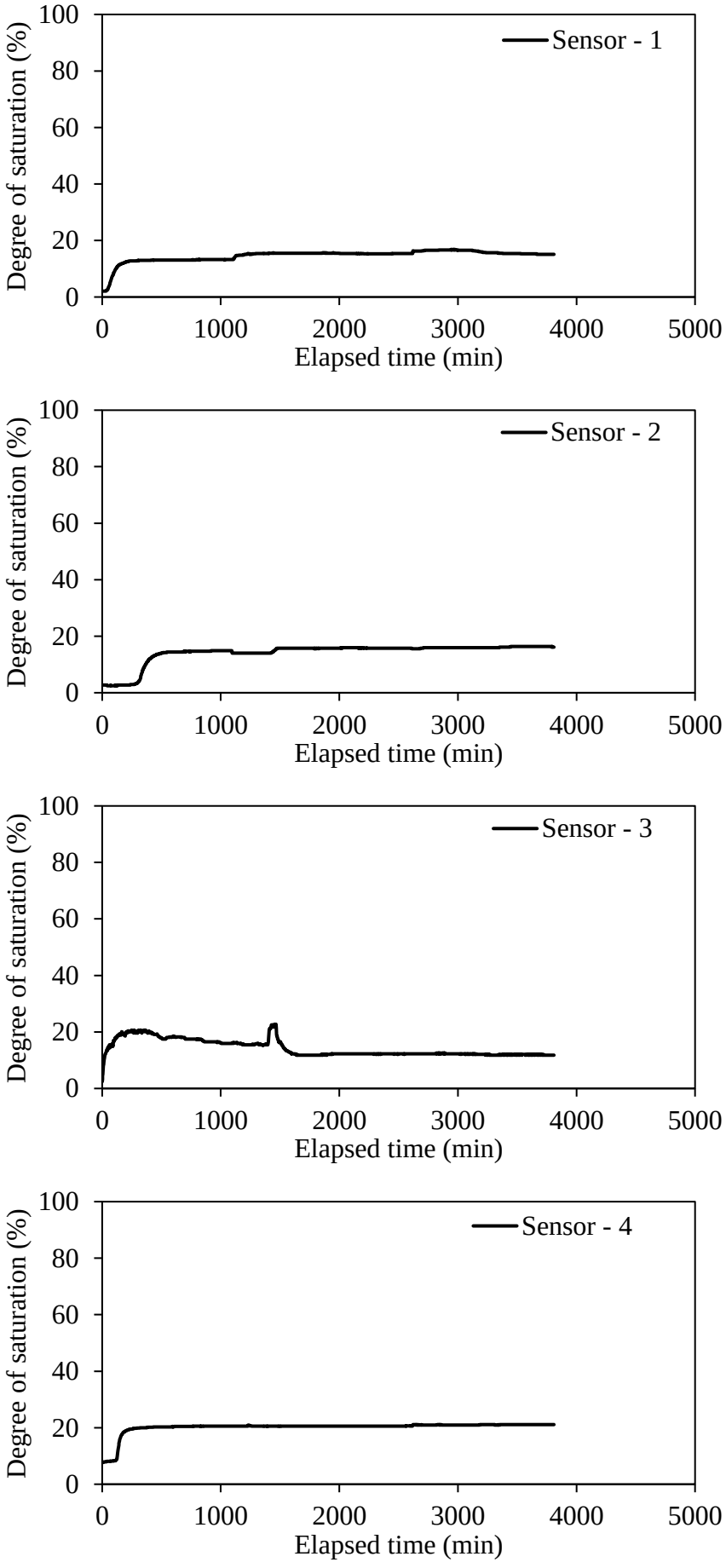

Figure 4 - 12 Saturation degrees of sensors 1, 2, 3, and 4 for Case 3

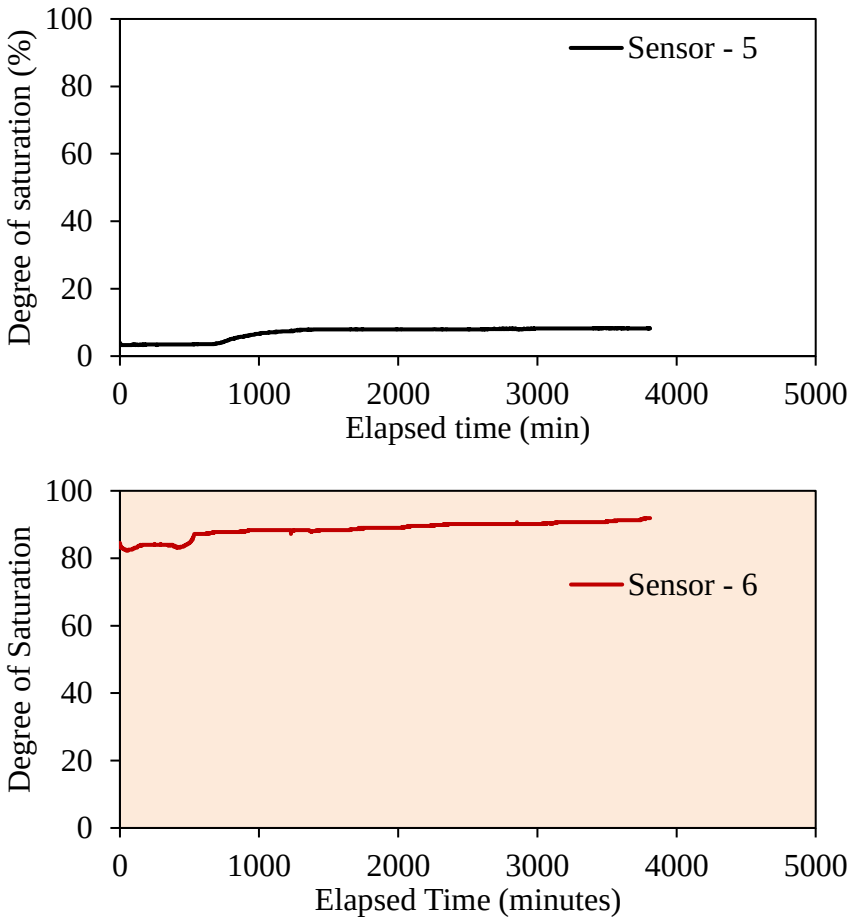

Figure 4 - 13 Saturation degrees of sensors 5, and 6 for Case 3

Case 4 - Drawdown Case - DL_II DD

Case 4 (DL_II DD) model is tested after the drawdown period. Case 4 tested with a rainfall of 3.72 mm/hr for 3880 minutes (66 hours). Figure 4 - 14 shows the time histories of the contaminated layer and drainage layer exits. Also, Table 4 - 5 shows the percentage of the final amount of drained water from different exits. Almost 99% of cumulative water goes out from the drainage layer. There is no water flow under the drainage layer until 466 minutes. After 466 minutes, the water started to flow out the drainage layer, and it continued until the end of the test. Case 4 has a higher cumulative drainage percentage compare to Case 3. This difference is nearly 8%, and it is considered to be as a result of the high initial moisture content of the contaminated layer at Case 3.

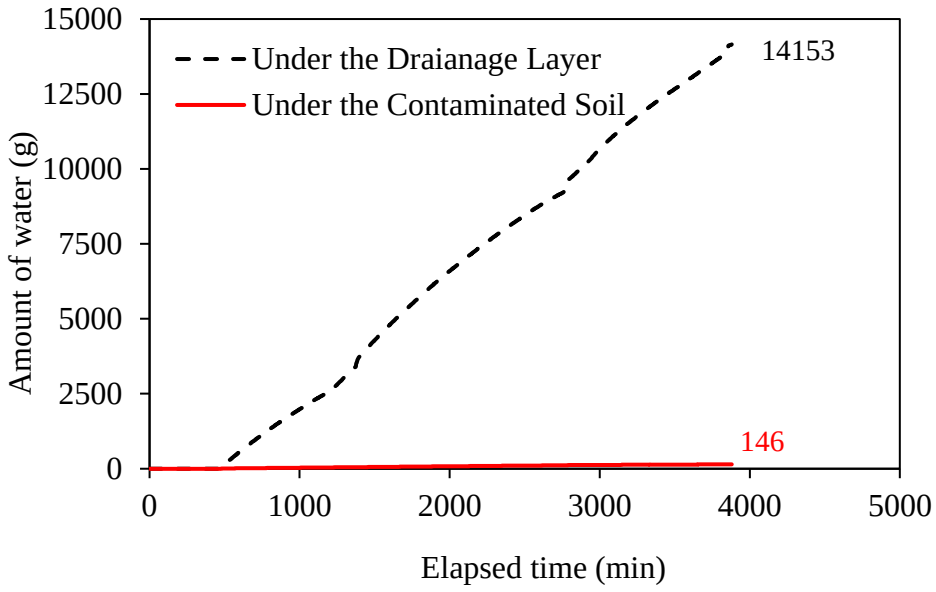

Figure 4 - 14 Time history of the drainage water for Case 4

Table 4 - 5 Total drained water from exits for Case 4

Exit	Exit location	Amount of water (g)	Percentage (%)	Amount of water each layer (g)
1	Under the drainage layer	3314	23	14153
2	Under the drainage layer	4191	29	
3	Under the drainage layer	2369	17	
4	Under the drainage layer	4279	30	
5	Under the contaminated layer	142	1	146
6	Under the contaminated layer	4	0	

The saturation degrees recorded from sensors are presented in Figure 4 – 15, and Figure 4 - 16. The saturations near the rainfall application region had high saturation values. The sensors inside the drainage layer had similar saturation values. Sensor – 6, which is inside the contaminated layer, did not show a significant change during the experiment. It is nearly constant. Also, the sensors inside the drainage layer did not have considerable change after the rainfall application. Their saturation degrees are roughly equal to initial saturation degrees. Instead, sensor 2 had a different pattern than the other sensors inside the drainage layer. It has a fluctuating change. It might depend on the calibration equation of the sensor. Especially at the lower degrees of saturation values, a perfect calibration is very difficult for the coarse soil.

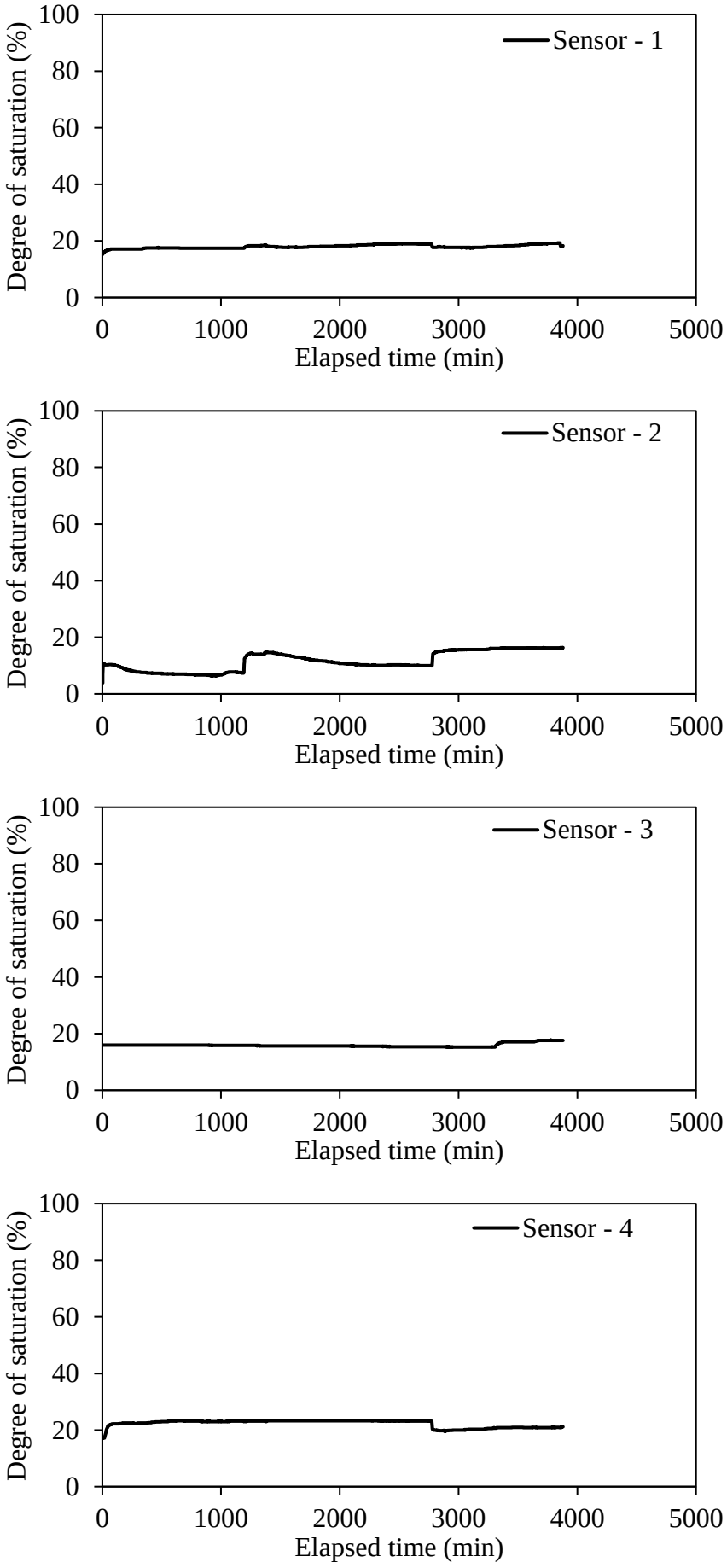

Figure 4 - 15 T Saturation degrees of sensors 1, 2, 3, and 4 for Case 4

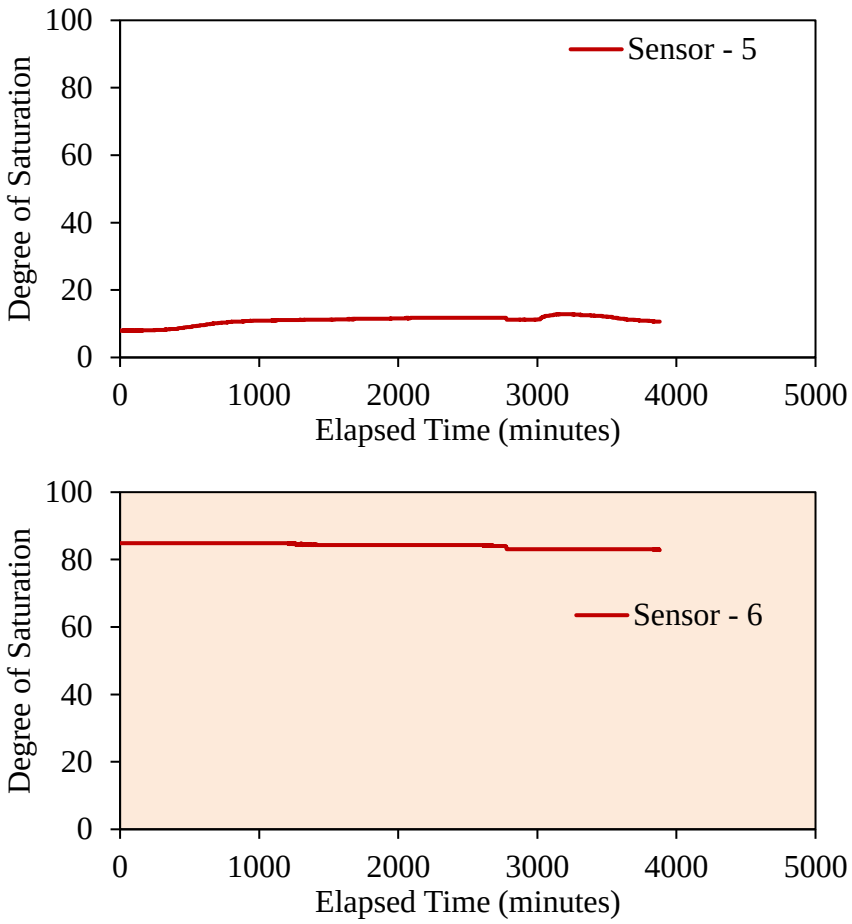

Figure 4 - 16 Saturation degrees of sensors 1, and 2 for Case 4

4.3.3 Drainage Layer Model Results for the DL_III

The DL_III models were tested under two different cases: optimum moisture content case and drawdown case. The prepared model geometry and the location of the sensors are presented in Figure 4 – 17. Totally six sensors were used in the experiments. Four sensors inside the contaminated layer (sensor 3, sensor 4, sensor 5, and sensor 6), and two sensors inside the drainage layer (sensor 1, and sensor 2).

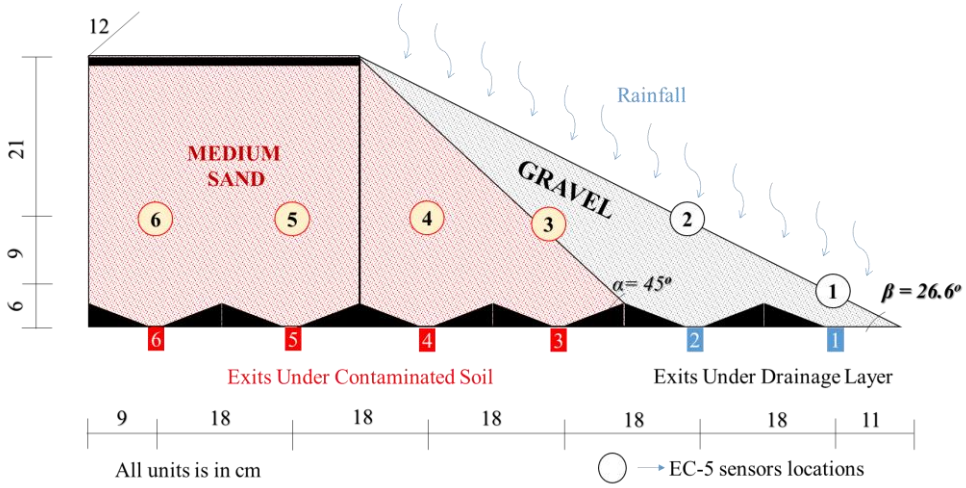

Figure 4 - 17 Experiment system for the DL_III models

Case 5 - Optimum Moisture Content Case - DL_III OMC

Case 5 (DL_III OMC) model was subjected to a rainfall of 2.79 mm/hr for 4140 minutes (69 hours). The initial saturation degrees (before rainfall application) were around 75% to 80% for the contaminated layer and 12% to 20% for the drainage layer.

Figure 4 - 18 shows the time histories exit under the contaminated layer and drainage layer. Also, Table 4 - 6 shows the percentage of the drainage amount from different exits at the end of the test. According to Figure 4 – 18, Case 5 had the highest cumulative drainage water percentage compare to all cases under the contaminated soil. 57% of cumulative drainage water flowed out under the contaminated layer.

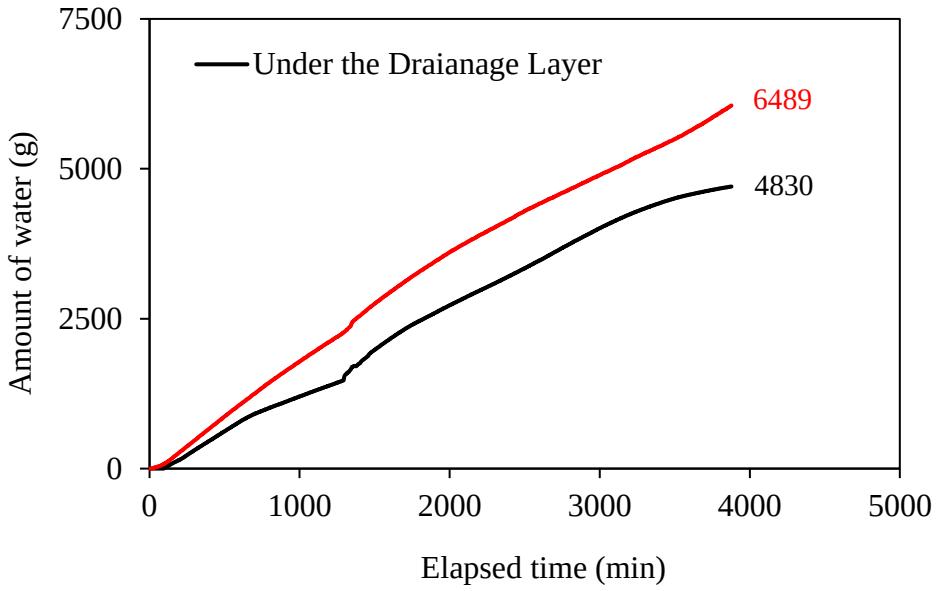

Figure 4 - 18 Time history of the drainage water for Case 5

Table 4 - 6 Total drained water from exits for Case 5

Exit	Exit location	Amount of water (g)	Percentage (%)	Amount of water each layer (g)
1	Under the drainage layer	2800	25	4830
2	Under the drainage layer	2030	18	
3	Under the contaminated layer	2474	22	6489
4	Under the contaminated layer	2202	20	
5	Under the contaminated layer	829	7	
6	Under the contaminated layer	983	9	

The degree of saturation versus time is presented in 4 – 19 and 4 – 20. From sensor readings, a slight decrease can be seen at the sensor – 6 for not apply rainfall on it. However, a slight increase in saturation degrees was seen in sensor – 1 under the drainage layer. Other sensors had nearly constant changing during the experiment. It might be explained that during the tank preparation period, the other sensors had already reached the maximum storage capacity. Because of that, they do not have any changing in saturation during the rainfall application period. Moreover, sensor 3 show some fluctuation, it is considered that the calibration equation or data logging system were sensitive at this sensor during the testing period. Therefore, a fluctuated saturation degree was obtained. As an average, sensor - 3 also had a constant saturation degree during Case 5.

Consequently, due to a high amount of drainage under the contaminated layer, the suggested system does not give satisfactory results in terms of water interception approaches. Only 43% percent of the water flowed under the drainage layer. That is because, at the drainage layer III models, the impervious pavement layer does not cover all surface of the contaminated soil. So, the rainfall directly enters the contaminated region. Consequently, the water under the contaminated area has a higher percentage than the drainage layer.

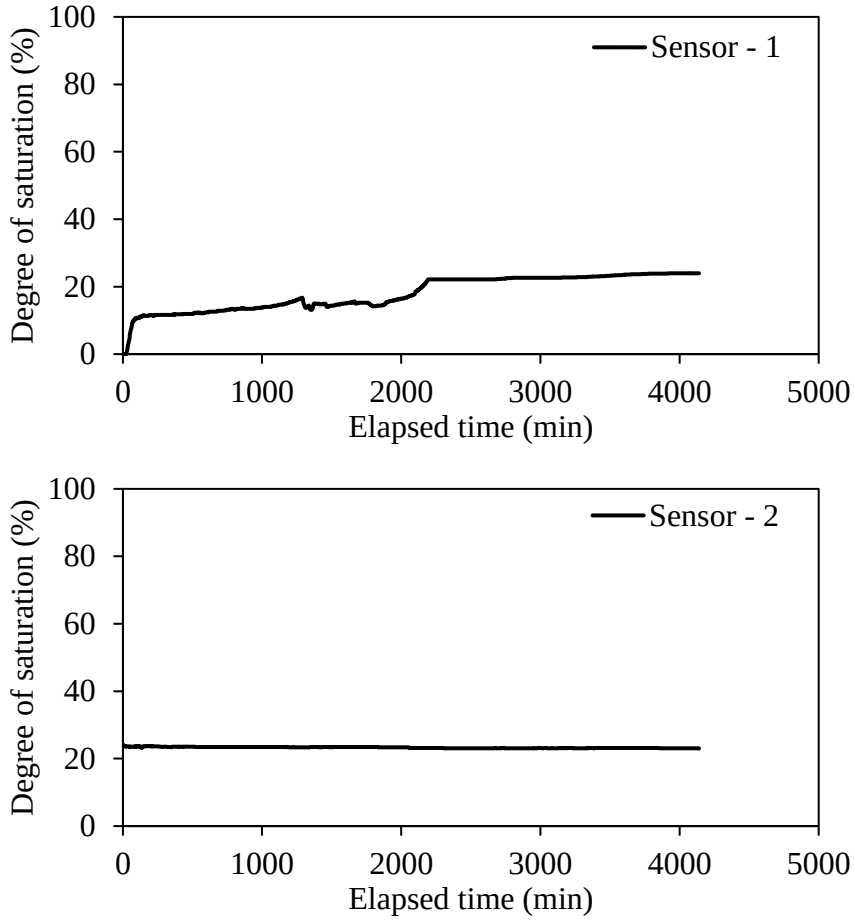

Figure 4 - 19 Saturation degrees of sensors 1, and 2 for Case 5

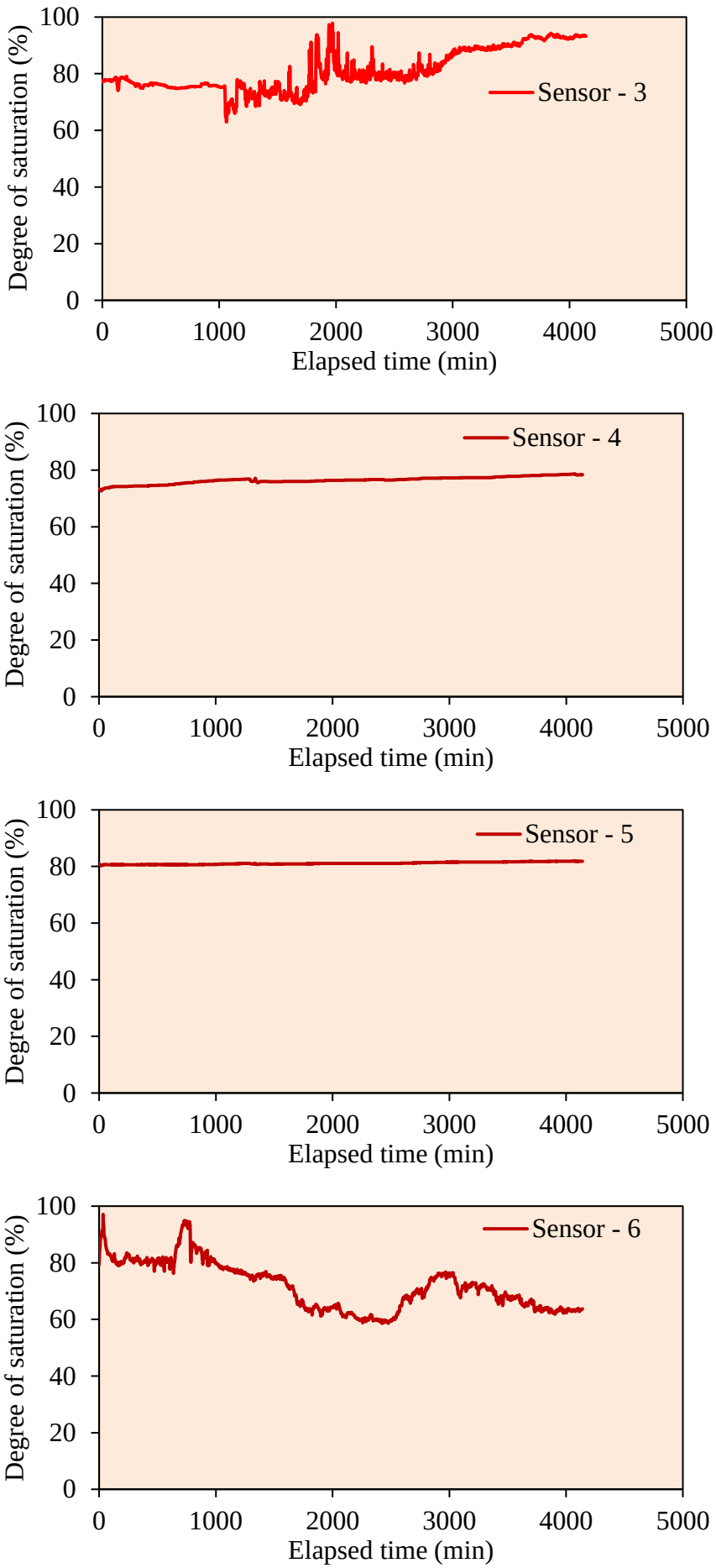

Figure 4 - 20 Saturation degrees of sensors 3, sensors 4, sensors 5, and 6 for Case 5

Case 6 - Drawdown Case - DL_III DD

Case 6 (DL_III DD) model is tested after the drawdown period. Case 6 tested with a rainfall of 3.02 mm/hr for 4080 minutes (68 hours). Figure 4 - 21 shows the time histories of the contaminated layer and drainage layer exits. Also, Table 4 - 7 shows the percentage of the drainage amount from different exits. Due to a high amount of cumulative drainage under the contaminated layer, the suggested system does not give satisfactory results in terms of water interception approaches. Only 46% percent of the cumulative drained water flowed under the drainage layer. That is because, at the drainage layer III models, the rainfall directly applied to the contaminated region. Consequently, the water under the contaminated layer has a higher percentage than the drainage layer.

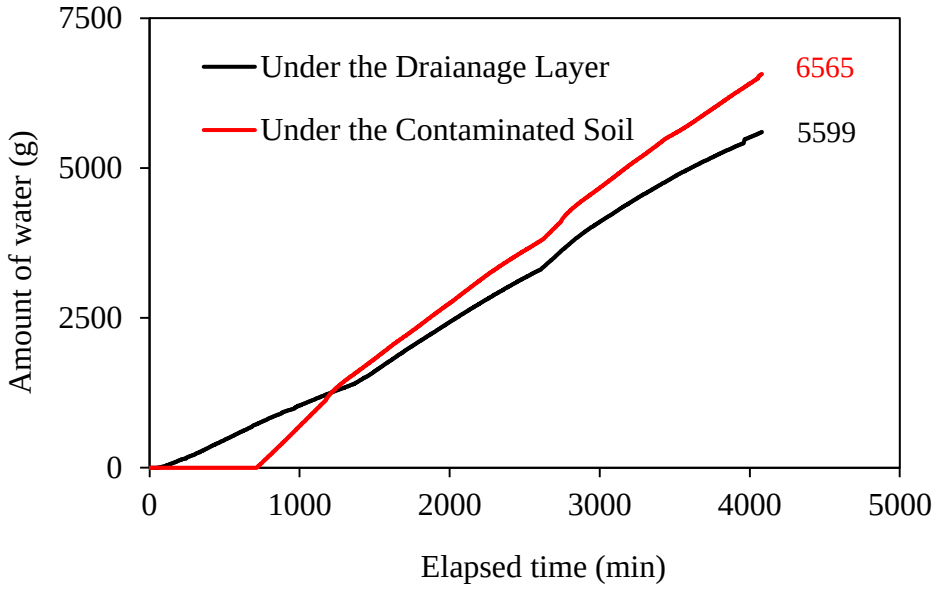

Figure 4 - 21 Time history of the drainage water for Case 6

Table 4 - 7 Total drained water from exits for Case 6

Exit	Exit location	Amount of water (g)	Percentage (%)	Amount of water each layer (g)
1	Under the drainage layer	2715	22	55989
2	Under the drainage layer	2884	24	
3	Under the contaminated layer	2942	24	6565
4	Under the contaminated layer	1810	15	
5	Under the contaminated layer	801	7	
6	Under the contaminated layer	1013	8	

The degree of saturation versus time is presented in 4 – 22 and 4 – 23. From sensor readings, constant saturation degrees were obtained for all of the sensors. The sensor – 6 has the lowest saturation degrees inside the contaminated layer due to its distant location from applied rainfall. Also, the sensors under the drainage layer (Sensor 1 and 2) are almost constant before the rainfall application and during the testing period. It might be explained as the drainage layer has already reached maximum storage capacity before the rainfall application. And the applied rainfall directly flows out from the drainage layer during the testing period.

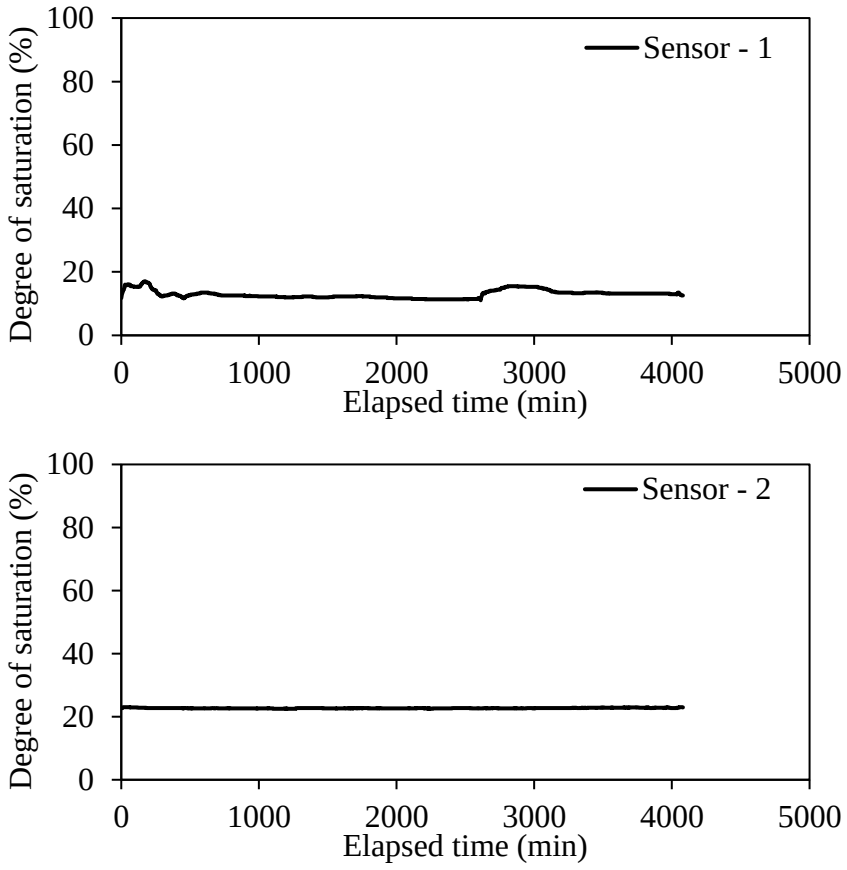

Figure 4 - 22 Saturation degrees of sensors 1, and 2 for Case 6

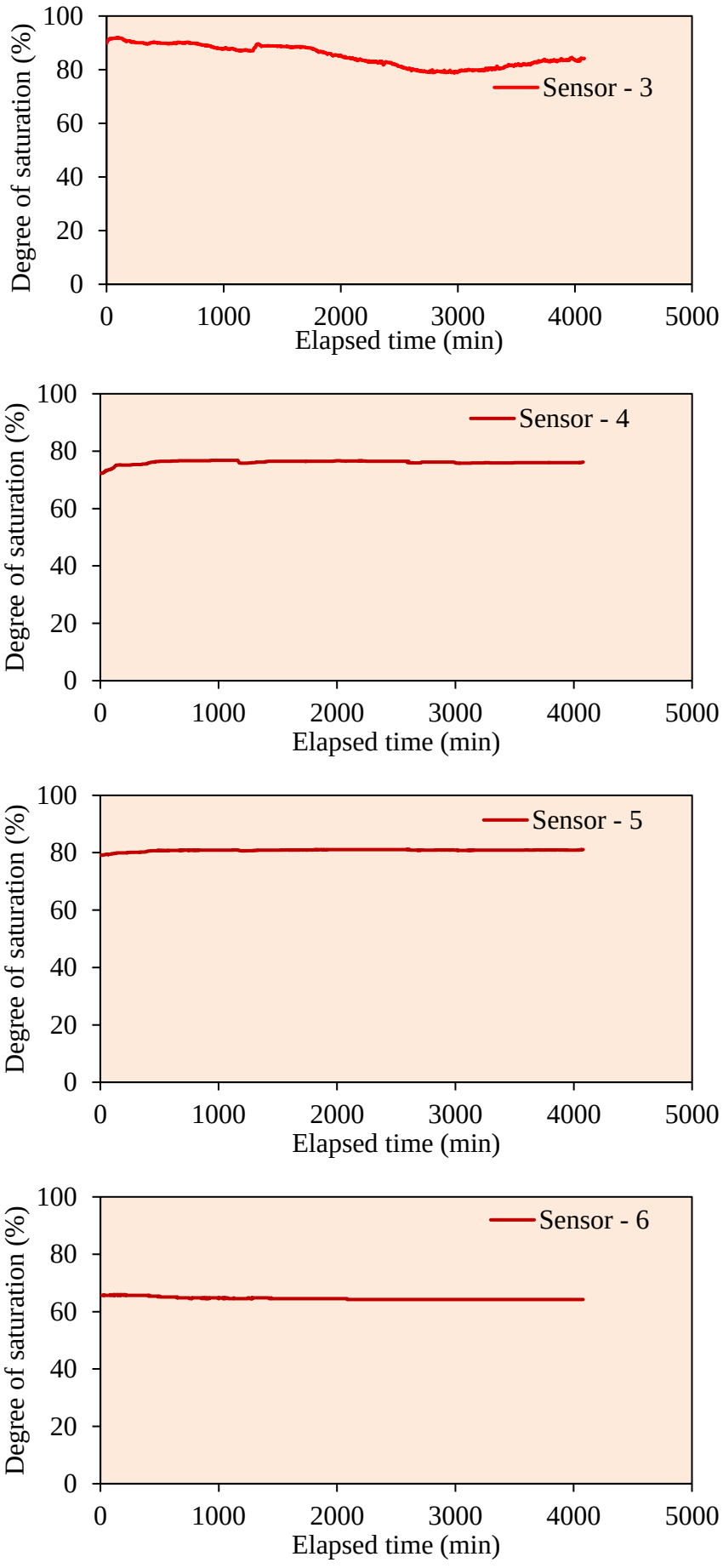

Figure 4 - 23 Saturation degrees of sensors 3, 4, 5, and 6 for Case 6

4.4 Discussions on Drainage Layer System Results

One of the main objectives of this research is to investigate the application of geogenic contaminated soil as embankment material in the core of the embankment. For that reason, the second approach, which is the use of a drainage layer, is suggested. The efficiency of the proposed system is tested experimentally. A drainage layer is planned to construct with the available in-situ coarse soil, which is coarser than the contaminated soil that is considered to be utilized. Three different utilization geometry were tested with different initial moisture content and different rainfall rates. The performance of the tested models is shown in Section 4.3.

The performance of models was examined according to the changing of saturation degrees in both layers (contaminated layer and drainage layer) and time histories of cumulative drained water. According to experimental, it is understood that if the contaminated soil is only placed under the impervious pavement layer, the drainage layer system became beneficial with respect to water interception capacity. DL_I and DL_II models had nearly directed 98% cumulative drainage water from the drainage layer at the drawdown cases (Case 2 and Case 4).

Effects of utilization geometry

Three different utilization geometry were investigated. Table 4 - 8 and Table 4 -9 show the cumulative directed water from exits at the optimum moisture content prepared cases, and the drawdown prepared cases, respectively. It is seen that nearly 98% of cumulated drained water is directed under the drainage layer at the drawdown models of DL_I and DL_II. That is because at the DL_I and DL_II, the rainfall is only applied only over the drainage layer. Therefore, the contaminated layer is not exposed to the direct wetting process. Also, the higher saturated hydraulic conductivity difference (more than 100 times) between the contaminated layer (MS) and drainage layer (GP) generates gravitational follow inside the drainage layer. Because of that DL_I and DL_II, have more promising results.

On the other hand, the DL_III model, which is not placed only under the impervious asphalt layer higher percentage of cumulative drained water flowed out from the contaminated layer. At the DL_III model, the drawdown case (Case 6), which has the highest directed water percentage under the drainage layer, has only 46% of the cumulative drainage.

According to results, it is seen that the exits which are close rainfall application area has a higher cumulative drainage percentage comparing to far ones under the contaminated layer. It is considered that the infiltrated water might escape to the contaminated layer from the drainage layer. Because of that exits near the drainage layer has a higher drainage amount than the far ones (Table 4 - 8 and Table 4 - 9).

It is suggested that a utilization method only under the impervious pavement layer (DL_I model and DL_III model) gives promising results compare to DL_III model. According to

obtained results, utilization with an impermeable surface layer might be a better option according to the water interception approach.

Table 4 - 8 Directed water percentage from each exit at the OMC prepared cases

Exits	DL _I Case_1	DL _II Case_3	DL _III Case_5
Exit 1	27	17	25
Exit 2	25	33	18
Exit 3	26	23	22
Exit 4	11	17	19
Exit 5	6	5	7
Exit 6	5	4	9

Table 4 - 9 Directed water percentage from each exit at the DD prepared cases

Exits	DL _I Case_2	DL _II Case_4	DL _III Case_6
Exit 1	22	23	22
Exit 2	35	29	23
Exit 3	20	17	24
Exit 4	21	30	15
Exit 5	1	1	7
Exit 6	1	0	8

Time-dependent barrier performance

The time-dependent barrier performance of models was investigated. Figure 4 -24 to Figure 4 – 31 show the time-dependent drainage percentage both under the contaminated layer and drainage layer Case 1 to Case 6, respectively. The changing of cumulative drained water within 30 minutes time period was selected for the understanding of the time-dependent performance of the drainage layer models. Then, the ration of drained water from each layer was calculated by dividing the total cumulative amount. According to Figure 4 – 24 and Figure 4 – 26, it is seen that the optimum moisture content prepared cases (Case 1 and Case 3) have drainage under the contaminated layer at the beginning of the experiment. However, after a specific time, the water started to flow out from the drainage layer. After the equilibrium, the drainage ration of

both layers becomes constant. It is considered that initial drainage under the contaminated layer is caused by non-storable water, which comes from the preparation of moisture content.

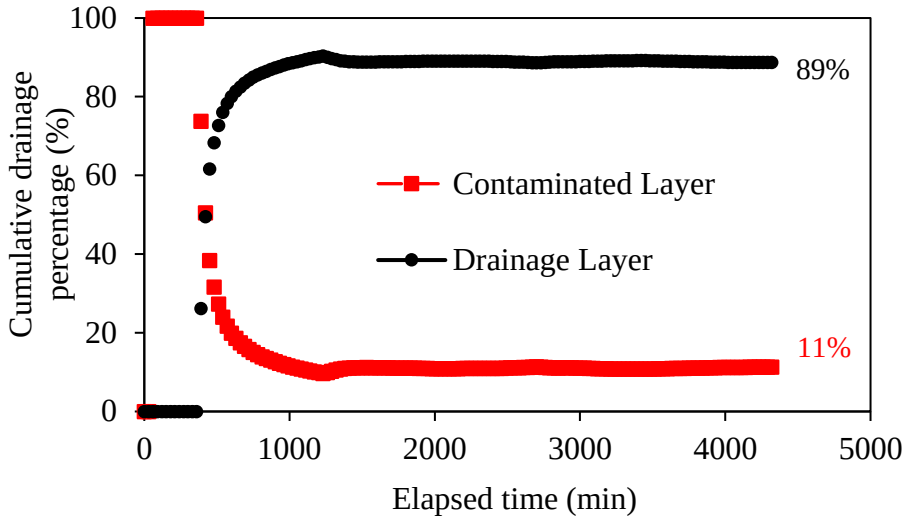

Figure 4 - 24 Time-dependent barrier performance of Case 1

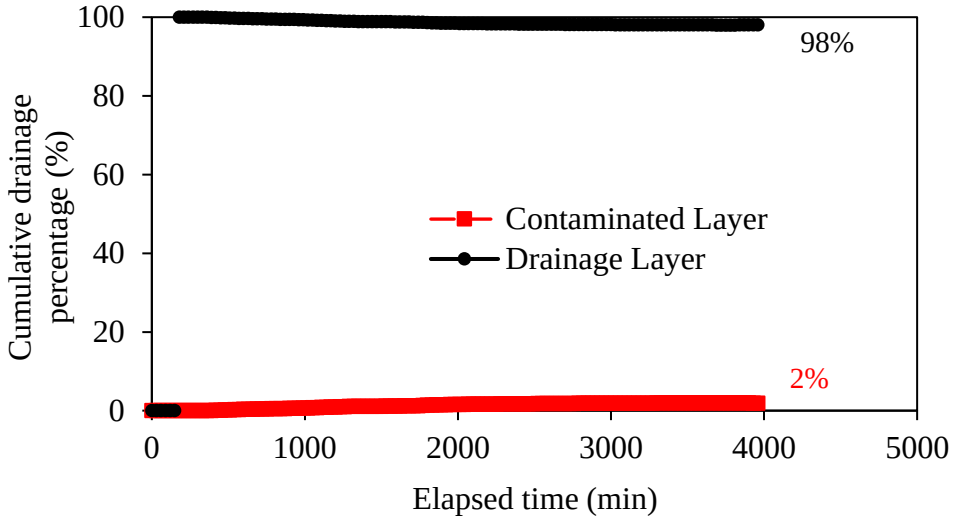

Figure 4 - 25 Time-dependent barrier performance of Case 2

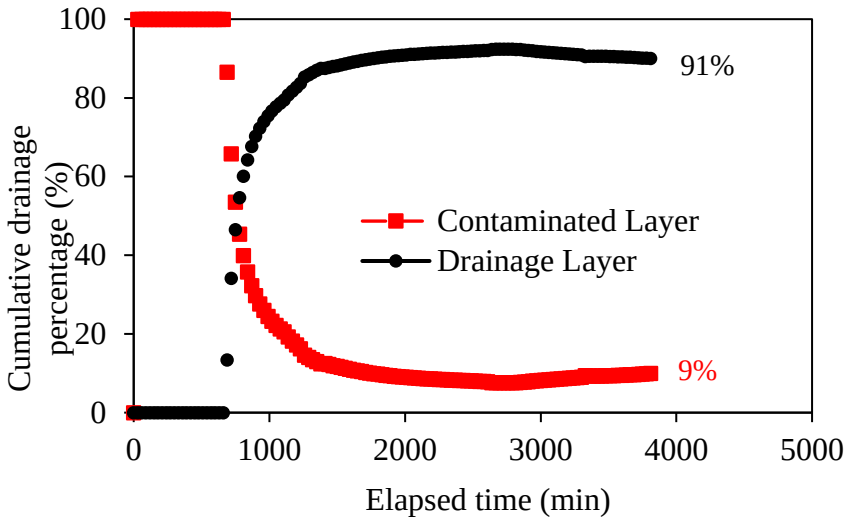

Figure 4 - 26 Time-dependent barrier performance of Case 3

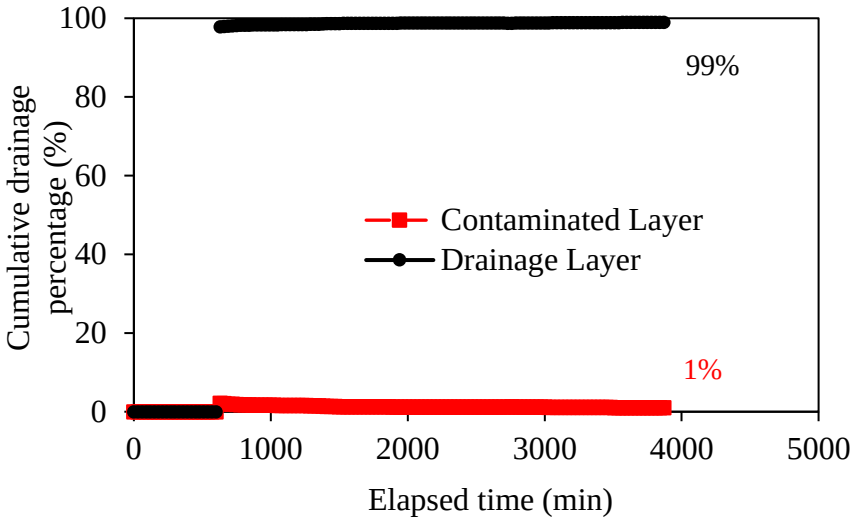

Figure 4 - 27 Time-dependent barrier performance of Case 4

On the other hand, according to Figure 4 – 25 and Figure 4 – 27, which are tested under the drawdown conditions (Case 2 and Case 4) nearly all of the water percolated from the drainage layer. These results also showed that the initial water drainage from the contaminated layer is caused by the higher preparation moisture content of the contaminated layer (MS).

In contrast, the results which belong to Case 5 and Case 6 have a different pattern. Due to direct rainfall over the contaminated layer, the water which drained under the contaminated layer has a higher percentage of drainage. Although the drainage layer directed nearly half of the water in Case 6, DL_III model has the lowest drainage ration inside three investigated models. It can be seen that the models which are placed under the impermeable pavement layer are more effective according to water interception capability.

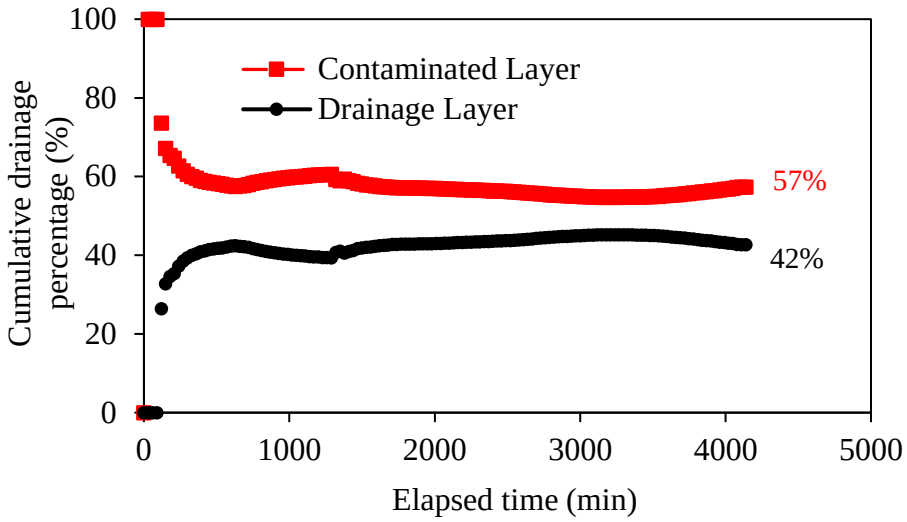

Figure 4 - 28 Time-dependent barrier performance of Case 5

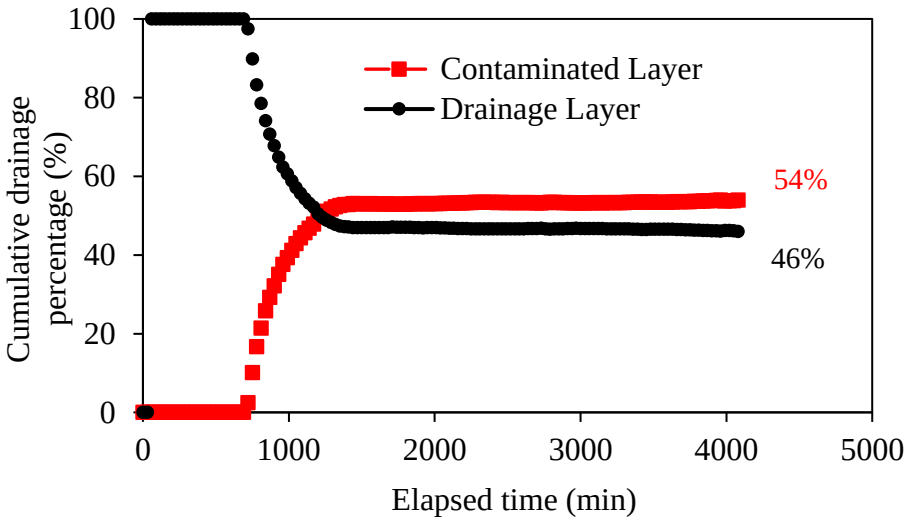

Figure 4 - 29 Time-dependent barrier performance of Case 6

4.5 Summary and Conclusions

In this chapter, the performance of suggested approach two, which is the drainage layer system, was investigated based on the laboratory infiltration box test. The effects of utilization geometry and initial preparation water content were discussed. The main objectives obtained in this chapter can be summarized as follows.

A drainage layer system with coarser material at the embankment shoulder and finer material (contaminated layer) in the embankment core is an alternative way for the utilization of geogenic contaminated soil in the embankment.

The drainage layer models I (DL_I) and model II (DL_II), which are deposited the contaminated soils only under the impervious layer, have a higher barrier efficiency compare to drainage layer model III (DL_III). The water interception capacity (more than 90 % of the cumulative drainage).

Because of the initially higher free water inside the tank for the optimum moisture content (OMC) prepared cases (Case 1, Case 3, and Case 5), higher bottom percolation is obtained under the contaminated layer. On the other hand, the drawdown (DD) cases have comparable lower percolation under the contaminated layer. However, the difference between OMC prepared cases and DD cases are approximately 10%.

According to drawdown case results, it is seen that the drainage layer model is reversible. They can continue their serviceability after saturation and drainage period.

Experimental results show that if the saturated hydraulic conductivity of embankment shoulder material is 100 times higher than saturated hydraulic conductivity of embankment core material (contaminated layer), the drainage layer system works fairly with the placement of contaminated soil under the impermeable pavement layer.

CHAPTER 5: WATER BALANCE AND CONTAMINANT TRANSPORT

5.1 General Remarks

The purpose cover system is to reduce the infiltration of rainwater into the contaminated layer, and consequently, to reduce the generation of leachate. The estimation of water amount, which may react with the contaminant, is a crucial task for geoenvironmental engineers. The answer ultimately depends on the quantity of water percolating from the cover system. Investigators have conducted extensive water balance analyses for landfill cover systems (Khire et al. 1997; Koerner and Daniel 1997; Benson et al. 2001)The quantity of water percolating to an underlying waste layer from a cover system depends on several factors, such as the hydrological conditions of the landfill site, the cross-sectional composition of the cover system, the surface, and the existence or nonexistence of vegetation. Predictions of the migration of rainwater, which generally pass through the cover system, may be simulated using traditional equations or numerical codes. For understanding the water flow inside in an embankment with a cover system, a water balance and contaminant transport analysis was conducted. This analysis is completed in two parts. At first, a water balance analysis was performed using conventional equations for the cover layer. The water balance analysis has solved with the analytical method of the HELP model proposed by Thornthwaite & Mather, 1955. At the second stage, a one-dimensional finite element contaminant transport analysis was performed with the advective-dispersive solute transport approach. Kyoto city was selected as the investigation site, and its average monthly precipitation and mean temperature over the past thirty years were used as the input data.

5.2 Water Balance in Cover Soil for Minimizing Geo-Environmental Impacts

The conceptual water balance for a cover is shown in Figure 5 - 1. It shows the pathway of rainwater when it passes through a cover system at a waste landfill site (Koerner and Daniel 1997; Khire et al. 1997). Infiltration precipitation (rainwater) can be minimized by (1) the effect of the evapotranspiration in the surface layer, (2) the effect of water retention in the surface layer, (3) the effect of the surface runoff of precipitation due to surface inclination, (4) the effect of drainage from the drainage layer, and (5) the effect of the low hydraulic conductivity of the barrier layer in the final cover system. Estimations of the infiltration of rainwater or melted

snow into a cover system are usually accomplished using one of the many available water balance analysis models.

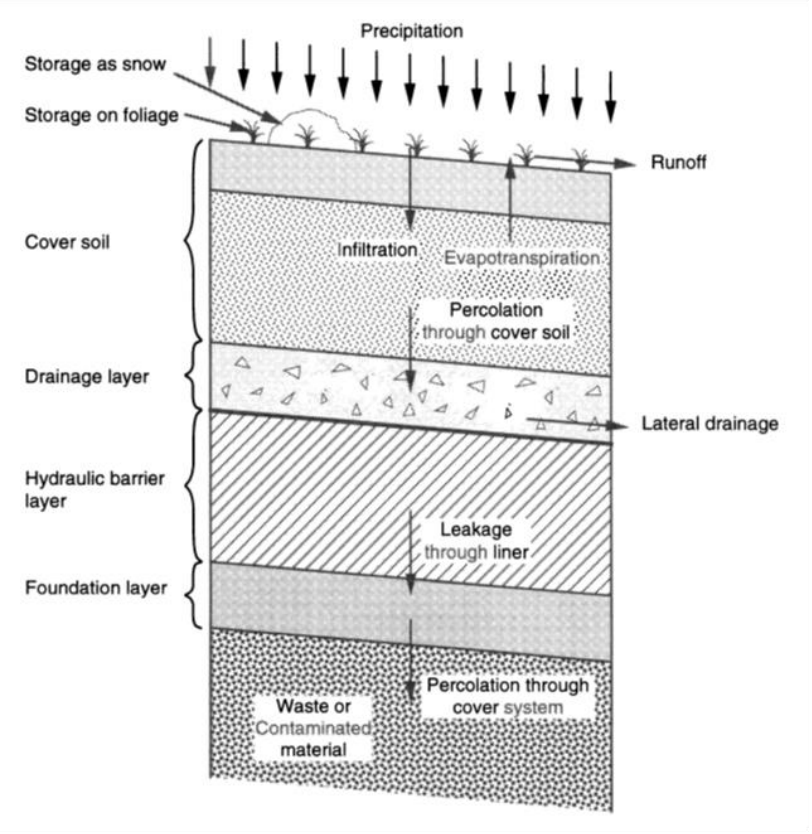

Figure 5 - 1 Water movement in landfill cover from (Koerner and Daniel 1997)

Schroeder et al. (1984) simulate the hydrologic processes for active or closed landfills by performing sequential water balance calculations using a two-dimensional approach, which considers all flow to be vertical, except at the lateral drainage layer, where the flow can be vertical or lateral. The simulation progresses with time, and the water balance process is thought to be steady-state within each time step. A conceptualization of the HELP model is shown in Figure 5 - 2. Each water balance parameters are separately calculated in the subsurface profile (Figure 5 – 2). The hydrologic processes considered in the model include precipitation, surface water storage, surface water evaporation, runoff, infiltration, plant transpiration, soil water storage, vertical flow through non-barrier soil layers, drainage layers and bottom percolation. Water balance analyses for landfill cover systems, using the Schroeder et al. (1984), model, have been performed in several studies (Thornthwaite and Mather 1955; Fenn et al. 1975; Koerner and Daniel 1997; Khire et al. 1997; Benson et al. 2001; Kamon et al. 2002). This model may be performed analytically or numerically. In the present study, a water balance analysis solved analytically. This procedure has also been recommended by Koerner & Daniel (1997).

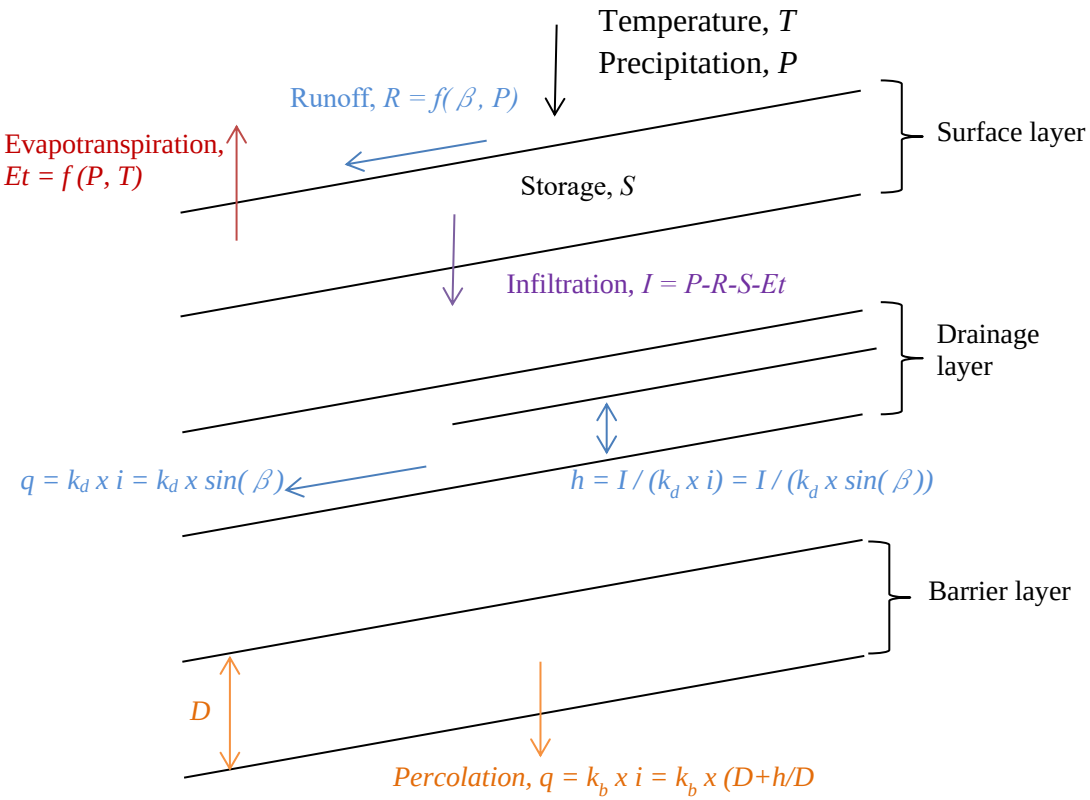

Figure 5 - 2 Representation of the water balance model

The water balance for a cover system can be expressed in terms of water inflows and outflows and storage changes for a given cover system volume over some arbitrary time interval, and it is named as a mass conservation law. It can be expressed by equation 5.1

$$I = P - R - S - Et \tag{5.1}$$

where I is the water quantity infiltrating into the drainage layer from the surface layer [L], P is the average monthly precipitation [L], R is the quantity of surface runoff [L], S is the quantity of water that can be retained in the surface layer [L], and Et is the quantity of water loss due to evapotranspiration [L]. Surface runoff, R can be estimated according to by following equation (Fenn et al. 1975):

$$R = P \times C \tag{5.2}$$

where C is the runoff coefficient, C is defined by the type of soil and the angle of the surface layer in the cover system (β). Typical runoff coefficients for completed landfi11 covers are given in Table 5.1. In this study, C is selected as 0.18, according to Fenn et al., (1975).

Table 5 - 1 Suggested runoff coefficients (From Fenn et al. 1975)

Description of Soil	***Slope***	***Runoff Coefficient***
Sandy Soil	Flat (≤2%)	0.05-0.10
Sandy Soil	Average (2%-5%)	0.10-0.15
Sandy Soil	Steep (≥7%)	0.15-0.20
Clayey Soil	Flat (≤2%)	0.13-0.17
Clayey Soil	Average (2%-5%)	0.18-0.22
Clayey Soil	Steep (≥7%)	0.25-0.35

Evapotranspiration, *Et*, provides direct water loss and the transpiration by the plants on the surface layer. Evapotranspiration depends on climatic conditions and the quality of vegetation. Since the determination of evapotranspiration is complicated, it can be simplified by the empirical formula expressed in Equations (5.3a), (5.3b), and (5.3c) (Thornthwaite and Mather, 1955), and can be defined as a function of the average temperature and the duration of sunlight:

$$Et = 0 \qquad for \qquad T \leq 0^{o}C \tag{5.3a}$$

$$Et = 0.53N\left(\frac{10T}{H_a}\right)^{a} \qquad for \qquad 0^{o}C<T<27^{o}C \tag{5.3b}$$

$$Et = N\left(-0.015T^{2} + 1.093T - 14.208\right) \qquad for \qquad T \geq 27^{o}C \tag{5.3c}$$

where *Et* is the unadjusted daily potential evaporation [*L*], T is the average monthly temperature (°*C*), H_a is the dimensionless annual heat index, *a* is a dimensionless empirical factor that is computed as in equation (5.4). Daily unadjusted evaporation values are converted to monthly by multiplying the results with the monthly duration of sunlight, *N*. *N* is assumed from the latitude at which the investigated site is located. Details on the relationship between *N* and the latitude are given in Koerner and Daniel (1997).

$$a = \left(6.75\times10^{-7}\right)H_a^{3} - \left(7.71\times H_a^{2}\right) + 0.01792\,H_a + 0.49239 \tag{5.4}$$

$$H_a = \sum_{i=0}^{i=n}(H_i)^{1.514} \tag{5.5}$$

$$H_i = (0.2\ T)^{1.514} \qquad for \qquad T \geq 0^o C \tag{5.6}$$

The amount of water that a soil can store depends mainly on the type as well as the thickness of the soil layer. Figure 5 – 3 shows commonly used parameters to describe soil moisture content. Dry soil refers to oven-dried soil, and it is devoid of water for any practical purposes. When plants are inside soil media, and the plant roots exist can remove the water by transpiration. Plants remove water until they wilt the plant wilting point (*PWP*). The 1500-kPa definition is reasonably representative for plants in more humid environments, but for semi-arid and arid environments, the wilting point can be 4000-10,000 kPa. The field capacity (*FC*) of a soil is the highest water content at which water is held in soil under the gravitational forces. When the water content of soil rises above field capacity, water drains downward by gravity until field capacity point. The cover will not flow as long as the soil water content does not exceed field capacity, and the water content in the cover will not drop below the wilting point (Koerner and Daniel 1997). Saturation occurs all the pores of the soil are filled with water. No additional water can be retained once the soil has reached saturation. Extra water after the soil state reached the saturation is directed as surface runoff. At the unsaturated state, the available water in the cover is assumed to be the difference between field capacity and wilting point.

In the water balance analysis, the maximum quantity of water that can be retained in a unit volume of the surface layer, S_{max} (mm), is determined by:

$$S_{max} = (\theta_{FC}) \times H_{root} \tag{5.7}$$

where H_{root} is the thickness of the surface layer (m). The quantity of water retained in the surface layer is decreased, as shown in equation (5.8a) given by Koerner and Daniel (1997). When the precipitation infiltrates into the surface layer, the quantity of water retained in the surface layer is added to the quantity of water retained in the previous month and the quantity of infiltration of the concerned month (equation (5.8b)). However, the quantity of water that exceeds the maximum quantity of water that can be retained in the surface layer, S_{max}, cannot be stored, in other words:

$$S_i = (S_{max}) \times 10^{\frac{0.455}{S_{max}}\, x\, (I - UPET \times N)} \tag{5.8a}$$

$$S_i = (P - R - Et)_i + S_{i-1} \tag{5.8b}$$

where S_i is the possible water retention quantity of the surface layer in the i^{th} month (mm).

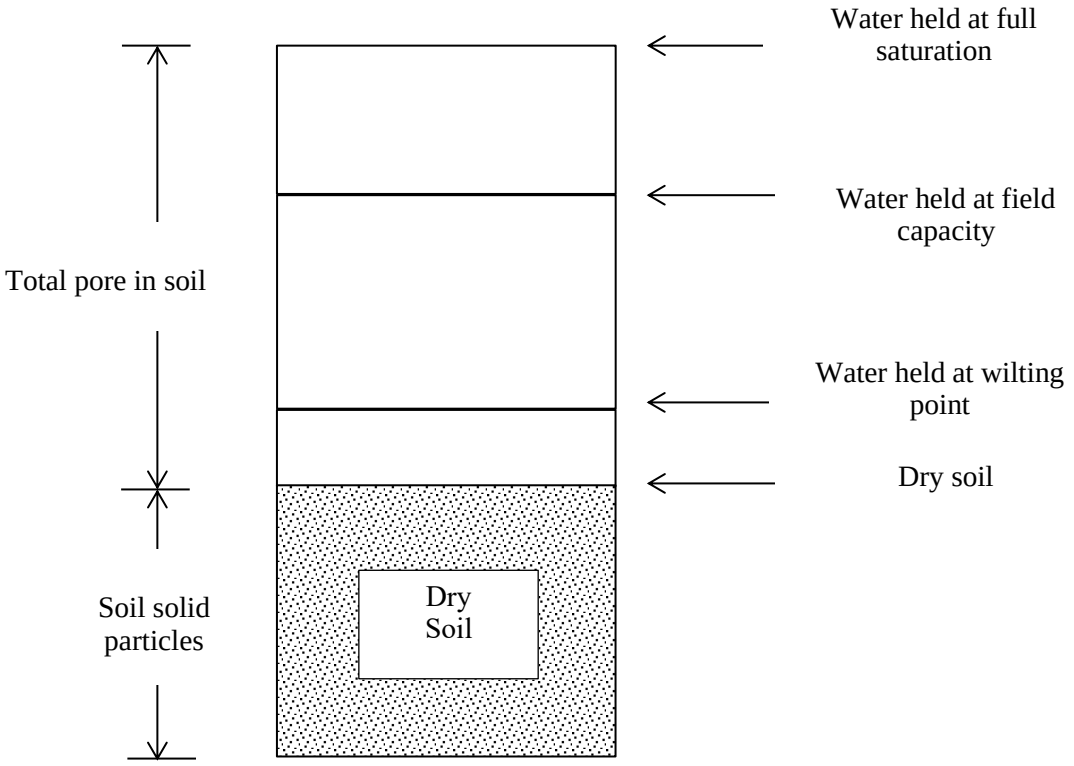

Figure 5 - 3 Representation of water retention in soil

5.2.1 Estimation of Water Balance Analysis for Kyoto City

The estimation process of water balance analysis is calculated for the Kyoto city, Japan. The assumed calculation profile and the characteristic values of the constituent layers of the cover systems are shown in Figure 5.4. The Kyoto city is located latitude 35 degrees north. For this analysis, the average monthly precipitation and mean temperature obtained from the Japanese Meteorology Agency over the past thirty years (1985-2015) were used as the input data (Table 5.2). The maximum water storage in the root zone (S_{max}) is estimated as 30 mm using equation (5.7).

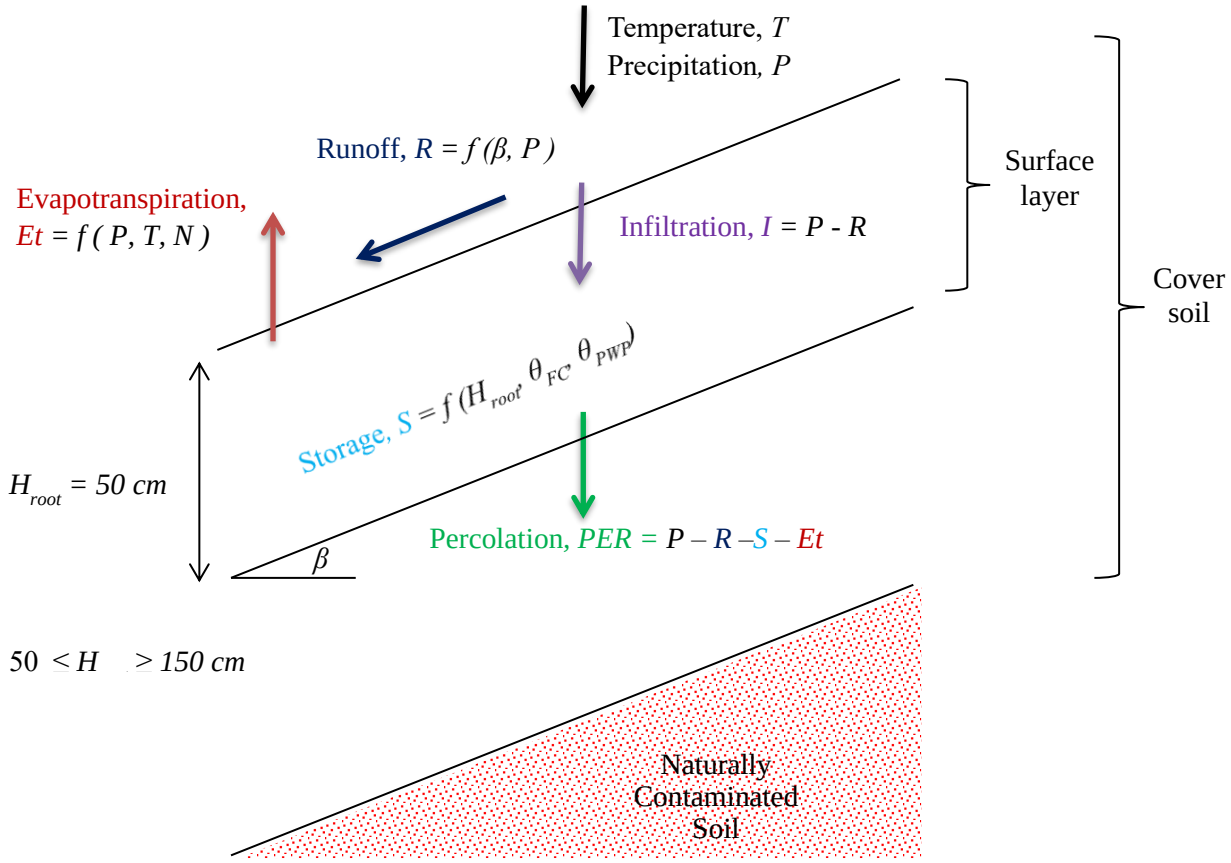

Figure 5 - 4 Assumed calculation profile for cover soil

5.2.2 Results and Discussions

The rainwater interception for an embankment cover system depends on the changes in weather conditions at the investigated site. The input data of the weather conditions used are the monthly precipitation, the daily mean temperature, and the average daily amount of solar radiation are shown in Table 4.2. The assumed structural profile is shown in Figure 5 – 4.

Table 5.2 shows the changes in the quantity of water percolating from the cover systems in Kyoto. The top surface layer, which is affected by vegetation zone, is selected as 50 mm. Runoff was predicted with respect to the in-situ precipitation and surface slope. The maximum predicted runoff occurred in July a significant amount of 40 mm/month Figure 5 - 5 and Table 5 - 2. The maximum monthly precipitation for Kyoto occurs in July (222.3 mm), which has 4.22 times of driest month in January (52.6 mm) (Gulsen et al. 2019).

The calculated monthly infiltration values for the surface layer were shown in Figure 5 - 5. The infiltration can be calculated anywhere inside the cover layer. In this research, the infiltration was calculated just below the surface layer, with an idea the precipitation minus surface runoff is equal to the infiltration. The maximum infiltration is calculated for in July (182.3 mm).

The quantity of water percolating from the surface layer to the embankment is 417.7 mm/year. The quantity of percolated water that passed through the surface layer into embankment depends on the amount of precipitation. Although the summer precipitation of Kyoto is heavier than in winter, the monthly maximum percolation occurs in March (74.1 mm/month). This is because of that the quantity of percolation decreases with the increase in evapotranspiration during periods of the high-temperature summer season. Although high precipitation was recorded, the percolation didn't occur in August.

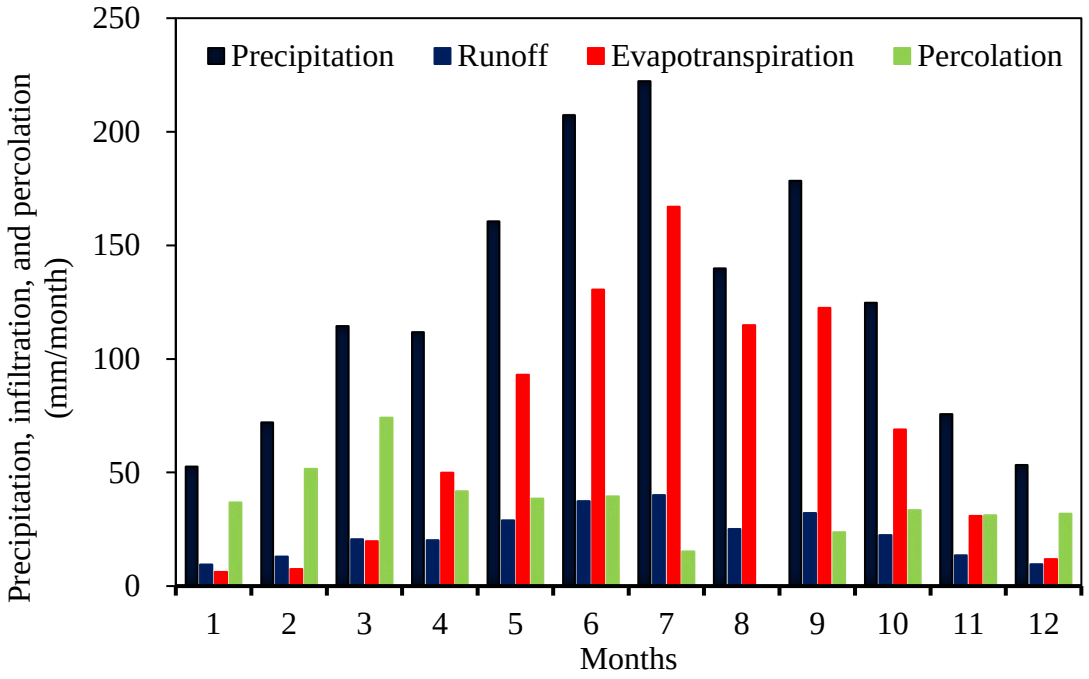

Figure 5 - 5 Results of water balance analysis for embankment cover

Table 5 - 2 Results of water balance analysis for cover systems at Kyoto city

Parameter	Jan	Feb	Mar	April	May	June	July	August	Sep	Oct	Nov	Dec
Avg. Temp	5.1	5.7	8.9	14.5	19.4	23.5	27.6	28.9	24.8	18.6	12.6	7.4
Heat Index	1.0	1.2	2.4	5.0	7.8	10.4	13.3	14.3	11.3	7.3	4.1	1.8
Duration of Sunlight	26.1	25.5	30.9	32.7	36.3	36.3	36.9	34.8	30.9	29.1	25.8	25.5
Precipitation	52.6	72.0	114.5	111.8	160.5	207.3	222.3	139.9	178.4	124.7	75.7	53.3
Runoff	9.5	13.0	20.6	20.1	28.9	37.3	40.0	25.2	32.1	22.5	13.6	9.6
Infiltration	43.1	59.1	93.9	91.7	131.6	170.0	182.3	114.7	146.3	102.3	62.1	43.7
Evapotranspiration	6.2	7.5	19.8	49.9	93.0	130.6	167.0	114.8	122.4	68.9	30.9	11.9
Percolation	36.9	51.6	74.1	41.8	38.6	39.4	15.2	0.0	23.7	33.4	31.2	31.8

5.3 One-Dimensional Numerical Simulation of Contaminant Transport

A one-dimensional simulation was evaluated a finite element advective-dispersive contaminant transport code (Dtransu-2D). This software is a free computer program that is used in engineering practice for simulating the hydrology and contaminant transport behavior of soils. In the second stage, the water balance analysis results were used as input parameters for finite element simulation. As shown in Figure 5 - 6, the model was simulated as a one-dimensional flow and had a horizontal extent of 1 m and a vertical extent of 5.5 m. A uniform grid consisting of 11 elements in the vertical direction with 24 nodes was used to estimate the contaminant transport. The top 3 elements of the model were designated to be finer soil, and they were considered as a cover layer with a thickness of 1.5 m. The next five cells being the coarse grain soil, and these elements were assigned as a naturally contaminated soil with a depth of 2.5 m. The remaining three cells had the same soil properties with the naturally contaminated soil but were identified as clean natural soil. The model input values in Table 5 – 3.

The net percolation, which had already obtained from water balance analysis, was applied at a depth of 5 m as a source of infiltration. The model boundary conditions were free-flux on the side and on the bottom. Both the cover layer and contaminated soil in the core of embankments were designated as unsaturated at the initial boundary condition with a fixed matric suction value (10 kPa). The simulation was conducted for 3650 days' (10 years') period.

Table 5 - 3 Model input parameters

Modeling parameters		Values
Timestep	Initial	1 day
	Tolerance	0.001 day
	Maximum	3650 day
Convergence tolerances		0.05
Vertical dispersion coefficient		0.1 m
Longitudinal dispersion coefficient		0.01 m
Molecular coefficient * Tortuosity		4.32×10^{-5} m^2/day
Retardation factor		1
Decay Rate		-
Input precipitation		1.14×10^{-3} m/day

In this study, two different soils were used. They were classified as sand and gravel. Their engineering properties were decided based on the experimental data by Vachon et al. (2015). The SWCCs, which can be seen in Figure 5 - 7, were estimated using Vachon et al. (2015) experimental results. The sand was assigned as a cover layer due to its relatively low conductivity at the initial stage compare to gravel. The gravel was assigned as embankment

material due to its beneficial embankment filling. Also, the primary source of contaminated soil is the excavated rocks from mining applications, tunneling etc. For that reason, it was thought that the gravel could be prepared as a core material from the excavated natural contaminated rock.

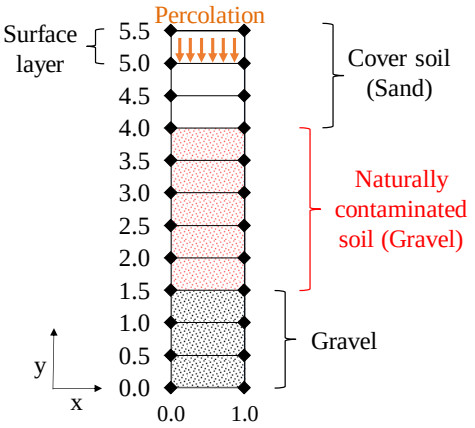

Figure 5 - 6 One-dimensional finite element simulation model

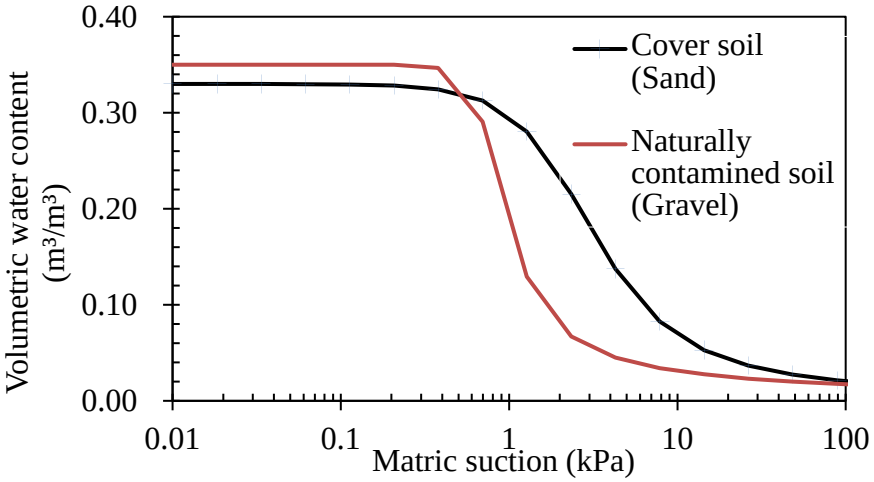

Figure 5 - 7 Soil water characteristic curves (data taken from Vachon et al. (2015))

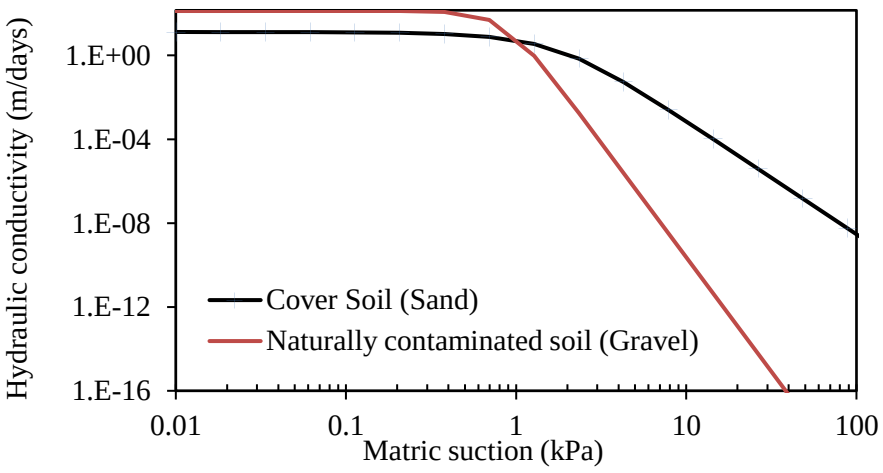

Figure 5 - 8 Hydraulic conductivity functions (data taken from Vachon et al. (2015))

At the second stage, a one-dimensional steady-state model simulation was conducted. The values of the simulation parameters are listed in Table 5 - 3. The initial distribution of matric suction was assumed to be linear and equals to the 10 kPa. The net precipitation, which was calculated from the water balance analysis, was applied as a uniform input up to 3650 days with a constant value. During this analysis, seepage flow and advection/dispersion are considered. The contaminant concentration was applied as Co, in the core of the embankment (naturally contaminated soil). Co is an initial unit concentration, and it is used as constant during the all-time steps.

The analysis results are shown in Figure 5 - 9. It reveals that the contamination level under the embankment increases with time and decreases with depth. The contamination concentration at a depth of 0.5 m was 5.13×10^{-4} times the Co after 3 days' elapse. At the same depth, the concentration increased to 1 × Co when the time increased to 1825 days (Figure 5 - 9). Thereafter, the concentration reached the same level as the core of the embankment. With the same understanding, the concentration at 1 m from the source did not reach a substantial level until the 1460 days. At that time, the concentration is equal to 0.328 × Co, and the concentration became the same as the source with time 1825 days (Figure 5 - 9). The contamination at a depth of 1.5 m from the source was affected after the time 1460 days, and it reached the source concentration at the time 2190 days. It could be seen from the results that the elapsed time dramatically affects the concentration level, and it takes a relatively long time to reach the same concentration level as the source.

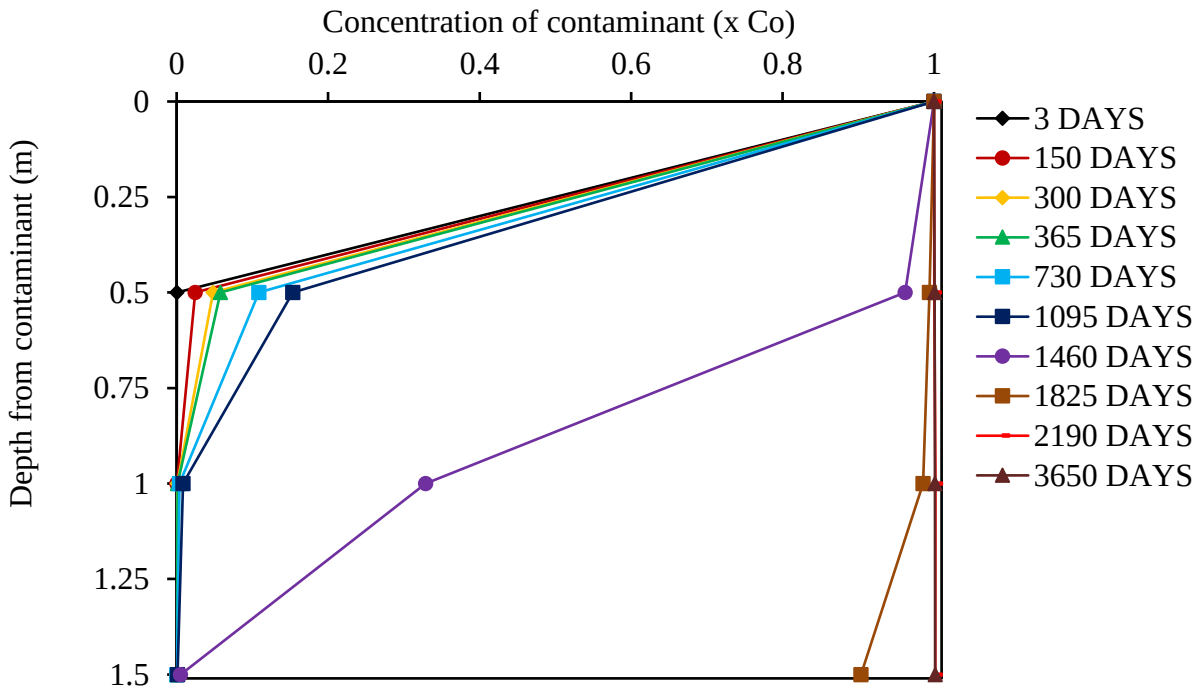

Figure 5 - 9 Concentration distribution under the embankment

5.4 Summary and Conclusions

In this chapter, a water balance analysis is calculated using traditional equations. In the water balance analysis, the average monthly precipitation and mean temperature, which is obtained from the Japanese Meteorology Agency over the past thirty years (1985-2015) for Kyoto city, were used as the input data. According to the results, annually, approximately 28% of precipitation gets into from the surface layer to the cover soil. The maximum percolation occurs in March. The quantity of infiltrated water that passed through the surface layer into embankment depends on the amount of precipitation. The summer precipitation of Kyoto is heavier than in winter. However, the quantity of percolation decreases with the increase in evapotranspiration during periods of high temperature in the summer season. Although high precipitation was recorded, the percolation didn't occur for August and September due to the high amount of evapotranspiration.

In the second stage, a 1D contaminant transport model was used. Both seepage flow and advection/dispersion properties were considered in the model. The model solution was conducted using the free available software Dtransu-2D. Based on the proposed solution, the influences of time and depth from the source were investigated. The result shows that the contamination level 1.5 m from the source reaches the same contamination level with naturally contaminated soil inside the embankment after 2190 days.

In conclusion, the water balance results show that the annual percolation is about 28% of precipitation. Although during the contaminated transport analysis, continuous unit concentration, and rainfall applied, the bottom contamination values from 1.5 meters far from the source are not equal to the unit source concentration within a 6-years period. This is a promising outcome for the utilization of naturally contaminated soil in the embankments with a suitable design concept.

CHAPTER 6: CONCLUSIONS AND FUTURE RESEARCH DIRECTIONS

6.1 Major Conclusions

The general conclusions regarding the study on the utilization of naturally contaminated soils in the embankments are presented as follows:

CAPILLARY BARRIER TEST

1. For the gravel as a contaminated soil overlain by medium sand as a cover soil, the capillary barrier successfully works. In contrast, for the silica sand as a contaminated soil versus medium sand as a cover soil, the capillary barrier did not work. It is considered that at the equilibrium state with the slope angle 26.6 degrees, hydraulic conductivity of gravel is smaller than k of cover soil, while k of silica sand is larger than the hydraulic conductivity of cover.
2. Initial water content does not affect the occurrence of a capillary barrier. That is because the capillary barrier takes place after the equilibrium matric suction came true inside the soil media regarding with preparation slope angle.
3. Soil configuration plays a crucial role than rainfall intercity. During the experiments, CB did not take place at the cases constructed by silica sand overlain by medium sand with slight rainfall intensities, too. However, the cases constructed with silica sand overlain by gravel had the capillary barrier effect both heavy and slight rainfall intensities.
4. The capillary barrier effect is a reversible phenomenon. As a result of drawdown cases, it is understood that CB can recover itself after saturation and drainage periods. This depends on the specific water absorption capacity of soils in the testing condition case.
5. The distribution of water content is higher near the outlets. In the experiments, only drainage holes were used as exits; however, in the field applications, wider drainage areas are generally available. This result may be a restriction of a laboratory tank test.

DRAINAGE LAYER TEST

6. A drainage layer system with coarser material at the embankment shoulder and finer material (contaminated soil) in the embankment core is an alternative way for the utilization of geogenic contaminated soil in the embankment.
7. The contaminated soil, which is placed under the impermeable pavement layer cases gave more pleasing results in order to water interception capacity (more than 90 %

drained). It depends on the shelter function of the impermeable layer above the contaminated soil. Hence, less amount of water enters inside the embankment core.

8. Initial water content does not dramatically affect the drainage layer system performance (approximately 10% difference of drained water between optimum water content cases and drawdown cases). It may depend on the specific water absorption capacity of soils. Within the particular condition, soil can retain the same amount of water, although initial water content is different.
9. Drainage layer systems are also reversible. The conclusion is obtained according to drawdown case results, which are conducted after saturation and drainage. It may depend on the specific water absorption capacity of soils, too.
10. If the saturated k of embankment shoulder material is 100 times higher than saturated k embankment core material, the drainage layer system works moderately with the placement of contaminated soil under the impermeable pavement layer. The difference between k creates preferential follow at the shoulder area.

WATER BALANCE AND CONTAMINANT TRANSPORT

11. According to the results, annually, approximately 28% of precipitation gets into from the surface layer to the cover soil. The maximum percolation occurs in March. The summer precipitation of Kyoto is heavier than in winter. However, the quantity of percolation decreases with the increase in evapotranspiration during periods of high temperature in the summer season. Although high precipitation was recorded, the percolation didn't occur for August and September due to the high amount of evapotranspiration.
12. 1D contaminant transport model was used. Both seepage flow and advection/dispersion properties were considered in the model. Although during the contaminated transport analysis, continuous unit concentration, and rainfall applied, the bottom contamination values from 1.5 meters far from the source are not equal to the unit source concentration within a 6-years period.

6.2 Further Recommendations

In the course of this study, some recommendations for future research direction were identified as follow:

1. The results of experimental studies may be verified with numerical simulations. After that, the experimental results can be implied with the in-situ scale numerical works for an understanding of field performance.
2. Long-term performance of the suggested system is needed to be investigated for a better understanding of actual works over the required service life. Therefore, in-situ scale investigations may be future steps for approving the effectiveness of proposed methods.
3. Apart from the embankment, the possibility of the utilization of geogenic contaminated soil should be investigated in other civil engineering structures such as in recreational parks, creating forests on the coastal belt, in the dams, or retaining structures as backfill.

REFERENCES

Abdolahzadeh, A. M., Vachon, B. L. and Cabral, A. R. (2011) 'Evaluation of the Effectiveness of a Cover with Capillary Barrier Effect to Control Percolation into a Waste Disposal Facility', *Canadian Geotechnical Journal*, 48(7), pp. 996–1009. doi: 10.1139/t11-017.

Aitchison, G. D. (1965) 'Moisture Equilibria and Moisture Changes in Soils beneath Covered Areas'. Butterworth.

Albright, W. H. *et al.* (2004) 'Field Water Balance of Landfill Final Covers', *Journal of Environmental Quality*, 33(6), pp. 2317–2332. doi: 10.2134/jeq2004.2317.

Alloway, B. J. (2013) *Heavy Metals in Soils: Trace Metals and Metalloids in Soils and their Bioavailability*. doi: 10.1007/978-94-007-4470-7.

Azizian, M. F. *et al.* (2003) 'Environmental impact of highway construction and repair materials on surface and ground waters: Case study. Crumb rubber asphalt concrete', *Waste Management*, 23(8), pp. 719–728. doi: 10.1016/S0956-053X(03)00024-2.

Bedient, P. B., Rifai, H. S. and Newell, C. J. (1999) *Ground Water Contamination: Transport and Remediation*. Prentice Hall PTR.

Benson, C. *et al.* (2001) 'Field Evaluation of Alternative Earthen Final Covers', *International Journal of Phytoremediation*, 3(1), pp. 105–127. doi: 10.1080/15226510108500052.

Billstein, M., Svensson, U. and Johansson, N. (1999) 'Development and Validation of a Numerical Model of Flow Through Embankment Dams – Comparisons with Experimental Data and Analytical Solutions', *Transport in Porous Media*, 35(3), pp. 395–406. doi: 10.1023/A:1006531729446.

Birle, E., Heyer, D. and Boso, M. (2010) 'Technical Safeguards for Earth Constructions with Contaminated Soils and Recycled Materials of Low Permeability', in *Proceedings of the 6th International Congress on Environmental Geotechnics*.

Bonaparte, R. and Yanful, E. K. (2001) 'Covers for Waste', in *Geotechnical and Geoenvironmental Engineering Handbook*.

Bradl, H. B. (2005) *Heavy Metals in the Environment : Origin, Interaction and Remediation*. Elsevier Academic Press.

Briaud, J.-L. (2013) *Geotechnical Engineering: Unsaturated and Saturated Soils*. Wiley.

Choo, L.-P. and Yanful, E. K. (2000) 'Water Flow through Cover Soils Using Modeling and Experimental Methods', *Journal of Geotechnical and Geoenvironmental Engineering*, 126(4), pp. 324–334. doi: 10.1061/(ASCE)1090-0241(2000)126:4(324).

D'Amore, J. J., Al-Abed, S. R., Scheckel, K. G. and Ryan, J. A. (2005) 'Methods for Speciation of Metals in Soils', *Journal of Environmental Quality*. Madison, WI: American Society of Agronomy, Crop Science Society of America, Soil Science Society, 34, pp. 1707–1745. doi: 10.2134/jeq2004.0014.

Daniel, D. E. (1993) *Geotechnical Practice for Waste Disposal*. Springer US.

Daniel, D. E. and Shackelford, C. D. (1988) 'Disposal Barriers that Release Contaminants only by Molecular Diffusion', *Nuclear and Chemical Waste Management*.

Delleur, J. W. (1999) *Handbook of Groundwater Engineering*. CRC Press.

DiVenere, V. J. (2019) *Weathering and Soils*. Available at: http://www.columbia.edu/~vjd1/soils.htm (Accessed: 1 March 2019).

Duriez, S. (2005) *On the Use of Groundwater Contaminant Transport Modelling in Risk Assessments*. Chalmers University of Technology.

Edelstein, M. and Ben-Hur, M. (2018) 'Heavy Metals and Metalloids: Sources, Risks and Strategies to Reduce Their Accumulation in Horticultural Crops', *Scientia Horticulturae*, pp. 431–444. doi: 10.1016/j.scienta.2017.12.039.

Edlefsen, N. E. and Anderson, A. B. C. (1943) 'Thermodynamics of Soil Moisture', *Hilgardia*, 15(2), pp. 31–298. doi: 10.3733/hilg.v15n02p031.

Fenn, D., Hanley, K. J. and Degeare, T. V. (1975) *Use of the Water Balance Method for Predicting Leachate Generation From Solid Waste Disposal Sites: a Current Report on Solid Waste Management*.

Floyd, P. A. and Winchester, J. A. (1978) 'Identification and Discrimination of Altered And Metamorphosed Volcanic Rocks Using Immobile Elements', *Chemical Geology* 21(3–4), pp. 291–306. doi: 10.1016/0009-2541(78)90050-5.

Fredlund, D. G., Rahardjo, H. and Fredlund, M. D. (2012) *Unsaturated Soil Mechanics in Engineering Practice*. John Wiley & Sons, Inc.

Fredlund, D. G. and Xing, A. (1994) 'Equations for the Soil-Water Characteristic Curve', *Canadian Geotechnical Journal*, 31(4), pp. 521–532. doi: 10.1139/t94-061.

Freeze, R. A. and Cherry, J. A. (1979) *Groundwater*. Prentice-Hall.

van Genuchten, M. T. (1980) 'A Closed-form Equation for Predicting the Hydraulic Conductivity of Unsaturated Soils', *Soil Science Society of America Journal*, 44(5), pp. 892–898. doi: 10.2136/sssaj1980.03615995004400050002x.

GEO-SLOPE International Ltd. (2008) *Contaminant Modeling with CTRAN/W 2007, Geo-SLOPE international Ltd.*

Gross, B. (2005) *Water Balance Evaluations for Monitored Evapotranspirative Cover Systems At Three Sites in the Semi-Arid and Arid Southwest U.S.* The University of Texas at Austin.

Gulsen, F. *et al.* (2019) 'Numerical Investigation on Utilization of Natural Contaminated Soil in the Embankments', In: Zhan L., Chen Y., Bouazza A. (eds) Proceedings of the 8th International Congress on Environmental Geotechnics Volume 1. ICEG 2018.

Hanamura, T. (1990) 'Japan's New Frontier Strategy: Underground Space Development', *Tunnelling and Underground Space Technology incorporating Trenchless*. Pergamon, 5(1–2), pp. 13–21, (In Japanese). doi: 10.1016/0886-7798(90)90058-r.

Harnas, F. R. (2015) *Development of Dual Capillary Barrier System Using Recycled Materials*. Nanyang Technological University.

Hattori, S., Ohta, T. and Kiya, H. (2003) 'Engineering Geological Study on Exudation of Acid Water from Rock Mucks', *Journal of the Japan Society of Engineering Geology*. Japan Society of Engineering Geology, 43(6), pp. 359–371, (In Japanese). doi: 10.5110/jjseg.43.359.

Heerten, G. and Koerner, R. M. (2008) 'Cover Systems for Landfills and Brownfields', *Land Contamination & Reclamation*, 16(4), pp. 343–356. doi: 10.2462/09670513.904.

Hilf, J. W. (1956) 'Investigation of Pore-water Pressure in Compacted Cohesive Soils', *Bureau of Reclamation /US*.

Igarashi, T. *et al.* (2008) 'Leaching Behavior of Arsenic from Various Rocks by Controlling Geochemical Conditions', *Minerals Engineering*. Pergamon, 21(3), pp. 191–199. doi: 10.1016/j.mineng.2007.07.014.

Inazumi, S. *et al.* (2018) 'Remediation of Heavy Metals Polluted Soil Using Metal Insolubilizing Materials', *Journal of Environmental Protection*, 09(07), pp. 770–789. doi: 10.4236/jep.2018.97048.

Jaishankar, M. *et al.* (2014) 'Toxicity, mechanism and health effects of some heavy metals', *Interdisciplinary Toxicology*, 7(2), pp. 60–72. doi: 10.2478/intox-2014-0009.

Japan Meteorological Agency (2018) *Primary Factors behind the Heavy Rain Event of July 2018 and the Subsequent Heatwave in Japan from Mid-July | World Meteorological Organization*. Available at: https://public.wmo.int/en/media/news-from-members/primary-factors-behind-heavy-rain-event-of-july-2018-and-subsequent-heatwave (Accessed: 9 March 2020).

Kamon, M., Inazumi, S. and Katsumi, T. (2002) 'Performance Evaluations of Landfill Cover Systems with Sludge Barriers', *Journal of the Souteast Asian Geotechnical Engineering Society*, 33, pp. 113–132.

Katsumi, T. (2015) 'Soil Excavation and Reclamation in Civil Engineering: Environmental Aspects', *Soil Science and Plant Nutrition*, 61, pp. 22–29. doi: 10.1080/00380768.2015.1020506.

Khan, F. I., Husain, T. and Hejazi, R. (2004) 'An Overview and Analysis of Site Remediation Technologies', *Journal of Environmental Management*, 71(2), pp. 95–122. doi: 10.1016/j.jenvman.2004.02.003.

Khan, S. *et al.* (2008) 'Health Risks of Heavy Metals in Contaminated Soils and Food Crops Irrigated with Wastewater in Beijing, China', *Environmental Pollution*. Elsevier, 152(3), pp. 686–692. doi: 10.1016/J.ENVPOL.2007.06.056.

Khire, M. V., Benson, C. H. and Bosscher, P. J. (1997) 'Water Balance Modeling of Earthen Final Covers', *Journal of Geotechnical and Geoenvironmental Engineering*, 123(8), pp. 744–754. doi: 10.1061/(ASCE)1090-0241(1997)123:8(744).

Klute, A., Van Genuchten, M. T. and Wierenga, P. J. (1986) 'Solute Dispersion Coefficients and Retardation Factors', in. John Wiley & Sons, Ltd, pp. 1025–1054. doi: 10.2136/sssabookser5.1.2ed.c44.

Koerner, R. M. and Daniel, D. E. (1997) *Final Covers for Solid Waste Landfils and Abandoned Dumps*. Thomas Telford Publishing. doi: doi:10.1680/fcfswlaad.02610.

Koohmishi, M. (2019) 'Hydraulic Cconductivity and Water Level in the Reservoir Layer of Porous Pavement Considering Gradation of Aggregate and Compaction Level', *Construction and Building Materials*. Elsevier Ltd, 203, pp. 27–44. doi: 10.1016/j.conbuildmat.2019.01.060.

Krahn, J. and Fredlund, D. G. (1972) 'On Total, Matric and Osmotic Suction', *Soil Science*, 114(5).

Lebeau, M. and Konrad, J.-M. (2009) 'Pavement Subsurface Drainage: Importance of Appropriate Subbase Materials', *Canadian Geotechnical Journal*, 46(8), pp. 987–1000. doi: 10.1139/T09-021.

Li, J. *et al.* (2016) 'Potential for Leaching of Arsenic from Excavated Rock after Different Drying Treatments', *Chemosphere*, 154, pp. 276–282. doi: 10.1016/j.chemosphere.2016.03.129.

Liu, L. *et al.* (2018) 'Remediation Techniques for Heavy Metal-Contaminated Soils: Principles and Applicability', *Science of the Total Environment*, 633, pp. 206–219. doi: 10.1016/j.scitotenv.2018.03.161.

Merrill, K., Friedman, H. and Goodale, G. (2002) 'Design Considerations for GCLs Used in Alaska Landfills', in *Cold Regions Engineering*. Reston, VA: American Society of Civil Engineers, pp. 922–937. doi: 10.1061/40621(254)80.

Ministry of the Environment, G. of J. (2019) *Ministry of the Environment, Government of Japan*. Available at: https://www.env.go.jp/en/water/index.html (Accessed: 3 January 2019).

Mizukami, M., Kato, K. and Ohmori, S. (1995) 'Metal-Rich Sludgy Sediments Deposited in the Seikan Undersea Tunnel', *Shigen-Chishitsu*. The Society of Resource Geology,

45(254), pp. 391–400 (In Japanese). doi: 10.11456/shigenchishitsu1992.45.391.
Morris, C. E. and Stormont, J. C. (1997) 'Capillary Barriers and Subtitle D Covers: Estimating Equivalency', *Journal of Environmental Engineering*, 123(1), pp. 3–10. doi: 10.1061/(ASCE)0733-9372(1997)123:1(3).
Mualem, Y. (1976) 'A New Model for Predicting the Hydraulic Conductivity of Unsaturated Porous Media', *Water Resources Research*, 12(3), pp. 513–522. doi: 10.1029/WR012i003p00513.
Naidu, R., Sumner, M. E. and Harter, R. D. (1998) 'Sorption of Heavy Metals in Strongly Weathered Soils: An Overview', *Environmental Geochemistry and Health*, 20(1), pp. 5–9. doi: 10.1023/A:1006519009465.
Nishiumura, T. *et al.* (2011) 'Microporous Membrane Technology for Measurement of Soil-Water Characteristic Curve', *Geotechnical Testing Journal*, 35(1), pp. 1–9.
Nyhan, J. W. (2005) 'A Seven-Year Water Balance Study of an Evapotranspiration Landfill Cover Varying in Slope for Semiarid Regions', *Vadose Zone Journal*, 4(3), pp. 466–480. doi: 10.2136/vzj2003.0159.
Parent, S. É. and Cabral, A. (2006) 'Design of Inclined Covers with Capillary Barrier Effect', *Geotechnical and Geological Engineering*, 24(3), pp. 689–710. doi: 10.1007/s10706-005-3229-9.
Pierzynski, G. M., Sims, J. T. and Vance, G. F. (2005) *Soils and Environmental Quality*.
Rahardjo, H. *et al.* (2012) 'Performance of an Instrumented Slope Covered by a Capillary Barrier System', 138(4), pp. 481–490. doi: 10.1061/(ASCE)GT.1943-5606.0000600.
Ross, B. (1990) 'The diversion capacity of capillary barriers', *Water Resources Research*, 26(10), pp. 2625–2629. doi: 10.1029/WR026i010p02625.
Sawada, M., Mimura, M. and Yoshimura, M. (2017) 'Infiltration Control Using Capillary Barriers for Conservation of Historical Tumulus Mounds', *Japanese Geotechnical Society Special Publication*, 5(2), pp. 5–10. doi: 10.3208/jgssp.v05.002.
Schroeder, P., Lloyd, C., Zappi, P., McEnroe, P., Sjostrom, J. W., & Peyton, R. L. (1984) 'The Hydrologic Evaluation of Landfill Performance (HELP) Model: Engineering Documentation for Version 1', *U.S. Environmental Protection Agency*.
Sharma, H. D. and Reddy, K. R. (2004) *Geoenvironmental Engineering: Site Remediation, Waste Containment, and Emerging Waste Management Technologies*. Wiley.
Shimpo, A. *et al.* (2019) 'Primary Factors behind the Heavy Rain Event of July 2018 and the Subsequent Heat Wave in Japan', *SOLA*, advpub. doi: 10.2151/sola.15A-003.
Siegel, F. R. (2002) *Environmental Geochemistry of Potentially Toxic Metals*.
Stormont, J. C. (1996) 'The Effectiveness of Two capillary Barriers on a 10% Slope', *Geotechnical and Geological Engineering*, 14(4), pp. 243–267. doi: 10.1007/BF00421943.
Stormont, J. C. and Morris, C. E. (1998) 'Method to Estimate Water Storage Capacity of Capillary Barriers', *Journal of Geotechnical and Geoenvironmental Engineering*, 124(4), pp. 297–302. doi: 10.1061/(ASCE)1090-0241(1998)124:4(297).
Tabelin, C. B. *et al.* (2014) 'Leaching of boron, arsenic and selenium from sedimentary rocks: I. Effects of contact time, mixing speed and liquid-to-solid ratio', *Science of the Total Environment*, 472, pp. 620–629. doi: 10.1016/j.scitotenv.2013.11.006.
Tabelin, C. B. *et al.* (2018) 'Arsenic, selenium, boron, lead, cadmium, copper, and zinc in naturally contaminated rocks: A review of their sources, modes of enrichment, mechanisms of release, and mitigation strategies', *Science of the Total Environment*, 645, pp. 1522–1553. doi: 10.1016/j.scitotenv.2018.07.103.
Tami, D. *et al.* (2004) 'Design and Laboratory Verification of a Physical Model of Sloping

Capillary Barrier', *Canadian Geotechnical Journal*, 41(5), pp. 814–830. doi: 10.1139/t04-036.

Thornthwaite, C. W. and Mather, J. R. (1955) 'The water balance', *Institute of Technology Publications in Climatology*, 8(1).

Vachon, B. L., Abdolahzadeh, A. M. and Cabral, A. R. (2015) 'Predicting the diversion length of capillary barriers using steady state and transient state numerical modeling: case study of the Saint-Tite-des-Caps landfill final cover', *Canadian Geotechnical Journal*, 52(12), pp. 2141–2148. doi: 10.1139/cgj-2014-0353.

Van Genuchten, M. Th. (1980) 'A Closed‐form Equation for Predicting the Hydraulic Conductivity of Unsaturated Soils', *Soil Science Society of America Journal*, 44 (5), pp. 892–898. doi:10.2136/sssaj1980.03615995004400050002x

Von Maubeuge, K., Egloffstein, T. and Vollmert, L. (2015) 'Road Noise Barriers as Longitudinal Waste Deposits - Lined Slopes with Geosynthetics Protecting the Environment', *The 15th Asian Regional Conference on Soil Mechanics and Geotechnical Engineering*, (November).

Warren, J. K. (2010) 'Evaporites through time: Tectonic, climatic and eustatic controls in marine and nonmarine deposits', *Earth-Science Reviews*, 98(3–4), pp. 217–268.

Warren, R. W., Hakonson, T. E. and Bostick, K. V. (1996) 'Choosing the most effective hazardous waste landfill cover', *Remediation*, 6(2), pp. 23–41. doi: 10.1002/rem.3440060205.

Wilkinson, B. *et al.* (2009) *Global geologic maps are tectonic speedometers-Rates of rock cycling from area-age frequencies, Geological Society of America Bulletin,* 21(5) , pp. 760-779. doi: 10.1130/B26457.1.

Wuana, R. A. and Okieimen, F. E. (2011) 'Heavy Metals in Contaminated Soils: A Review of Sources, Chemistry, Risks and Best Available Strategies for Remediation', *ISRN Ecology*, 2011, pp. 1–20. doi: 10.5402/2011/402647.

Yano, T. *et al.* (2010) 'Saturated-Unsaturated Hydraulic Properties of Porous Asphalt Mixture', *Doboku Gakkai Ronbunshuu E*, 66(4), pp. 452–465 (In Japanese). doi: 10.2208/jsceje.66.452.

Yokobori, N., Igarashi, T. and Yoneda, T. (2015) 'Leaching Characteristics of Heavy Metals from Mineralized Rocks Located Along Tunnel Construction Sites', in Lollino, G. et al. (eds) *Engineering Geology for Society and Territory - Volume 6*, pp. 429–433.

Zhang, M.-K., Liu, Z.-Y. and Wang, H. (2010) 'Use of Single Extraction Methods to Predict Bioavailability of Heavy Metals in Polluted Soils to Rice', *Communications in Soil Science and Plant Analysis*, 41(7), pp. 820–831. doi: 10.1080/00103621003592341.

Zhao, Q. and Kaluarachchi, J. J. (2002) 'Risk Assessment at Hazardous Waste-Contaminated Sites with Variability of Population Characteristics', *Environment International*, 28(1–2), pp. 41–53. doi: 10.1016/S0160-4120(02)00003-X.

Zornberg, J. G., Bouazza, A. and McCartney, J. S. (2010) 'Geosynthetic capillary barriers: current state of knowledge', *Geosynthetics International*, 17(5), pp. 273–300. doi: 10.1680/gein.2010.17.5.273.

Zornberg, J. G., LaFountain, L. and Caldwell, J. A. (2003) 'Analysis and Design of Evapotranspirative Cover for Hazardous Waste Landfill', *Journal of Geotechnical and Geoenvironmental Engineering*, 129(5), pp. 427–438. doi: 10.1061/(ASCE)1090-0241(2003)129:6(427).